STATUS OF THESIS

Title of thesis	MATHEMATICAL MODELING AND STATISTICAL EVALUATION OF COGENERATION PLANT IN TROPICAL REGION

I, AKLILU TESFAMICHAEL BAHETA, hereby allow my thesis to be placed at the Information Resource Centre (IRC) of Universiti Teknologi PETRONAS (UTP) with the following conditions:

1. The thesis becomes the property of UTP
2. The IRC of UTP may make copies of the thesis for academic purpose only
3. The thesis is classified as

☐ Confidential

[√] Non-Confidential

If the thesis is confidential, please state the reason:

_____

_____

The contents of the thesis will remain confidential for _____ years.

Remarks on disclosure:

_____

_____

Endorsed by

_____   _____
Signature of Author   Signature of Supervisor

Permanent   Addis Ababa University   Dr. Syed Ihtsham-Ul-Haq Gilani
Address: Faculty of Technology (N)
            Addis Ababa, Ethiopia

Date:___August 27 / 2010   Date: 30th, August, 2010

UNIVERSITI TEKNOLOGI PETRONAS

MATHEMATICAL MODELING AND STATISTICAL EVALUATION OF

COGENERATION PLANT IN TROPICAL REGION

by

AKLILU TESFAMICHAEL BAHETA

The undersigned certify that they have read, and recommend to the Postgraduate Studies Programme for acceptance this thesis for the fulfilment of the requirements for the degree of Doctor of Philosophy in Mechanical Engineering.

Signature:

Main Supervisor: Dr. Syed Ihtsham-Ul-Haq Gilani

Date: 30th. August, 2010

Signature:
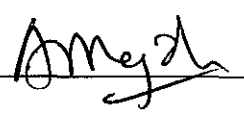
Head of Department: Dr. Ahmad Majdi Bin Abdul Rani

Date: 30/8/2010

MATHEMATICAL MODELING AND STATISTICAL EVALUATION OF

COGENERATION PLANT IN TROPICAL REGION

by

AKLILU TESFAMICHAEL BAHETA

A Thesis

Submitted to the Postgraduate Studies Programme

as a Requirement for the Degree of

DOCTOR OF PHILOSOPHY

MECHANICAL ENGINEERING

UNIVERSITI TEKNOLOGI PETRONAS

BANDAR SRI ISKANDAR

PERAK

AUGUST, 2010

DECLARATION OF THESIS

Title of thesis	MATHEMATICAL MODELING AND STATISTICAL EVALUATION OF COGENERATION PLANT IN TROPICAL REGION

I, AKLILU TESFAMICHAEL BAHETA

hereby declare that the thesis is based on my original work except for quotations and citations which have been duly acknowledged. I also declare that it has not been previously or concurrently submitted for any other degree at UTP or other institutions.

Witnessed by

_____

Signature of Author

Permanent   Addis Ababa University
Address: Faculty of Technology (N)
                 Addis Ababa, Ethiopia

Date: _August 27 2010_

_____

Signature of Supervisor

Dr. Syed Ihtsham-Ul-Haq Gilani

Date: _30th August, 2010_

DEDICATION

This dissertation is dedicated to my father Tesfamichael Baheta Desta and my sister Abeba Tesfamichael Baheta

ACKNOWLEDGEMENTS

ABSTRACT

The widespread use of gas turbines and cogeneration plants as a means of independent power generation have provided a considerable momentum for further study of cogeneration plant. Furthermore, in the design of new systems and an existing system improving their performance is a challenging task. This is largely achieved by studying the system performance as a whole or as an individual component. In order to do that, greater understanding of the behaviour of the plant during off-design operation and identifying the potential components that have wide margin of improvement are important.

Thus, this thesis is concerned with a detailed investigation of how off-design conditions affect the cogeneration performance and the associated exergy destruction or loss. To carry out the investigation a new modeling procedure based on component matching is developed. The model is used to predict the design performance, off-design performance, and the exergy destruction of the cogeneration plant. The cogeneration plant consists of gas turbine and heat recovery steam generator. The gas turbine compressor has variable stator vanes whose position may be set to control the inlet air flow to the compressor. During off-design the variable vanes are re-staggered to improve the overall cogeneration performance. Two modes of gas turbine operation are identified. The first mode is for part load less than 50% running to meet the part load demand. This is achieved by controlling the fuel flow and air bleeding at the downstream of the compressor to avoid surge formation. The second mode of operation is for part load greater than 50% and running to meet both the part load demand and the exhaust gas temperature set value by simultaneously regulating the fuel feeding and the variable vanes opening. To accommodate change of compressor parameters during variable vanes re-stagger correction coefficients are introduced.

The unavailable information such as the compressor and turbine design point data are obtained using energy and mass conservation, and thermodynamic properties ratio relationships. The compressor and turbine maps are developed using scaling method

from similar configuration known component maps. Both energy and exergy models of the components are developed. First, an energy based components model and their interactions using modified component matching concept are developed. To support the calculations required for off-design analysis, a computer program is developed in MATLAB software. The effect of variation of load on the cogeneration parameters such as fuel consumption, temperatures, pressure ratios, variable vanes opening, efficiencies, specific fuel consumption, and steam production rate are examined. The simulated results are compared with available actual data. Furthermore, statistical errors evaluation using Minitab program indicated that the error mean and standard deviations values were small and hence the developed model represents the real process.

Once the model has been validated, based on the inlet and outlet properties of each component the exergy analysis is performed to find out the exergy destruction or loss in each component. Sensitivity analysis of the effect of ambient temperature on the cogeneration performance is carried out. It is found that the smaller the ambient temperature, the better is the gas turbine performance in the first mode of operation. In the second mode of operation the VVs is modulated to maintain the turbine exhaust gas temperature. Consequently, effect of ambient temperature on the thermal efficiency is not significant; but the higher the ambient temperature, the higher is the overall performance of the cogeneration plant at a given load.

ABSTRAK

Penggunaan meluas turbin gas dan loji penjanaan bersama sebagai kaedah penjanaan kuasa bermandiri telah memberikan deras untuk kajian lanjut loji penjanaan bersama. Tambahan pula, dalam rekaan sistem baru dan sistem yang sedia ada, meningkatkan prestasi adalah tugas yang mencabar. Hal ini sebahagian besar dicapai dengan mempelajari sistem secara keseluruhan atau prestasi komponen individu. Bagi melaksanakan hal ini, perilaku loji semasa operasi 'off-design' harus dikaji, serta mengenalpasti komponen yang berpotensi untuk diperbaiki.

Oleh yang demikian, fokus tesis ini ialah penyiasatan terperinci tentang pengaruh situasi 'off-design' terhadap prestasi penjanaan bersama dan penghancuran atau kerugian eksergi yang berkaitan. Bagi melaksanakan kajian ini, prosedur model baru berdasarkan penyesuaian komponen dibangunkan. Model ini digunakan untuk meramal prestasi operasi 'on' dan 'off-design', serta kehancuran eksergi logi penjanaan bersama. Logi penjanaan bersama terdiri daripada turbin gas dan penjana wap panas pemulihan. Turbin gas pemampat mempunyai bilah-bilah stator bolehubah yang ditetapkan untuk menentukan aliran udara masuk ke pemampat. Pada waktu operasi 'off-design', bilah-bilah stator disusun untuk meningkatkan prestasi keseluruhan penjanaan bersama. Selanjutnya, dua mode operasi turbin gas dikenalpasti. Mod yang pertama adalah untuk operasi beban-separa, dengan operasi kurang daripada 50% kapasiti penuh. Ini dicapai dengan mengawal aliran bahan api dan udara di hilir pemampat untuk mengelakkan pembentukan gelombang. Mod kedua operasi ini adalah untuk beban 'beban-separa' yang lebih besar daripada 50% dan berjalan untuk memenuhi permintaan beban dan nilai suhu gas buang yang ditetapkan. Ini dapat dicapai dengan menetapkan sekaligus aliran bahan bakar dan saiz bukaan bilah-bilah stator boleh-ubah. Bagi membolehkan perubahan parameter pemampat apabila bukaan bilah disusun kembali, pekali pembetulan diperkenalkan.

Maklumat pemampat dan turbin yang tidak sedia ada seperti data rekaan diperolehi menggunakan persamaan tenaga dan pemuliharaan jisim serta hubungan

nisbah termodinamik. Peta pemampat dan turbin diperolehi menggunakan kaedah penskalaan peta komponen. Model untuk tenaga dan eksergi setiap komponen diusahakan. Pertama sekali, model komponen berasaskan persamaan tenaga diperoleh; interaksi komponen dikaji menggunakan konsep padanan. Bagi menjalankan pengiraan yang diperlukan untuk analisa 'off-design', sebuah program komputer dibangunkan menggunakan perisian MATLAB. Kesan variasi beban pada parameter penjanaan bersama seperti penggunaan bahan bakar, suhu, nisbah tekanan, bukaan stator boleh-ubah, kecekapan, penggunaan bahan bakar spesifik serta kadar pengeluaran wap dikaji. Keputusan simulasi dibandingkan dengan data sebenar yang sedia ada. Selanjutnya, penilaian ketepatan statistik menggunakan program Minitab menunjukkan nilai rata-rata mendekati sifar dengan sisihan piawai yang kecil. Justeru, disimpulkan bahawa model ini mewakili situasi nyata.

Setelah model disahkan, berdasarkan karakteristik pada saluran masuk dan saluran keluar bagi setiap komponen, analisis eksergi dijalankan untuk mengetahui kerugian eksergi di setiap komponen. Analisis sensitiviti kesan suhu persekitaran pada prestasi proses 'penjanaan bersama' telah dilaksanakan. Dalam mod operasi pertama, didapati bahawa prestasi turbin gas lebih baik apabila suhu persekitaran semakin rendah. Dalam mod kedua operasi VVs dimodulasi untuk menjaga suhu ekzoz turbin gas. Akibatnya, kesan suhu persekitaran pada kecekapan terma tidak signifikan, tetapi semakin tinggi suhu persekitaran, semakin tinggi prestasi keseluruhan dari loji penjanaan bersama pada tahap beban yang diberikan.

TABLE OF CONTENTS

LIST OF TABLES

LIST OF FIGURES

NOMENCLATURES

A	Surface area [m^2]
Cogen	Cogeneration
c_{pa}	Specific heat of air at constant pressure [kJ/kg K]
c_{pg}	Specific heat of gas at constant pressure [kJ/kg K]
c_{pgec}	Specific heat of gas in economizer [kJ/kg K]
c_{pgev}	Specific heat of gas in evaporator [kJ/kg K]
d	Diameter [m]
e	Error tolerance [%]
GT	Gas turbine
HRSG	Heat recovery steam generation
h	Enthalpy [kJ/kg]
I	Irreversibility [kW]
LHV	Lower heating value [kJ/kg]
LMTD	Log mean temperature difference [K]
$\dot{m}$	Mass flow rate [kg/s]
N	Rotational speed [rpm]
p	Pressure [kPa]
pr	Pressure ratio
$\dot{Q}$	Heat transfer rate [kW]
R	Characteristic gas constant [kJ/kg K]
s	Specific entropy [kJ/kg K]
T	Temperature [K]
U	Overall heat transfer coefficient [W/m^2 .K]
V	Velocity [m/s]
VVs	Variable Vanes
$\dot{W}$	Power [kW]
w	Specific power [kW/kg]
x	Fraction of steam
z	Elevation [m]

Greek symbols

α	VVs percentage opening [%]
γ	Specific heat ratio
η	Efficiency
π	Fraction of pressure drop
τ	Torque [N.m]
ψ	Exergy [kW]

Subscripts

1,2,3,4,5,6,7	Designate the state of the working fluid station in the plant process
pt	Polytropic turbine
pc	Polytropic compressor
$term$	Terminating
gb	Gearbox coupling
gen	Generator
g	Exhaust gas
M	Map
MD	Map design point
D	Calculated design point
sm	Scaled map
b	Bleed
f	Fuel
cc	Combustion chamber
t	Turbine
c	Compressor
sat	Saturated state
v	Saturated vapor
fw	Feedwater
$fw2$	State of the feedwater leaving the economizer
ev	Evaporator

ec	Economizer
eca	Economizer assumed
ecc	Economizer calculated
i	Inlet
e	Exit
o	Dead state
cv	Control volume
rev	Reversible
act	Actual
I	First law
II	Second law
comp	Component
dest	Destruction
sg	Stack gas

Superscripts

CH	Chemical
TM	Thermomechanical

CHAPTER 1

INTRODUCTION

1.1 Cogeneration Overview

The requirement placed on the supply of electricity and heat in the future is the conversion of primary energy forms in a manner that is efficient and as non-polluting as possible. The emissions could be lowered if the efficiency of the energy conversion unit increases or switches to low carbon fuels. Among all fossil fuels, natural gas burning results in the lowest levels of Green House Gas (GHG) emissions. Furthermore, the successive energy crises and proposals of law to limit amount of GHG emission, like the Kyoto Protocol, have stimulated the study of more efficient ways for the use of the available energy in fuels. Therefore, to improve the ability of power plants to convert energy to useful form, utility companies have introduced a cogeneration plant using more than one prime mover [1].

Cogeneration may be defined as the simultaneous production of electrical or mechanical energy and useful thermal energy from a single energy source by capturing heat from an exhaust gas that would otherwise be rejected to the environment. Cogeneration plant can operate at efficiencies greater than those achieved when heat and power are produced in separate processes. Hence they produce less emission than conventional power and heat sources. Cogeneration systems are classified by the type of prime mover used to drive the electrical generator. The five main types currently in use are steam turbines, gas turbines, reciprocating engines, microturbines and combined cycle gas turbines [2, 3]. New systems currently under development include fuel cells and Stirling engines.

Cogeneration was initially introduced in Europe and the USA around 1890 [4]. During the first decades of the twentieth century, most industries had their own

1

power generation units with a steam furnace turbine, operating on coal. Many of those units were cogeneration units. Moreover, 58% of power generated by various industries in the USA was actually generated by cogeneration units [4]. Later, a period of decline followed. Industrial cogeneration dropped to 15% of the total power generation potential until 1950 and, after that, continued its descending course to as low as 5% in 1974. However, due to the abrupt rise of fossil fuel prices since 1973, and the energy policy motives provided at a National level the trend has been reversed not only in the USA but also in Europe, Japan etc.

Typically, cogeneration systems have overall efficiencies of between 65% and 85% [5]. This is because the heat that is rejected in the power cycle is used for a useful purpose rather than rejected to the atmosphere, as is the case with large centralized power production. Cogeneration systems can achieve energy saving in the range of 15-40% when compared against the supply of electricity and heat from conventional power stations and boilers [6, 7]. Consequently, the reduction in primary fuel consumption and emissions including CO_2 is significant.

In the history of energy conversion, gas turbine is relatively a new plant. The first practical gas turbine used to generate electricity ran at Neuchatel, Switzerland in 1939, and was developed by the Brown Boveri Company [8, 9]. The design of this machine is illustrated in Figure 1.1. Because the origin of this gas turbine lies simultaneously in the electric power field and in aviation, there have been a profusion of "other names" for the gas turbine. For electrical power generation and marine applications it is generally called a gas turbine, also a combustion turbine (CT) [9].
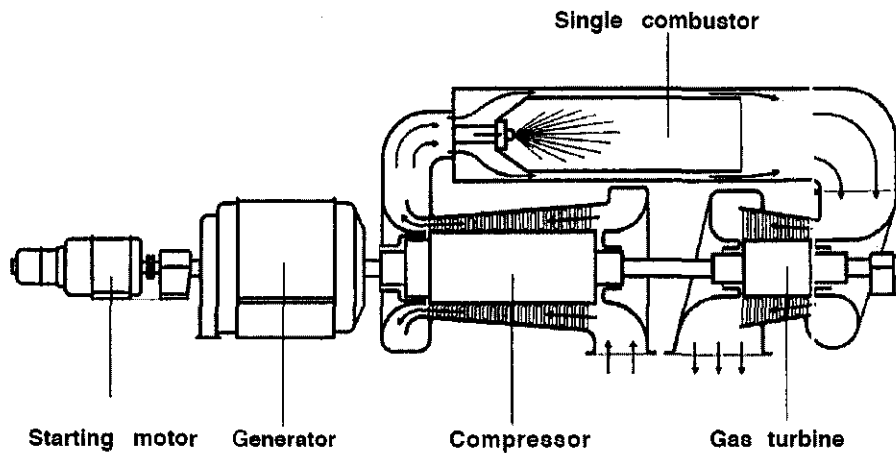
Figure 1.1 Layout of the single stage gas turbine set [8]

Figure 1.2 shows a typical single shaft gas turbine thermodynamic cycle representation (a) on temperature entropy diagram and (b) on pressure volume diagram. The working fluid (air) enters into air intake duct. After the air passes through the air intake duct, the temperature of ambient air remains constant as there is no energy input but its pressure drops from p_1 to p_2. Then, it is compressed by the compressor to state point 3 to a temperature and pressure T_3 and p_3, respectively. The high pressure and temperature air is admitted to the combustion chamber where it mixes with fuel and is heated by chemical energy of fuel released during combustion process from temperature T_3 to temperature T_4. The combustion gas with temperature T_4 and pressure p_4 is admitted into the turbine. In the turbine it expands from state point 4 to state point 5, thus transferring its energy to the turbine blade in the form of mechanical work. The turbine is connected to the compressor and the generator by a shaft and gear box, respectively. As a result the mechanical work from the turbine drives both the compressor and the generator.

In Figure 1.2, the two states, 3s and 5s, they are not the actual thermodynamic cycle state points but two supplement points. State points 3s and point 3 have the same pressure but different temperatures. Point 3 is the final state of the compressed air after undergoing an actual polytropic compression process with a pressure rising from p_2 to p_3 whereas state 3s is the final state of air after undergoing an ideal isentropic compression process with the same initial and final pressures. Similarly, point 5 is the air state point after undergoing an actual polytropic expansion process

3

whereas point 5s is the state point after undergoing an ideal isentropic expansion process with the same initial and final pressures.

(a) Temperature entropy diagram   (b) Pressure volume diagram
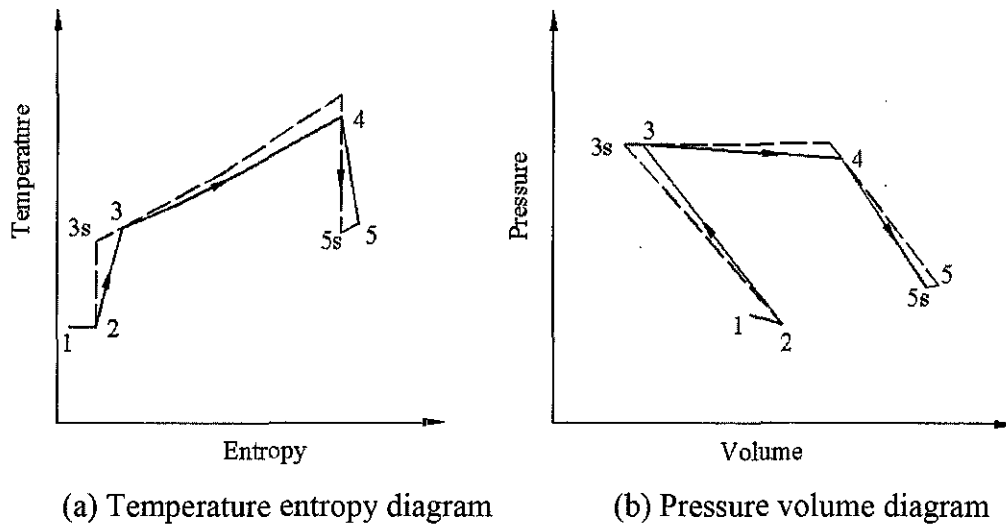
Figure 1.2 Single shaft thermodynamic cycle

A schematic representation of UTP single shaft gas turbine based cogeneration plant is shown in Figure 1.3. Air as working fluid enters into the compressor where energy is added to bring it to a higher pressure and temperature. It then enters to the combustor where it is burned with fuel to raise it to a higher temperature. The burned gas expands through the turbine and produces mechanical energy. A portion of the energy produced is used to run the compressor which is rigidly coupled to the turbine and the excess power is used to drive the generator. The turbine exhaust gas is used to recover heat in the form of steam in the Heat Recovery Steam Generator (HRSG).
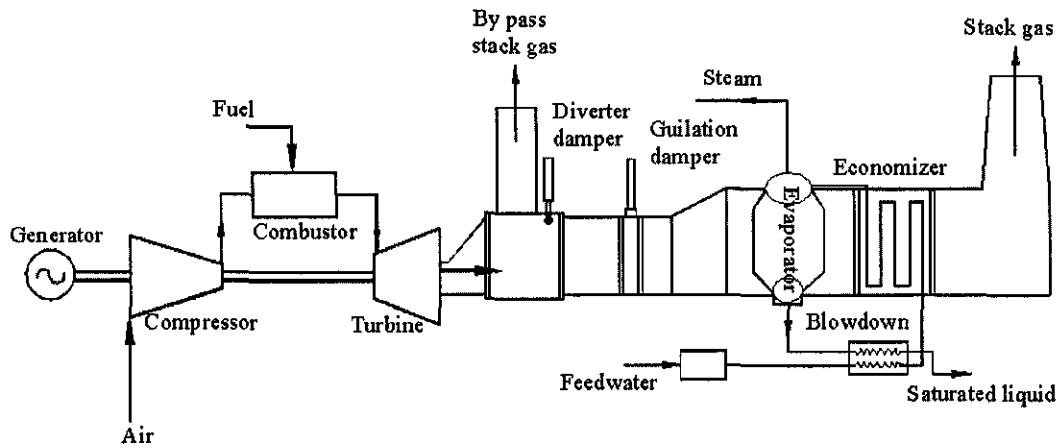
Figure 1.3 Schematic representation of UTP single shaft gas turbine cogeneration plant

In gas turbine system high pressure and temperature gas expands in the turbine to a given pressure to produce mechanical power, which can be converted to electricity through an electrical generator. The exhaust gas temperature of the gas turbines at full load is in the range of 450–600°C [10]. This is well suited to produce medium to high temperature process steam using HRSG. However, this range of temperature is not achieved in all gas turbine types and part load running conditions. In order to get this temperature either the gas turbine should run near to the full load or should be designed so that the air flow entering to the gas turbine is controlled after a certain part load. For that, a gas turbine working in a cogeneration plant usually involves variable geometry compressor to control the air flow. Hence, gas turbine engines played a significant role in the advancement of the cogeneration capabilities.

An industrial gas turbine may operate at different part load and ambient conditions globally that leads to off-design situation of the cogeneration plant. Even in a day, the gas turbine may be operating and delivering shaft power to maintain production with large change in ambient temperature. The gas turbine performance is sensitive to its load setting, ambient temperature and geographic location [11]. Therefore the operation of cogeneration plants involves frequent changes of operating conditions within the plant and its components. These change are caused by variations in electrical and steam loads as well as seasonal and daily changes of outside air parameters. This establishes the need to ensure that the cogeneration will

perform as desired over the range of conditions, considering a wide range of changes of load and initial conditions.

One method to do this is to build the engine, and then test it under a comprehensive set of conditions. It can be performed with better accuracy; however, this method is proven to be expensive and time consuming task. Another equally effective method to analyse the system is to model the system component mathematically and then tie the component models together with a computer simulation. This reduces or eliminates costly and time consuming testing of the physical hardware. In order to examine the cogeneration performance during off-design operation and identify the component that has potential performance improvement, thermodynamics model and analysis play a big role. Energy analysis is based on the first law of thermodynamics and concerned with the conservation of energy. On the other hand, exergy analysis is based on both the first and second laws, and generally allows process inefficiencies to be better pinpointed than an energy analysis, and efficiencies to be more rationally evaluated. It is also used to identify and quantify both the consumption of exergy used to drive a process (due to irreversibilities) and the exergy losses i.e. the transportation of exergy to the environment. Based on energy model many gas turbine engine models and simulations have been developed and reported among other literatures [12-14]. However, a few have addressed integration of all of the various components of a cogeneration plant in a system model including the variable geometry compressor effect.

1.2 Problem Statement

In order to determine the performance of either the cogeneration plant or its components at the early development stage experimental tests of prototypes of either the whole engine or its main components were the only available method. However, this procedure was not only costly, but also time consuming [14]. Furthermore, cogeneration/gas turbine usually operates at part load conditions for a considerable part of their lifetimes and hence the off-design performance needs to be studied in

detail [15]. For the performance prediction a mathematical modeling using computational techniques are considered to be the most economical solution [14].

Efforts are continually required in order to improve the plant performance and increase both the power generation and fuel efficiency of the cogeneration plant. In this regard to identify where the major losses are occurring in the system and the equipments that have the potential for performance improvement and trends which may aid in the design of future plants, exergy analysis is useful [16, 17]. This again needs mathematical modeling of the cogeneration plant. Other uses of mathematical modeling of the cogeneration plant are:

- To check and confirm projected engine performance data provided by the engine manufacturer while the engine is still in the design and test phase.

- To assess the effect of climate conditions on the plant performance before installation.

- Sensitivity analyses for change of parameters.

- To assess engine performance for healthy monitoring purpose.

The methodology to be used for performance prediction depends on the availability of performance data [18]. Mathematical modeling of gas turbine engine performance requires multivariate maps of their rotating components. However, a major impediment to the development of component map based engine models is the lack of available component data [19]. These maps are in general obtained experimentally; but sometimes they can be predicted with reasonable accuracy using geometric properties of the components [13]. Design, manufacturing and test of compressors and turbines are very expensive and hence, these data are usually proprietary to the engine manufacturer and with scant information normally provided, the estimation of suitable component performance maps remains, at best a difficult task [20].

In the cases where experiments are not possible there are various methods to develop component performance maps, e.g., stage by stage, row by row and scaling methods. In stage by stage method the performance behaviour of the compressor stage is completely described by the stage characteristics [21]. The stages are stacked to form the component model where the discharge conditions of one stage are used

7

as the inlet conditions to the following stage. However the calculation process requires assumptions and several iterations. The following quantities are assumed to be known [19, 21].

- Operating line data. Unique compressor or turbine performance data.
- Gas path dimensions. Stage stacking analysis requires the mean radius and effective annulus area at the inlet of each stage be known.
- Flow angles. The stage stacking also requires the absolute air flow angle at the inlet to each stage must be known.
- Stage characteristics.

The row by row analysis is similar to stage by stage analysis. But in this method the stage characteristics are allocated into two virtual contributions of stator and rotor rows [21]. This will reduce the iterative procedure required to arrive the stage characteristics. However, the knowledge of the entire stage parameter is necessary that could be allocated to the stator and the rotor rows.

A more common alternative way is to scale available performance maps of similar components. This method has been used successfully to generate fixed geometry compressor and turbine component maps for gas turbine simulation purpose [22-24]. This technique involves scaling of available component map to produce another component unknown map, if both components have the same configuration and their design data are known. However, if the gas turbine consists of variable geometry, for each geometry setting, the engine's performance parameters changes [25]; thus, some means of predicting the variable geometry effect on engine performance is required [19]. Hence, the performance maps developed using the scaling method cannot be any more useful except at the design point setting.

In general, the stage by stage and row by row methods require detail geometric dimensions of the components to develop component performance maps. Furthermore, generating performance maps from experimental data are expensive and time consuming, and the scaling method performance maps development works only for fixed geometry components or at design point setting of the variable geometry component. Therefore, to carry out the gas turbine based cogeneration

plant model for performance prediction and exergy analyses this research proposed a new method that modified the existing component matching method considering a variable geometry and air bleeding compressor effect.

1.3 Research Objective

The objectives of this work are:

1. To develop new mathematical and simulation model with statistical evaluation for a variable geometry gas turbine based cogeneration plant.

2. To investigate the energetic, including change of ambient temperature effect, and exergetic performances of the cogeneration plant and its components working under tropical climate conditions.

In order to achieve the objectives of the research the following activities are carried out:

- The design point of the cogeneration is determined.
- The compressor and turbine models are develop based on the first law of thermodynamics, performance maps and correlations obtained from simulation and actual data.
- Mathematical model of other main components such as combustor, air inlet exhaust ducts, and HRSG are developed.
- Exergy based modeling of each component are formulated.
- The components models are linked together to form a whole cogeneration model.
- The cogeneration plant model is validated with actual plant data and statistical evaluation results are shown.
- Effect of different ambient temperatures on the cogeneration performance is examined.
- Exergy analysis of cogeneration plant is carried out.

1.4 Scope of the Research

The research presented in this thesis could be used to examine performance, parametric effect and exergy analyses of a cogeneration plant.

- The cogeneration plant under investigation consists of single shaft gas turbine as the actual tests data gathered from Universiti Teknologi PETRONAS (UTP) Gas District Cooling (GDC) plant single shaft gas turbine.

- The model is developed using modified component map matching method because the other methods require detail geometric dimensions data of the plant components [26, 27].

- Shut down and start up of a utility supplying cogeneration plant encounters very rarely as they are intended for continuous operation. Therefore, the model is developed to predict the performance and the exergy losses of the cogeneration plant under steady state condition.

- The validation is carried out based on the available actual tests data.

1.5 Research Methodology

A new method based on the component map matching is used to developed the cogeneration plant model. In order to overcome the unavailablity of the compressor and turbine maps, they are developed using scaling law. Prior to the scaling their design point data are determined using thermodynamics law and properties ratio relationships, where manufacturer's maps are used as input data. The data of existing compressor and turbine maps that are used in the scaling law were obtained from literature. As the compressor variable stator vanes opening change its perormance maps also change. To accommodate these change, the compressor maps parameters are modified by multiplying by their respective correction coefficients. On top of that the exergy destruction or loss of each cogeneration component was formulated and predicted for different part load conditions. To support the calculations required for design, off-design and exergy analyses a computer program has been developed in MATLAB environment.

The detail of the research methodology steps are:

- Identification of variables. An extensive literature review is done to define the processes and variables involved in the cogeneration cycle. Each process has key variables that directly impact on the performance of the component (like power, ambient temperature, pressure and fuel flow rate)

- Determination of the design point data. Manufacturer's maps information, thermodynamic laws and property relationships were used to determine the compressor and turbine design point data.

- Development of the maps. Based on scaling law the compressor and turbine maps are developed.

- Construction of the mathematical model. Here the energy and exergy models for each component are defined in terms of variables to be analysed.

- Development of flowcharts. The models were converted to a computer program in order to analyse the effect of the variables evaluated on the process. Subroutine of each flowchart is written in MATLAB environment. The set of necessary compatibility laws were used to integrate the component's models.

- Validation of the model. The simulation model results were compared with available actual data. Comparisons are made with the performance of UTP Gas District Cooling (GDC) plant data that is currently in operation.

- Statistical evaluation. Quantifying the error involved in the model prediction compared to the actual data.

- Simulations. Simulations are carried out to evaluate the different scenarios and answers to the fundamental questions about component and cycle performance.

- Exergy analysis. Exergy destruction and second law efficiency of each component and the cogeneration plant are carried out.

1.6 Outline of the Thesis

This thesis is divided into 5 chapters. The second chapter deals with literature review of a gas turbine based cogeneration plant. These include comparison of an ideal and actual gas turbine open cycle, the different types of cogeneration modeling methods,

and exergy analyses. Chapter 3 describes how the compressor and turbine design point data were determined and their component maps were developed. Detail theoretical bases of the various equations used to build the components energy and exergy models are described. It also contains all the subroutine flowcharts that are used in implementing the computer program. Chapter 4 contains results and discussion, validation with statistical evaluation, and effect of ambient temperature on each component and the whole power plant. In the same chapter the exergy destruction rate in each component and the whole cogeneration plant are included. Conclusions and recommendations for future work are presented in Chapter 5.

CHAPTER 2

LITERATURE REVIEW

2.1 Introduction

In this chapter literature review of a gas turbine based cogeneration plant is presented. This includes the different gas turbine based cogeneration modeling methods and exergy analyses.

There are numerous references on gas turbine theory and performance, notably [13, 28, 29] clearly described analysis of different gas turbine engine arrangements. Other gas turbine authors such as [13, 30, 31], indicated different gas turbine thermodynamic cycles analyses, but these studies are necessarily ideal case and they did not consider variable vane geometry component/s.

To perform prediction and study the operation of the gas turbine cycle it is necessary to develop the component models and simulate the gas turbine at the system level. Gas turbine based cogeneration model could be done at different level depending on the data available about the components. The following section indicates the different modeling methods of a gas turbine and its cogeneration.

2.2 Gas Turbine/Cogeneration Modeling Methods

The prominent components in the modeling of a cogeneration plant are compressor, combustor, turbine and HRSG. Furthermore, in the modeling of a gas turbine the compressor and turbine are represented by their maps or mathematical equations and thermodynamic relationships. There are several methods for the determination of the compressor and turbine models, all of varying accuracy and complexity. The following methods are reviewed:

13

- Streamline curvature method.
- Performance map based model.
- Stage stacking method.
- Row by row analysis.

2.2.1 Streamline Curvature Method

Streamline curvature (SLC), is a method based on an iterative procedure used for solving the through-flow problem in axial-flow turbomachines. It also has the intrinsic capability of being able to handle various shaped boundaries with ease [32]. Conceptually, using SLC method, the compressor is divided into a large number of adjacent stations as shown in Figure 2.1, known as quasi-orthogonals, which are usually located at, or between blade rows.
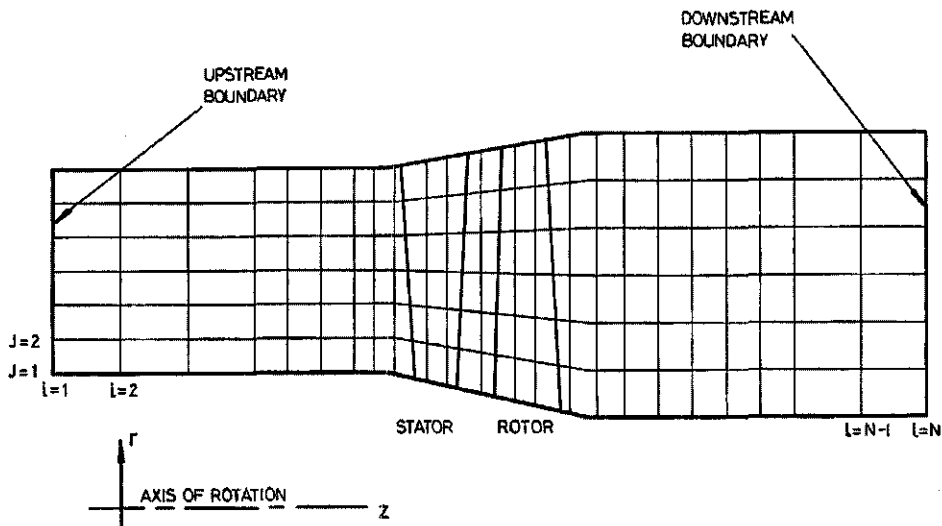
Figure 2.1 Grid arrangement of a typical axial flow component stage [33]

Gradients in both the meridional and spanwise directions are required for the streamline curvature analysis which are usually provided by external loss models and boundary layer development models. The general process for streamline curvature analysis is indicated in the form of flowchart in Figure 2.2 [34].

14

```
┌─────────────────────────────┐
│  At inlet boundary plane, select │
│  streamline locations with equal │
│  annulus area between them       │
│  (initially true at all axial stations │
│  includes annulus wall blockage) │
└─────────────────────────────┘
              │
              ▼
┌─────────────────────────────┐
│  Get φ and r_c from          │◄──────────────┐
│  streamline location         │               │
└─────────────────────────────┘               │
              │                                 │
              ▼                                 │
┌─────────────────────────────┐               │
│  Guess V_m at one location   │◄──────────┐   │
│  from local conditions       │           │   │
└─────────────────────────────┘           │   │
              │                             │   │
              ▼                             │   │
┌─────────────────────────────┐           │   │
│  Calculate V_m(r) from hub to tip using │ │   │
│  governing equation and closure         │ │   │
│  relations (include blockage, loss and  │ │   │
│  deviation)                             │ ┌──────────────────────┐
└─────────────────────────────┘           │ │ Streamline locations │
              │                             │ │ adjusted so that each│
              ▼                             │ │ streamtube contains  │
┌─────────────────────────────┐           │ │ portion of mass flow │
│  Determine overall mass flow rate │     │ │ specified at the inlet│
└─────────────────────────────┘           │ └──────────────────────┘
              │                             │         ▲
              ▼                             │         │
        ◇ Overall ṁ_calc = ṁ_actual ? ◇ ──No──┘      │
              │                                        │
             Yes                                       │
              │                                        │
              ▼                                        │
        ◇ Changes V_m, φ, and r_c within desired ◇ ──No─┘
              tolerance ?
              │
             Yes
              │
              ▼
      ┌──────────────┐
      │ Final result │
      └──────────────┘
```

Figure 2.2 General procedure for streamline curvature analysis method [34]

where $\dot{m}$ mass flow rate,

   φ flow coefficient or streamline slope,

   U tangential velocity,

   V_m meridional absolute velocity,

   r radius in the radial direction,

   r_c radius of curvature.

Using streamline curvature through-flow method Frost [33] developed a computer program for the analysis of the fluid motion in the meridional plane of axial flow turbomachines. The program allows calculations within blade rows. Equations for a steady, inviscid, incompressible flow in an arbitrary shaped turbomachine were

15

derived and a numerical method developed for their solution by McBride [35]. The result of this study was a blade-to-blade flow solution that can be used to construct a three-dimensional representation of the velocity and pressure fields in the turbomachine. Recently, Pachidis et al. [36] developed two-dimensional SLC Compressor Software to provide great flexibility, in the sense that it could be used as a performance prediction tool for compressors of a known design. It could be used as a development tool to assess the changes in performance of a known compressor after implementing small geometry changes.

However, the use of streamline curvature methods requires the complete compressor design data to be provided, including the coordinates within the actual blade passages. Furthermore, such information usually would not be available; as component geometric characteristics are property of the manufacturers. Therefore the streamline curvature model is not applicable to the research at hand.

2.2.2 Performance Map Based Model

The overall performance of a gas turbine engine is governed by the performance characteristics of its constituent components. If suitable component performance representation can be acquired or estimated, engine performance over a wide range of operating conditions can be predicted. The laws of compatibility of mass flow, work and rotational speed determine the matching between these components. This gas turbine matching procedure is adequately described by Cohen et al. [13] and, Walsh and Fletcher [29] has also described the component matching procedure.

Al-Hamdan and Ebaid [37] carried out turbine component matching between the centrifugal compressor and radial turbine for variable speed single shaft gas turbine to produce the equilibrium performance line. However, the matching was done for fixed geometry components and the results were not validated.

For different purpose different steady state models of fixed geometry gas turbines or gas turbine based cogenerations have been developed in the past [38-40]. Using typical component performance maps Zhang and Cai [38] analytically studied the part load characteristics of constant rotating speed single shaft gas turbine and its

16

cogeneration. One calculation example of the analytical solution is shown in Figure 2.3. It represents the typical part load performances of a constant speed single shaft gas turbine.
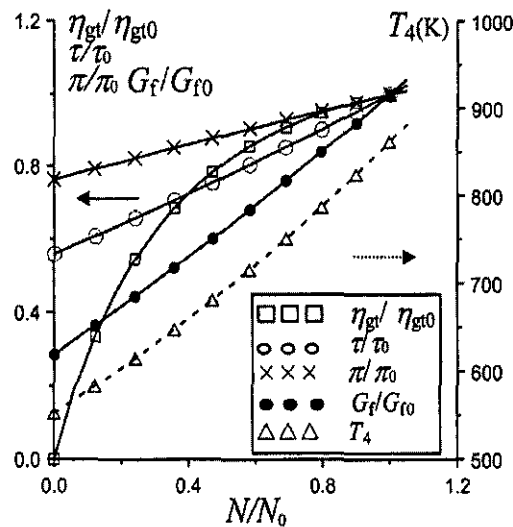
Figure 2.3 Typical part load performance of fixed geometry single shaft gas turbine [38]

In Figure 2.3 the meaning of the parameters are:

G_f fuel mass flow rate,

N power output,

π pressure ratio,

τ temperature ratio,

η_{gt} gas turbine efficiency,

T_4 gas turbine exit temperature and the subscript o stands for the design values.

However, the model results represent only a fixed geometry gas turbine. In the HRSG model, they have assumed constant heat transfer coefficients in the heat exchanger and the exhaust temperature is not maintained as it consists of fixed geometry compressor. Hence, the cogeneration results do not comply with a variable geometry gas turbine based cogeneration.

The general characteristics of single shaft microturbine set at variable speed operation was studied by Wang et al. [39]. The gas turbine composed of fixed geometry radial compressor and radial turbine and this study used typical

17

performance maps. The performance of single and double shaft cogenerations was compared by Najjar [40]. However, only the model and analysis of the heat recovery boiler were presented and the results were not validated.

In many cases the performance maps are not available, since the engine manufacturers consider them proprietary information. One solution is to produce the performance map from testing. Unfortunately this requires a good test facility and individual healthy components. A more common alternative is to scale available performance maps of similar components. Scaling method has already been used for the determination of compressor and turbine characteristics [22-24]. This technique involves scaling an existing map to match the design pressure ratio, mass flow rate and efficiency.

Using scaled maps two computer simulation tools GENeralized ENGine (GENENG/GENENG II) were developed by Fishbach and Koening [23]. The steady state design and off-design matching of turbofan and turbojet engines for performance evaluation at Lewis was accomplished with either GENENG/GENENG II computer code. However these codes do not accommodate variable cycle engine. A study of the effects of the design parameters on the performance of a fixed geometry co-turboshaft engine using scaled component maps was carried out by Okelah [24]. Sellers and Daniele [41] and recently Jones [42] described the scaling method and used for the gas turbine engine analysis.

The component matching method could not be used for this research directly because this method assumes the geometry of the components are fixed and there is no need to maintain the exhaust gas temperature. Furthermore, to use the scaling method for component maps development that would be used in the component matching; the basic assumption is that the two components under consideration should have geometric similarities. However, if one of the component consists of variable geometry, it is not suitable other than at the design point setting [20]. Hence, the component maps developed at the design point setting need modification to accommodate the variable geometry change.

2.2.3 Stage Stacking Method

Axial turbomachines, in general, consist of a series of stages; each stage has a row of moving rotor blades followed by a row of stator blades which is stationary with the casing. To develop the performance maps in this method the performance behaviour of the compressor stage is completely described by the stage characteristics [21]. To formulate the stage characteristics, first, the following dimensionless variables should be introduced:

- The stage flow coefficients.
- The axial velocity ratio.
- The circumferential velocity ratio.
- The degree of reaction defined as the ratio of the amount of work consumed by the rotor to the amount of work consumed by the entire stage. and
- The stage load coefficient.

These dimensionless variables are incorporated into the conservation equations of mass, momentum, and energy leading to a set of equations. These equations in conjunction with the stage loss coefficient are used to calculate the stage characteristics. The stages are stacked to form the component model where the discharge conditions of one stage are used as the inlet conditions to the following stage. However the calculation process requires assumptions and several iterations. The following quantities are assumed to be known [19, 21]:

- Operating line data, i.e., unique compressor or turbine performance data.
- Gas path dimensions, i.e., the mean radius and effective annulus area at the inlet of each stage.
- Flow angles. The stage stacking also requires the absolute air flow angle at the inlet to each stage must be known.
- Stage characteristics, i.e., pressure ratio, air mass flow rate and efficiency.

Using this method, Steinke [26] developed a FORTRAN computer code for predicting the off-design performance of multistage axial-flow compressors. Stage and cumulative compressor performance are calculated from representative meanline velocity diagrams located at rotor inlet and outlet meanline radii. The author mentioned, many of the correlations that are used in the model were normally

19

obtained from experimental data. These empirical correlations permit modeling the trends in stage and overall performance. However, he mentioned that the correlations may only be accurately applied to predict the performance of compressors similar to those compressor used in deriving the empirical correlations.

Muir et al. [19, 20] also studied the steady state performance of a single shaft free turbine engine consists of variable geometry compressor for health monitoring of Canadian Navy engines. For different variable vane positions, the performance of the engine was analysed with respect to compressor shaft speed. However, due to the absence of each stage characteristics, their performances were approximated by generalized stage characteristics.

Kim et al. [43] compared the part load performance of single and two shaft engines and their potential of modulating variable inlet guide vanes to level-up the heat recovery capacity for combined cycle plants. They have drawn the following conclusions from the study. Maintaining the turbine exhaust gas temperature at the set value by modulating the Variable Inlet Guide Vane (VIGV) is possible up to 40% and 50% load in the single and two shaft engines, respectively. The VIGV modulation produces a favorable influence over the combined cycle performance of the single-shaft configuration. However, the two shaft engine does not appear to be effectively improved by the VIGV modulation since the degradation of gas turbine performance counteracts the advantage of the higher performance of the steam turbine cycle. The model method was stage stacking method and row by row analysis for the compressor and the turbine, respectively.

The inputs for this method, i.e., the stage performance data and compressor aerodynamic design detail are usually proprietary to the engine manufactures [20]. To overcome this, estimated stage performance curves are inferred from available overall stage performance data.

2.2.4 Row by Row Analysis

The row by row analysis is similar to stage by stage analysis. But in this method the stage characteristics are allocated into two virtual contributions of stator and rotor

rows [21]. This will reduce the iterative procedure required to arrive the stage characteristics. However, the knowledge of the entire stage characteristics is necessary that could be allocated to the stator and the rotor rows. Schobeiri [21] has illustrated how to use blade total pressure loss parameter (blade profile and shock losses) to calculate the stage off-design efficiency. The total pressure loss parameter is a function of diffusion factor that is a blade property. Furthermore, the total pressure loss factor is obtained from experimentally developed graph at a known diffusion factor. Once the total pressure loss known, the loss coefficient can be calculated and then off-design efficiency is one minus the loss coefficient.

Wei [44] also developed an axial turbine loss models that would be used to develop overall performance map of turbine. In the calculation, the main input data are the stage inlet stagnation pressure and temperature, mass flow, turbine speed and geometric parameters of the stator and the rotor. These data are taken from experiments and the original design of the stage. Then the flow parameters at each section and the overall performance parameters of the stage are predicted row by row. The calculations are based on the principle of conservation of mass, momentum and energy over every blade row.

A one-dimensional row by row method for design and off-design performance analysis of axial compressor and turbine was developed by Attia [27]. For the compressor detail analysis, the modified diffusion factor with compressibility effects was utilized to get the total pressure loss which is used to determine the off-design efficiency. For the turbine off-design efficiency calculation the author used empirical relationships developed experimentally by other authors. Using similar method Ainley and Mathieson [45] calculated the performance of conventional axial flow turbine. In the calculation they used data derived from the analysis of a large number of turbine tests and other associated test work reported in other literatures. The method enables the performance of a turbine to be calculated over a wide range of its operation.

2.2.5 Combined Models and Other Studies

Using an existing simulation program where the compressor and turbine were modeled stage by stage and row-by-row methods, Kim [46] analysed the relationship between the part load performance and design performance of gas turbine and combined cycle plants. Furthermore, the results showed that the gas turbine with higher design performance exhibit superior part load performance.

Kim and Hwang [15] studied the part load performance analysis of recuperated gas turbine (a heat exchanger that heats the compressed air prior to entering the combustion chamber). The study considered engine configuration and various operation strategies to maintain the exhaust gas temperature. As a result, the combustor inlet temperature will be higher and enhance the part load efficiency. To accommodate the compressor and turbine variable geometry effects they have explained the importance of introducing correction coefficients and modification of the map properties according to the variable stator vanes opening angle. They have also mentioned that using VIGV modulation the turbine exhaust gas temperature can be kept until 30% air flow reduction. However, how these correction coefficients are developed is not mentioned and they are not also included. The model did not include cogeneration rather the exhaust gas was used for heating the compressed air entering to the combustor.

Jansen et al. [47] carried out experiment on single shaft gas turbine consists of variable geometry compressor and the results are indicated in Figure 2.4. As can be seen, though the variable stator vanes are regulated, the turbine exhaust temperature is maintained above 50% part load.
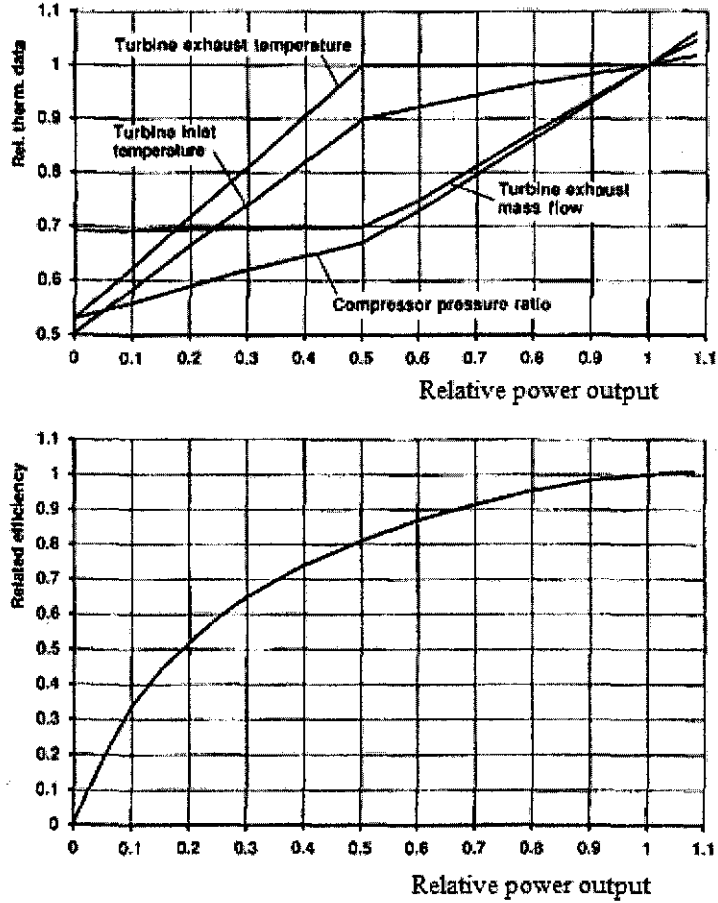
Figure 2.4 Test results of the V64.3 gas turbine thermodynamic properties with variable stator vanes modulation [47]

Generally, the methodology used to predict the turbine performance affect the accuracy of the result. Haglind and Elmegaard [18] used component maps and turbine constant methods to model aero-derivative gas turbine and compare the results. Turbine constant for gas turbine is a constant that governs the relation among flow capacity, pressure ratio and inlet temperature for the turbine given as:

$$C_T = \frac{W\sqrt{T_{in}}}{\sqrt{P^2_{in} - P^2_{out}}} \qquad (2.1)$$

Performance parameters namely compressor pressure ratio, mass flow, thermal efficiency, and exhaust gas temperature were examined and compared with the manufacturer data. The comparison showed that the turbine constant method has much deviation than the component map method. However, in both methods the compressor variable stator vanes effect is not taken into account.

Dorer [48] in 2007 reviewed available studies and projects of cogeneration systems to support the research of International Energy Agency (IEA). The review covered the performance assessment and empirical evaluation of residential cogeneration systems. The criteria that were considered in the assessment and evaluation were environmental, mainly primary energy demand and GHG (Green House gas Emissions) emissions, technical including the control and operation of cogeneration systems, and economic.

2.3 Exergy Based Cogeneration Plant Analysis

Exergy, also known as availability, is a measure of the maximum useful work that can be obtained when a system is brought to a state of equilibrium with the environment in reversible processes [49]. Therefore, a system delivers the maximum possible work as it undergoes a reversible process from the specified initial state to the state of its environment, that is, the dead state. A system is said to be in the dead state when it is in thermodynamic equilibrium with the surroundings. At the dead state, a system is at the temperature and pressure of its environment; it has no kinetic or potential energy relative to the environment; and it does not react with the environment [49]. Such information is useful when designing a thermal system or reducing sources of inefficiency in an existing system.

Across a control volume, the specific exergy on a mass basis, ψ, which expresses as the sum of thermomechanical and chemical contributions, is given as [50, 51]:

$$\psi = \psi^{TM} + \psi^{CH} = (h - h_o) - T_o(s - s_o) + \frac{V^2}{2} + gz_i + \psi^{CH} \qquad (2.2)$$

where h, s, and ψ^{CH} are the specific enthalpy, entropy, and chemical exergy, respectively. Furthermore, h_o and s_o denote the specific enthalpy and entropy, respectively, at the restricted dead state while V and z are the velocity and elevation of the bulk flows entering and exiting the control volume.

The maximum net work obtained when a pure substance or working fluid of a system existing at the environment state is brought into complete thermodynamic

equilibrium with the environment is called the chemical exergy, ψ^{CH} [52]. For hydrocarbons the chemical exergy is roughly approximated by the fuel heating value [50].

The thermomechanical exergy, ψ^{TM}, is the maximum theoretical work obtainable as the system passes from some given state to the restricted dead state. When evaluating the thermomechanical contribution, we can think of bringing the system without change in composition from the specified state to T_o, p_o, the condition where the system is in thermal and mechanical equilibrium with the environment. Depending on the nature of the system, this may be a hypothetical condition. When a difference in exergy or flow exergy between states of the same composition is evaluated, the chemical contribution cancels, leaving just the difference in the thermomechanical contributions. For a such calculation, it is unnecessary to evaluate the chemical exergy explicitly [51].

The use of exergy analysis in power plants or generally in thermal design has been discussed and demonstrated by numerous authors [16, 17, 49, 51, 53, 54]. Huang [55] shows that the performance evaluation of a combined cycle power plant based only on the first law of thermodynamics is not adequate, but the second law of thermodynamics must be taken into consideration to get a better evaluation. Horlock et al. [56] described a general approach to develop terms for exergetic efficiency of modern fossil fuel power plants. The focus was to study the effect of exergy analysis based on the gas turbine inlet temperature, and the level of steam injection into the gas turbine. Verkhivker and Kosoy [57] pointed out the principal processes which cause the destruction of exergy in a power generation cycle. These are the combustion process, the subsequent heating of the working fluid and the heat transfer in the heat exchangers.

An exergy analysis of a Braysson cycle (consists of Brayton and Ericsson cycles) for different cycle temperature and pressure ratios with ideal gas assumption was done by Zheng et al. [58]. Moreover, the results indicate the Braysson cycle specific work output and exergy efficiency were higher than that of Brayton cycle. Exergy based performance characteristics of heavy duty gas turbine in part load operating conditions was investigated by Song et al. [59]. The compressor VIGV was

controlled to maintain the turbine rotor inlet temperature for load between 80 and 100%. As a result the turbine exhaust gas temperature increases in this load range that can be used for heat recovery purpose. On the other hand, for load less than 80% the VIGV opening was fixed and temperature was not controlled. However, in analysis the HRSG was not included.

The performance of waste heat recovery based power generation system using the second law of thermodynamics for various operating conditions such as gas composition, specific heat, pinch point and gas inlet temperature was investigated by Butcher and Reddy [60]. This system consists of heat recovery for steam generation integrated to the steam turbine for power generation and the analysis did not consider the gas turbine which is the basic source of the exhaust gas.

Exergy model of a gas turbine cogeneration system with constant compressor and turbine isentropic efficiencies was developed by Si-Doek Oh et al. [61]. They studied effect of part load and ambient temperature on the gas turbine performance. However, they did not include the heat recovery in the energy analysis. Furthermore, to determine the inlet and exit properties of each component a constant isentropic efficiency is used that is expected to vary with the speed of the shaft and the air inlet temperature to the compressor. Consequently the part load operation results did not represent practical performance outputs. The cogeneration exergy analysis was also done only at full load condition.

Facchini et al. [62] performed exergy analysis off a combined power cycle using extremely high gas turbine inlet temperature. In their study, only a limited range of pressure ratios were used in the analysis. With the focus on latest gas turbines, the effect of the gas turbine inlet temperature on the exergy destruction was not analysed.

Sue and Chuang [63] investigated the effect of compressor inlet air cooling and fuel heating for efficiency improvements of combustion gas turbine based power generation system using exergy and energy concept. However, the analyses considered the whole plant as one unit and did not examine each component independently to identify where the big loss occur.

Huessein et al. [64] carried out exergetic analysis of a 120 MW steam power plant. Each component exergetic performance was evaluated independently. For the analysis, actual operating data at 80 MW were used. The results showed the maximum exergy loss was happened in the boiler while the minimum in condenser and feedwater heater. It also included the possible causes that contribute to the exergy losses. However, the analysis was done only at a single load (80 MW) and hence the exergy losses at another load are not known.

The way how the heat input defined to a power plant affect their thermal and exergetic efficiencies. To illustrate this Kanoglu et al. [65] considered a steam power plant, a diesel engine based cogeneration, and a geothermal power plant and calculated their thermal and exergetic efficiencies with different heat input definitions at a given inlet and outlet state property values of the plants.

Based on the first and second law of thermodynamics Abusoglu and Kanoglu [66] analysed diesel engine cogeneration plant. In the result the relative exergy of each component is included. However, the components energy and exergy analysis were carried out only at the engine full load condition.

Recently hypothetical cogeneration plants were examined based on both the first and second law of thermodynamics by Kanoglu and Dincer [67]. The cogenerations consists of four different power producing engines namely gas turbine, steam turbine, diesel engine and geothermal and 13.5 MW heat recovery producing hot water for building application. For comparison purpose the engines were assumed producing 10 MW power except the diesel engine 20 MW as more heat was used to produce power than heat in case of diesel engine cogeneration. The results showed that the comparison of the energy efficiencies favour diesel, steam and gas turbine cogenerations, respectively. While the exergy analysis favours the diesel and the geothermal cogenerations. However, the analysis was done only at a given engine and heat recovery load and hence this study did not show the scenario what will happen to both the exergy and energy efficiencies if the load changes. Moreover, the individual component thermodynamic analysis was not carried out and hence the significant component for performance improvement cannot be identified.

The literature review has shown that exergy analysis of a gas turbine integrated to a heat recovery with respect to wide range of load has not been examined. Hence, this thesis examines the effect of part load on the second law performance of the cogeneration plant in addition to the exergy analysis considering variable geometry compressor.

2.4 Summary

This chapter covered the efforts that have been made on the gas turbine/cogeneration system modeling and simulation methods and their exergy analysis. Most models, obviously, are based on fixed geometry compressor to evaluate performance or cycle analysis. A few have considered variable geometry compressors and turbines modeling and they have been done based on stage stacking or row by row method. Furthermore, these two approaches require each stage performance characteristics and detail geometric dimensions data and empirical loss correlation models of the compressor and the turbine. However, performance maps and geometric dimension data are property of the manufacturers. For this research the aforementioned approaches are not suitable as detail components data are not available. Therefore, this research proposed a new methodology based on component matching method that requires less input data. Once the model developed it is used to examine the performance, effect of different ambient temperatures and exergy of the cogeneration plant. The major contributions of the research are included in Chapter 5.

CHAPTER 3

METHODOLOGY

3.1 Introduction

The existing GT (gas turbine) based cogeneration plant modeling methods are reviewed in Chapter 2. However, they were found that these modeling methods require intensive information of each component. Therefore, in order to overcome this problem a new method is proposed that need minimum input information to model a GT based cogeneration plant. To address this in this chapter, first, the design point data calculation were carried out using the conservation of energy and mass concept and thermodynamic property ratio relationships. Once the design point calculated, the two most demanding components, i.e., compressor and turbine performance maps are generated using scaling method. Each component energy model is formulated and analysed. Then, the exergy destruction rate and second law efficiency model and analysis for each cogeneration component were carried out. Finally the new proposed model computer implementation is presented.

Off-design performance prediction of a cogeneration plant involves two processes. The first one is mathematical modeling of the cogeneration plant, where each component process is represented by a set of equations and the second process is investigating the model's behaviour by integrating and solving the set of equations using compatibility laws at the given conditions. The main components that determine the overall performance of the cogeneration plant are air intake duct, compressor, combustion chamber, turbine, exhaust duct and HRSG. The cogeneration plant layout with these components is shown in Figure 3.1.
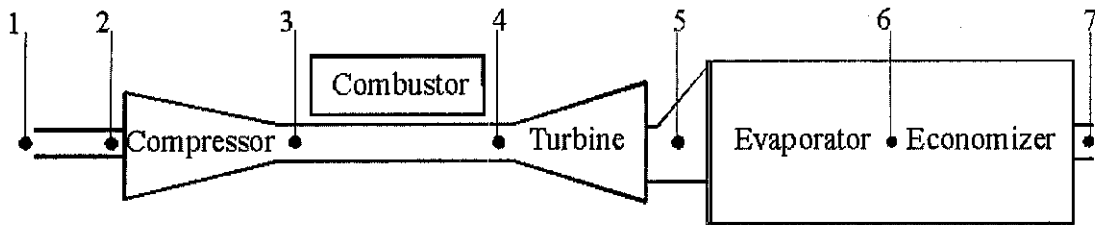
Figure 3.1 GT based cogeneration plant layout

The off-design modeling of the compressor and turbine involves their performance maps. Generally, the design point data and the performance maps of the critical components are either missing or partially available. Therefore, prior to the off-design modeling of the gas turbine the design point data should be calculated and the compressor and turbine performance maps should be developed.

3.2 Design Point Data Calculation and Performance Map Generation

The main components of a gas turbine are compressor, combustion chamber, turbine, and electric generator as shown in Figure 3.2. The compressor is the most complicated component to represent it mathematically. Because of its nature, a compressor is a relatively unstable device in that it moves airflow against an unfavourable pressure gradient.
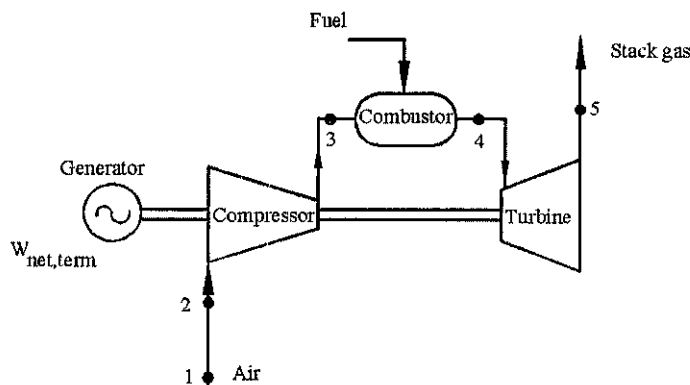
Figure 3.2 Schematic of the main components of a typical single shaft gas turbine

A major impediment to the development of component based gas turbine models is the lack of component performance maps. These maps are usually proprietary of the engine manufacturers. Hence, the estimation of suitable component performance

map remains, at best, a difficult task. When component performance maps are not available to estimate the compressor and turbine performance the scaling technique has been used successfully [22-24]. Usually in using scaling technique, the difficulty to develop the performance map of existing gas turbine is the lack of design point data to the researcher. This is because the manufacturer gives only the bare minimum data required for safe operation of the plant. As the scaling factor is obtained by comparing the known and unknown components design data point parameters, without these data it is very difficult to mathematically model the plant.

3.2.1 Design Data Calculation

Design point is defined as the particular point in the operating range of a gas turbine when the engine is running at the particular speed, pressure ratio, mass flow and temperature of the gas entering into the turbine. These parameters produce the required power that the engine components were designed. The design point is represented as a single point on the component characteristics. The engine operates over a wide range, deviating from its design point conditions. The deviation from design point performance is normally termed as off-design performance.

Among other parameters ambient air density is one of the parameter that affects a gas turbine performance. The ambient air density is a function of ambient temperature, pressure, and humidity. These conditions vary from day to day, and from location to location, it is convenient to define some standard conditions for gas turbines performance comparison purpose. The International Standards Organization (ISO) established standard conditions, which are: $15^{\circ}C$ temperature, 1.013bar pressure, and 60% relative humidity [68, 69]. The design point of compressor and turbine are defined by their pressure ratio, flow rate and efficiency. For calculation purpose, the design point properties such as compressor discharge pressure, combustor fuel consumption, turbine exhaust temperature, exhaust mass flow rate, and the generator terminal power output are taken from non conventional Taurus 60S maps indicated as DP in Figure 3.3 and Figure 3.4 at $15^{\circ}C$ and full load conditions [68]. Taurus 60S is the gas turbine engine type that is working in UTP in the cogeneration plant. These maps do not indicate both the surge and choke limits.

31

Unlike the conventional map where it uses efficiency versus inlet flow rate, and pressure ratio versus inlet flow rate for different corrected speeds these maps indicate only the effect of ambient temperature on the gas turbine performance.
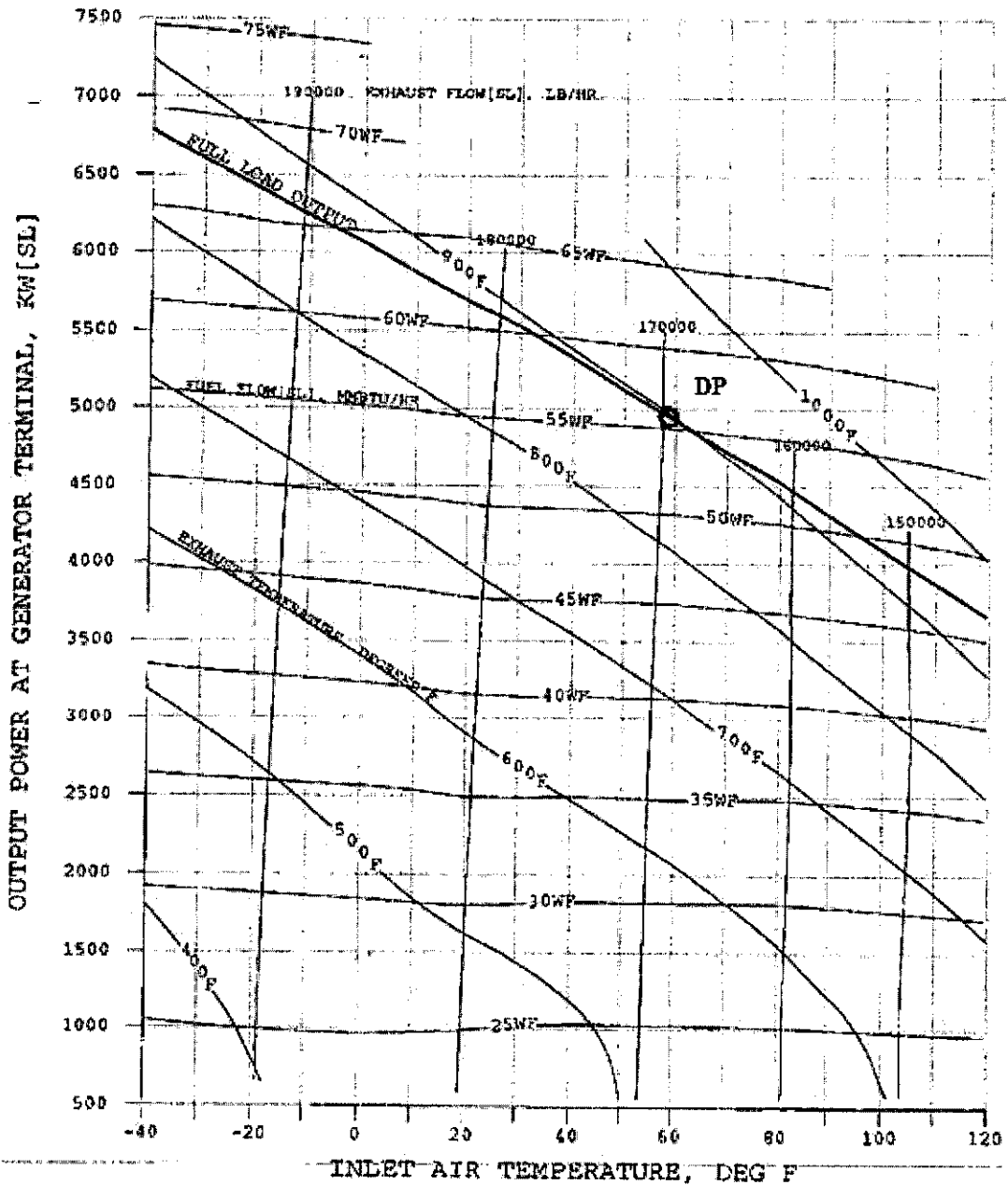
Figure 3.3 Variation of terminal power output, fuel consumption and exhaust gas
temperature with respect to ambient inlet air temperature at 1 atm. [68]
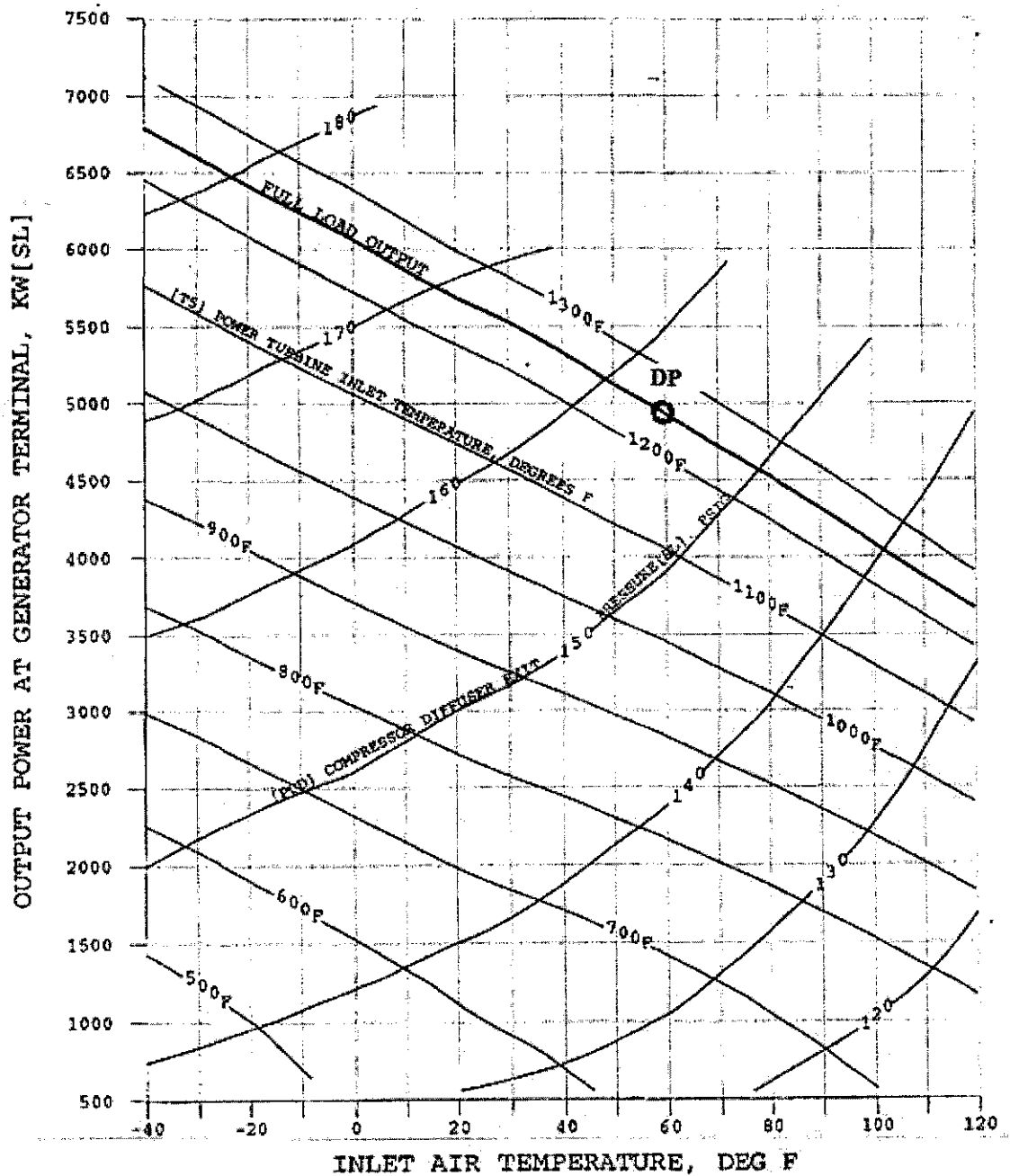
Figure 3.4 Variation of terminal power output, compressor discharge pressure and third stage turbine inlet temperature versus ambient temperature at 1 atm. [68]

3.2.1.1 Component Polytropic and Coupling Efficiencies

The values of compressor and turbine polytropic efficiencies are assumed to be 0.90 and 0.89, respectively with the current state of art design [70]. The mechanical friction causes some minor losses in the gearbox coupling, which reduces the output

of the turbine. This gearbox coupling efficiency is taken to be 98.20% and the generator power conversion efficiency is 96.40% obtained from manufacturer's document [68]. These losses are to be subtracted after the gas turbine net power has been determined to calculate the electrical generator terminal power output.

The compressor and turbine design point data are calculated using energy and mass conservations and thermodynamic property ratio relationships. The derivations of the equations are included in Appendix-A. The input numerical values are the data taken from the manufacturer's map and the assumed efficiencies. First, the compressor exit temperature is calculated using the following equation.

$$T_3 = T_2 \left(\frac{p_3}{p_2} \right)^{\frac{\gamma-1}{\gamma} \frac{1}{\eta_p}}$$
(3.1)

where $T, p, \gamma,$ and η_p are the temperature, pressure, specific heat ratio and polytropic efficiency, respectively. The meaning of the subscripts in the equations is based on their designation indicated in Figure 3.2.

Once the compressor exit temperature is known, the power input to the compressor can be calculated by the following equation.

$$\dot{W}_c = \dot{m} c_{p_a} (T_3 - T_2)$$
(3.2)

The compressor's isentropic efficiency can be calculated as:

$$\eta_c = \frac{\left(\frac{p_3}{p_2} \right)^{\frac{\gamma-1}{\gamma}} - 1}{\left(\frac{p_3}{p_2} \right)^{\frac{\gamma-1}{\gamma} \frac{1}{\eta_{pc}}}}$$
(3.3)

The total power produced by the turbine is given by:

$$\dot{W}_t = \frac{\dot{W}_{net,term}}{\eta_{gb} \eta_{gen}} + \dot{W}_c$$
(3.4)

where $\dot{W}_{net,term}$ is the gas turbine net terminal power output.

Once the total power produced by the turbine is known its inlet temperature is calculated from the following relationship.

$$T_4 = \frac{\dot{W}_t}{\dot{m}_g c_{pg}} + T_5 \tag{3.5}$$

The relationship between the turbine isentropic and polytropic efficiencies is used to calculate the turbine isentropic efficiency as follows:

$$\eta_t = \frac{1 - \left(\dfrac{p_5}{p_4}\right)^{\frac{\gamma-1}{\gamma}\eta_{pt}}}{1 - \left(\dfrac{p_5}{p_4}\right)^{\frac{\gamma-1}{\gamma}}} \tag{3.6}$$

The calculated design point values data using Eqs. (3.1) to (3.6) are summarized in Table 3.1. The mass flow rate discrepancy between the turbine and the compressor is the fuel added in the combustion chamber.

Table 3.1 Compressor and turbine calculated design point data

Component	Efficiency [%]	Flow rate [kg/s]	Pressure ratio
Compressor	86.08	21.01	12.05
Turbine	91.13	21.35	10.20

3.2.2 Development of Component Maps Using Scaling Method

Once the design data are calculated the component maps are developed using scaling method. The technique first calculates the scaling factors from comparison between the calculated design point data and design point of a known map. Then, each point

of the known map data is multiplied by its corresponding scaling factor to produce the unavailable map data.

The equations used to transform the known map data to the unknown map with the scaling factor SF are given by [24]:

$$pr_{sm} = SF_{PR}(pr_M - 1) + 1 = \frac{pr_D - 1}{pr_{MD} - 1}(pr_M - 1) + 1 \tag{3.7}$$

$$\dot{m}_{sm} = SF_{\dot{m}}\dot{m}_M = \frac{\dot{m}_D}{\dot{m}_{MD}}\dot{m}_M \tag{3.8}$$

$$\eta_{sm} = SF_\eta \eta_M = \frac{\eta_D}{\eta_{MD}}\eta_M \tag{3.9}$$

where pr_{sm}, $\dot{m}_{sm}$, and η_{sm} are the pressure ratio, mass flow rate and efficiency of the scaled map, respectively. The subscripts D and MD stands for the calculated and known map design point data while M is arbitrary point on the known map.

The methodology followed to develop the compressor and turbine maps is summarized in Figure 3.5.
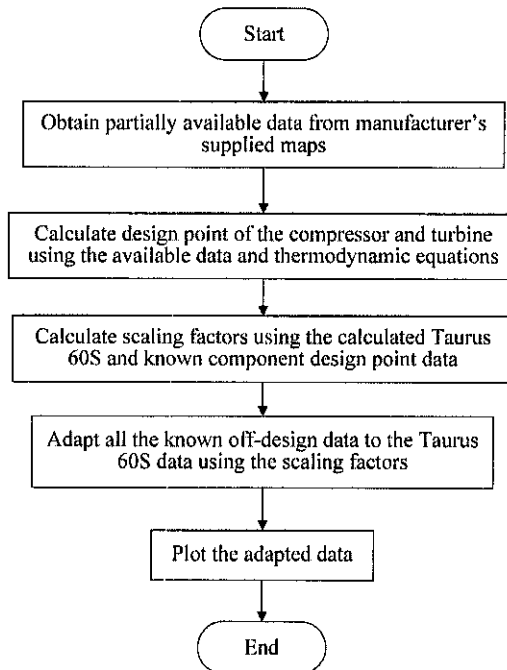
Figure 3.5 The flowchart indicates methodology used to get the component maps

36

The data used for scaling purpose are obtained from National Aeronautics and Space Administration (NASA) Lewis research centre that are released for public use [71, 72]. These compressor and turbine data are included in Appendix B. The calculated scaling factors to be used for map generation are summarized with their design points in Table 3.2.

Table 3.2 Summary of the design point data and scaling factors of the compressor and turbine

Component	Parameter	Design data of Tourus60S	Design data of literature map	Scaling factor
Compressor	PR	12.04	12.00	1.00
	$\dot{m}$	21.01	70.31	0.30
	η	86.16	85.10	1.01
Turbine	PR	10.20	1.76	12.13
	$\dot{m}$	21.35	18.43	1.16
	η	91.56	92.30	0.99

Using the above calculated scaling factors and the known map data of the compressor and turbine new data values for pressure ratio, mass flow and isentropic efficiency are calculated with the help of Eqs. 3.7 to 3.9. The converted data performance map plots are shown in Figure 3.6 to Figure 3.9.
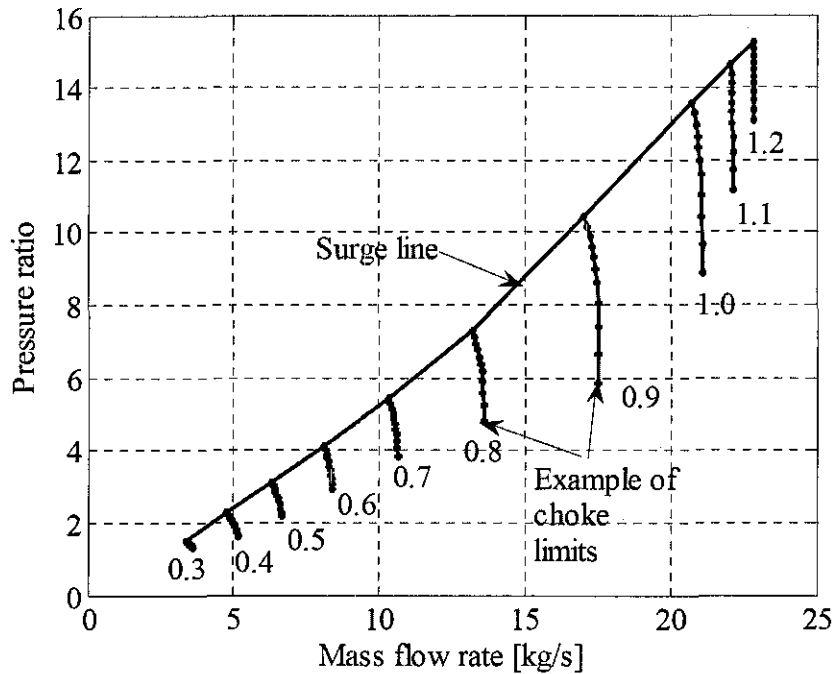
Figure 3.6 Scaled Taurus 60S compressor pressure ratio versus mass flow for different relative corrected speed ratios

The compressor map is a plot outlining the performance of the component over a wide variety of operating conditions. Figure 3.6 outlines the compressor map. The abscissa outlines the possible range of mass flow rates of the compressor, while the ordinate axis indicates the possible compressor pressure ratio for different relative corrected speed ratios. The corrected relative speed ratio is defined as $(N/\sqrt{T_2})/(N/\sqrt{T_2})_d$. For example, the solid line labelled 0.7 represents all the values of pressure ratio (as a function of mass flow) for a rotational speed which is 70% of the design rotational speed.

For a given speed, the point of operation lies between the choke limit (at high mass flows) and the surge line. The choke limit is where a speed line approaches vertical; indicating that a maximum mass flow is reached even though the pressure ratio is reduced.

On the other side of a speed line, as the pressure ratio increases the mass flow decreases, the surge line indicates a critical operating limit. The region of operation above the surge line in Figure 3.6 indicates unstable operating conditions normally leading to an undesirable compressor surge. Surge is a swift breakdown of the stable

38

compressor flow. This leads to a flow reversal so that it briefly goes backwards through the compressor from high to low pressure. Surge arises as the adverse pressure gradient across the compressor rises above that can be aerodynamically supported by the compressor blades and resulting mass flow. Often a compressor will quickly re-establish positive flow only to surge again leading to a cycle that can repeat multiple times in a second. This leads to a dynamic phenomenon consisting of large-amplitude low-frequency oscillations of flow rate and dangerous pressure pulsations [73]. Figure 3.7 shows the corresponding isentropic efficiency of the compressor for different relative corrected speed ratios.
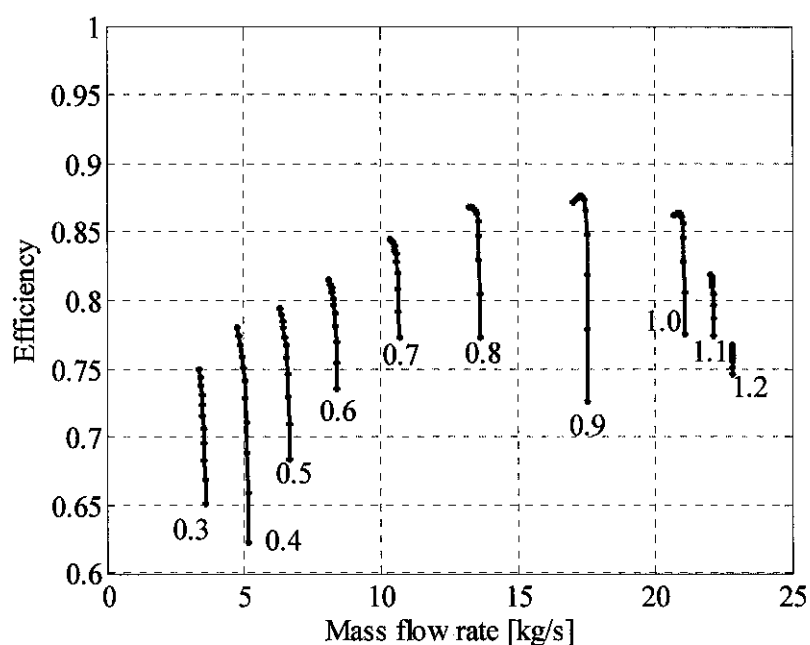
Figure 3.7 Scaled Taurus 60S compressor efficiency versus mass flow for different relative corrected speed ratios

The scaled turbine performance map is shown in Figure 3.8. The mass flow increases with pressure ratio and beyond a certain pressure ratio the Mach number between the aerofoil passages reaches unity and this restricts the amount of mass flow that can pass through the turbine. Under these operating conditions the turbine is said to be choked. Figure 3.8 shows the rotor is choked; and there is some variation of mass flow with turbine relative corrected speed. To account for this effect in the model, the flow is restricted to the maximum value of the turbine flow for a given speed. In actual engine, although the nozzle geometry does not change as a function of speed, the location of the choking point (and hence the nozzle throat

area) does change slightly due to boundary layer differences [32]. Figure 3.9 shows the corresponding turbine efficiency with respect to pressure ratio for different relative corrected speed ratios. The developed compressor and turbine performance maps would be used in the off-design analysis.
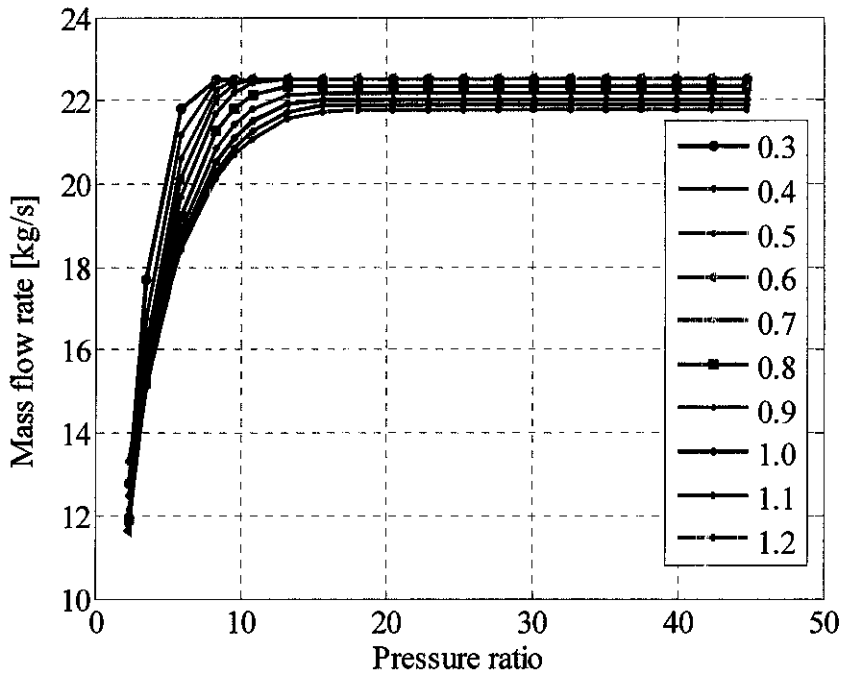
Figure 3.8 Scaled Taurus 60S turbine mass flow versus pressure ratio plot for different relative corrected speed ratios
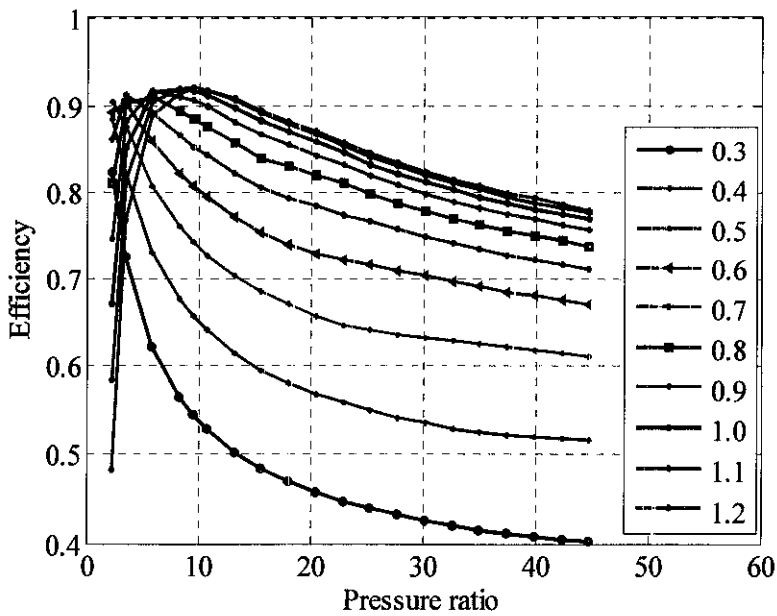
Figure 3.9 Scaled Taurus 60S turbine efficiency versus pressure ratio plot for different relative corrected speed ratios

40

3.3 Off-design Modeling and Analysis of a Cogeneration Plant

3.3.1 Air Intake Model

The air is drawn into the gas turbine and accelerated to the inlet velocity from a stagnation condition far from that of the inlet. Thus, the intake air properties entering into the intake duct is the same as the ambient condition (T_a and p_a).

$$T_1 = T_a \tag{3.10}$$

$$p_1 = p_a \tag{3.11}$$

Since there is no much temperature difference between the air intake duct and the ambient, the process is assumed to be adiabatic. The normal gas turbine installation has 38.1-101.6 mm of water intake pressure losses [74]. Hence the intake duct inlet and exit properties relationships, for temperature T_1 and pressure p_1 with intake duct pressure loss fraction, π_i, are:

$$T_2 = T_1 \tag{3.12}$$

$$p_2 = p_1(1 - \pi_i) \tag{3.13}$$

3.3.2 Compressor Model and Analysis

Compressor is one of the important component in evaluating the gas turbine performance. The purpose of a compressor is to increase the pressure of the air at the required flow rate while consuming a minimum power of the turbine. By its nature, it is a relatively unstable device because it moves airflow against an unfavourable pressure gradient. Steady state compressor component characteristics are presented in the form of pressure ratio versus the mass flow rate entering to the compressor for different relative corrected rotor speeds. Similarly, compressor efficiency versus mass flow rate is plotted for different relative corrected rotor speeds. These characteristic maps are indicated in Figure 3.6 and Figure 3.7. They would be used to

41

provide the governing equations of the model and simulation with the pressure and temperature rise across the compressor.

These maps are fully described mathematically by a number of dimensionless parameters or normalized parameters [37] as given in Eqs. (3.14) - (3.15):

$$\frac{\tau_c}{\delta} = f\left(\eta_c, \frac{N}{\sqrt{\theta}}, \frac{\dot{m}_a\sqrt{\theta}}{\delta}, \frac{p_3}{p_2}\right) \tag{3.14}$$

$$\frac{\tau_c}{d^2 p_2} = \frac{1}{2\pi} \frac{1}{\eta_c} \left(\frac{dN}{\sqrt{c_{pa}T_2}}\right)^{-1} \frac{\dot{m}_a\sqrt{c_{pa}T_2}}{d^2 p_1}\left[\left(\frac{p_3}{p_2}\right)^{\gamma_a-1/\gamma_a} - 1\right] \tag{3.15}$$

The work input to the compression, $\dot{W}_c$ is given by:

$$\dot{W}_c = d^2 p_2 \sqrt{c_{pa}T_2} \frac{\dot{m}_a\sqrt{c_{pa}T_2}}{d^2 p_2} \frac{1}{\eta_c}\left[\left(\frac{p_3}{p_2}\right)^{(\gamma_a-1)/\gamma_a} - 1\right] \tag{3.16}$$

where $\quad \theta = \dfrac{T}{T_{ref}}$ and

$$\delta = \frac{p}{p_{ref}}$$

The compressor exit temperature, T_3 is determined using the compressor property ratio relationships:

$$T_3 = T_2 + \frac{T_2}{\eta_c}\left[\left(\frac{p_3}{p_2}\right)^{(\gamma_a-1)/\gamma_a} - 1\right] \tag{3.17}$$

The specific heat of air is given by Eq. (3.18) and taken from [29].

$$c_{pa} = A0 + A1\ TZ + A2\ TZ^2 + A3\ TZ^3 + A4\ TZ^4 + A5\ TZ^5 + A6\ TZ^6 + A7\ TZ^7 + A8\ TZ^8 \tag{3.18}$$

where $TZ = (T_3+T_2)/1000$.

The specific heat ratio for ideal gas is a function of temperature and is given by:

$$\gamma_a = \frac{c_{pa}}{c_{pa} - R} \tag{3.19}$$

The constants $A0$, $A1$, $A2$, ..., $A8$ are given in Table 3.3.

Table 3.3 Constants required to calculate c_p of air and kerosene [29]

Constants			
A0	0.992313	B0	-0.718874
A1	0.236688	B1	8.747481
A2	-1.852148	B2	-15.863157
A3	6.083152	B3	17.254096
A4	-8.893933	B4	-10.233795
A5	7.097112	B5	3.081778
A6	-3.234725	B6	-0.361112
A7	0.794571	B7	-0.003919
A8	-0.081873	B8	0.055593
A9	0.422178	B9	-0.0016079
A10	0.000491		

The aforementioned compressor maps and thermodynamic relationships are good enough to represent a fixed geometry compressor. However, the compressor considered for this study is variable geometry type. Therefore, the model has to consider the effect of air bleeding and variable stator vanes modulation that is included in Section 3.3.2.2.

3.3.2.1 General Characteristics of Axial Compressor Variable Vane Systems

The application of controllable blades of inlet guide vane and stator vanes of particular compressor's stages makes it possible to simultaneously change inlet angles of flow onto blades of rotor rings of the stages. This is done by changing the setting angles of the blades of the variable stator vanes during part load of the gas turbine to maintain the set value exhaust gas temperature. In order to improve the overall fuel utilisation, the exhaust gas from the turbine is passed through a heat recovery steam generator to produce steam. Figure 3.10 illustrates the change in stator vane openings under part load operating conditions.

43
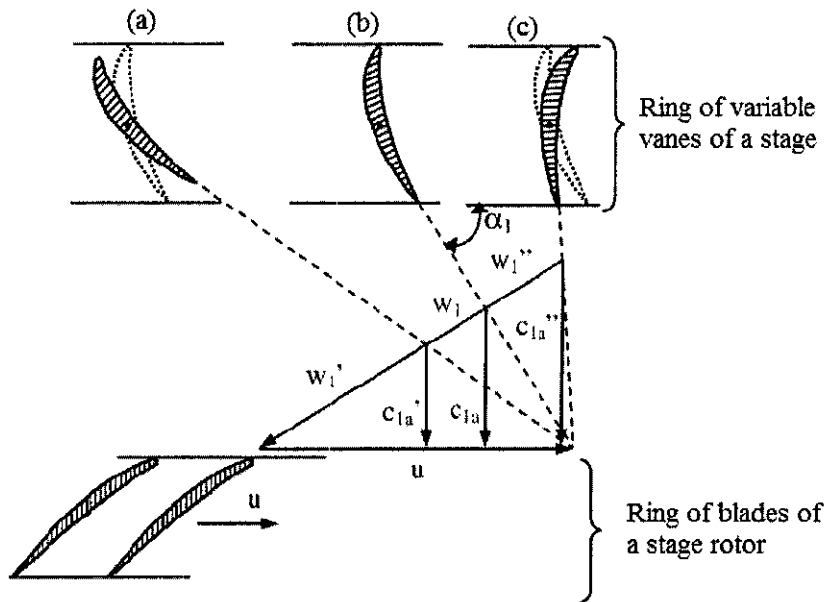
Figure 3.10 Regulating the variable vanes opening of a compressor stage by changing the setting angle of blades of stator vane rings to control the air flow velocity; (a) decreased axial velocity, (b) design axial velocity, (c) increased axial velocity [75].

Regulating the variable vanes opening would help to maintain the exhaust gas temperature and hence the steam generation. This in turn improves the total cogeneration efficiency. The increase and decrease of the air flow is proportional to the axial flow velocity. As can be seen in Figure 3.10, case (a) has low axial velocity consequently results in low air mass flow; case (b) axial velocity is at design point and it has the design point air mass flow; and case (c) has higher axial velocity and results higher air mass flow.

3.3.2.2 Compressor Variable Vanes System

The Variable Vanes (VVs) system position varies depending on the ambient inlet temperature and gas turbine power output values. This change of vanes position varies the effective volume of air which enters the compressor rotor. The axial compressor used in the gas turbine's VVs system consists of a single row of variable Inlet Guide Vanes (IGVs) and three rows of Variable Stator Vanes (VVs). Furthermore, it is observed that the cogeneration plant has two modes of operation,

that is, when the load is less than 50% and when it is greater than 50%. For load that is less than 50%, the cogeneration runs to meet the power demand. For load that is greater than 50%, the bleed valve is fully closed while the VVs are regulated to maintain the exhaust gas temperature at the set value, and the fuel flow regulated to meet the part load.

In the first mode of operation the bleed valve opening is regulated. It is designed to prevent engine surge by reducing backpressure imposed on the engine compressor during start up, shut down and low load operation. Furthermore, in this mode, VVs are fully opened (100%) whereas the compressor downstream air flow is regulated with the help of bleed valve [76]. Figure 3.11 shows compressor bleed air valve location. The following procedure is followed to obtain the percentage of air bleed mass flow rate in the first mode of operation.

1. Since the only parameter controlled in this mode is load, it is selected as a variable.

2. In general if a turbine is rotating at constant shaft speed with no air bleeding, then the air flow rate would be constant. However, the actual plant data shows that the flow is increasing as the load increases. Moreover, the trend follows a kind of parabolic curve. Therefore, a parabolic percentage bleed mass flow rate is assumed, i.e., $\dot{m}_b = a\dot{W}^2_{net,term} + b\dot{W}_{net,term} + c$.

3. With assumed a, b and c, simulation carried out for a set of input data.

4. Simulated compressor pressure ratio, fuel consumption, and power are compared with their corresponding actual plant collected data.

5. The third and fourth steps are repeated with another assumed a, b and c values until the error between the simulated and actual data fall within the given error tolerance.

6. To ensure consistency of the selected correlation, simulation is repeated with other sets of input data.

After a number of trial and error and validation with arbitrary chosen sets of data, the following correlation is selected:

45

$$\dot{m}_b = 1.2 \times 10^{-7} \dot{W}^2_{net,term} - 0.0024 \dot{W}_{net,term} + 13 \tag{3.20}$$

where $\dot{W}_{net,term}$ is the terminal power out put in kW.
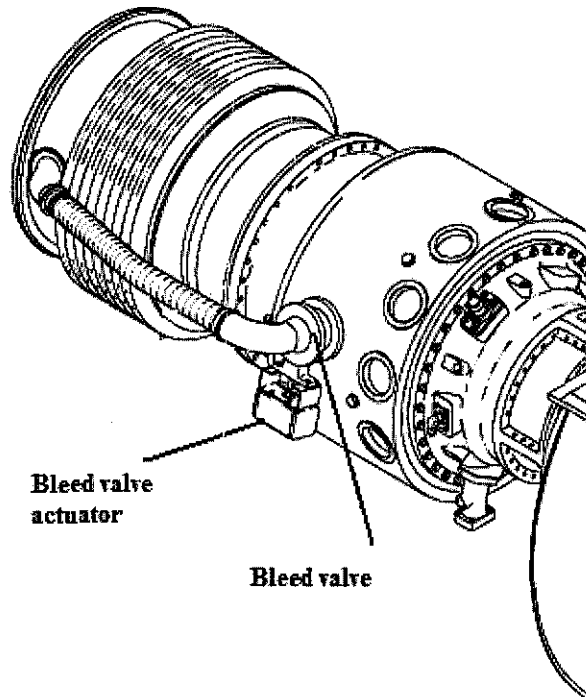
Figure 3.11 Compressor bleed air valve location [77]

When bleed valves downstream of a compressor are opened the compressor map is not affected [29]. However, for each position of the VVs in the second mode of operation, performance maps change. In order to accommodate this change, correction coefficient models are developed. The gas turbine data monitored and stored by Turbotronic device; but it does not monitor the absolute VVs angle rather it monitors the VVs percentage opening. To overcome the unavailability of VVs absolute angle opening, modeling is done based on VVs percentage opening. The procedure followed to find the correction coefficients at a given VVs percentage opening α is:

1. Simulate fixed geometry gas turbine model for a set of data;

2. Calculate the ratio of the fixed geometry simulated compressor pressure ratio data and the corresponding actual pressure ratio data;

3. Plot this ratio with respect to the actual VVs percentage opening;

Note: the variable stator vanes are ganged together and one average VVs percentage opening angle is used to represent the overall movement as they are operated by the same actuator lever;

4. A negative linear tend is observed and a correlation between the pressure ratio correction coefficient and VVs percentage opening is selected using curve fitting method;

5. However, the compressor VVs modulation not only affect the pressure ratio but also affect the mass flow rate and the efficiency to accommodate that similar tends are assumed;

6. With the assumed pressure ratio, flow rate and efficiency correction coefficients the variable geometry gas turbine model simulation is carried out with a set of data while maintaining the set value exhaust gas temperature;

7. Compare the simulated VVs percentage opening, compressor pressure ratio, fuel consumption and power with their corresponding actual measured plant data;

8. Modify the selected correction coefficients by trial and error until the comparison errors fall within the given error tolerance; and

9. Once the errors are within the given tolerance to ensure the selected correction coefficients consistency simulation is repeated for other sets of input data.

After a number of trial and error and validations it is found that the compressor flow correction coefficient coincides with the pressure ratio correction coefficient whereas the efficiency correction coefficient is different. The correction coefficients that are selected are given by:

$$CC_{pr} = 2.90667 \times 10^{-3} \alpha + 0.819787 \qquad (3.21)$$

$$CC_{\dot{m}} = 2.90667 \times 10^{-3} \alpha + 0.819787 \qquad (3.22)$$

$$CC_{\eta} = 1.66667 \times 10^{-4} \alpha + 0.9896667 \qquad (3.23)$$

For each VVs percentage opening, the new compressor performance map is obtained by multiplying the scaled performance map parameters with their respective

correction coefficients. Hence, at any percentage opening α the off-design compressor characteristic is given by:

$$\dot{m}_a = CC_{\dot{m}} \times \dot{m}_{a,sm} \tag{3.24}$$

$$pr = CC_{pr} \times pr_{sm} \tag{3.25}$$

$$\eta = CC_\eta \times \eta_{sm} \tag{3.26}$$

where $\dot{m}_{a,sm}, pr_{sm}, and \ \eta_{sm}$ are mass flow rate, pressure ratio and efficiency of compressor obtained from the scaled compressor performance map, respectively. Using the modified compressor performance map properties the rest of the parameters can be easily determined if any of the two dimensionless parameters are known.

3.3.3 Combustion Chamber Modelling and Analysis

Combustors are typically used in gas turbine cycles to heat the working fluid between the compressor and the turbine. This process increases the enthalpy and temperature of the working fluid. The additional energy is then extracted by the turbine. From conservation of energy viewpoint, the additional heat energy (or chemical energy of the fuel) is converted to mechanical energy by the turbine. A combustor model should simulate the temperature rise of the working fluid when it is combusted with the fuel and it should be integrated into the overall cogeneration gas turbine system.

Technical documentation of the gas turbine describes that during combustion NO_x and CO emissions are by-products of reaction of hydrocarbon fuel with air in the combustion process. At reaction temperatures above $1593°C$ high concentration of nitrogen oxides (NO_x) are produced [76]. CO is an intermediate product of oxidation of hydrocarbon fuel. At combustion temperatures below $1482°C$ CO does not completely oxidize to form carbon dioxide. In order to overcome these by-products formation the combustion chamber is SoLoNOx type. It is a lean premix

48

low emission combustion system designed to provide combustion reaction temperatures low enough to minimize NO_x formation and high enough to minimize CO emission.

The primary zone in the combustor is a near stoichiometric region which provides the incoming fuel and air mixture sufficient time to react and burn. The gas turbine requires approximately one-fourth of the total air it compresses to completely burn the supplied fuel. The excess air is used to cool the combustion chamber and mixes with the combustion products to reduce the gas temperature at the inlet of the first-stage turbine [76].

In modeling the combustor under steady state operation combustor efficiency, pressure drop and heat addition must be accounted for. Typical combustion chamber pressure loss and combustion efficiency are 3% of the compressor inlet pressure and 99%, respectively [18]. If the fraction of combustion pressure loss is in the combustor expressed as π_{cc}, the combustor exit pressure as a function of the combustor inlet pressure will be:

$$p_4 = p_3 (1 - \pi_{cc})$$ (3.27)

Using the combustor inlet conditions the amount of energy generated by the combustion of the fuel is calculated at the given power output. Walsh and Fletcher [29] provide curve fits for specific heat as functions of temperature and fuel-air ratio (FAR) at a pressure of one atmosphere. The characteristic gas constant is also given as a function of FAR. The change of enthalpy is calculated using the lower heating value (LHV) of the fuel. The LHV is used because all the water produced as a product of combustion will remain vaporized, until it is out of the turbine. Using the basic combustion principle, the FAR is:

$$FAR = \frac{\Delta H_{34}}{LHV \, \eta_{cc}} = \frac{c_{pg}(T_4 - T_3)}{LHV \, \eta_{cc}} = \frac{\dot{m}_f}{\dot{m}_a}$$ (3.28)

The gas turbine considered for this study are designed to operate under two types of fuel. The fuels are natural gas and liquid fuels (diesel). These fuels have various heating values and thus this affect the gas turbine output and heat rate. Furthermore

this effect is considered in the combustion chamber model. For calculation within 1% accuracy loss for natural gas, c_{pg} at the mean temperature is evaluated by [29]:

$$c_{pg} = (1.0001 + 0.9248FAR - 2.2078FAR^2)c_{pl} \tag{3.29}$$

where c_{pl} in [kJ/kg K] of combustion products of liquid fuel (diesel) in dry air is given by:

$$c_{pl} = A0 + A1Tz + A2Tz^2 + A3Tz^3 + A4Tz^4 + A5Tz^5 + A6Tz^6 + A7Tz^7 + A8Tz^8 + (FAR/(1+FAR))\begin{pmatrix} B0 + B1Tz + B2Tz^2 + B3Tz^3 + B4 Tz^4 + \\ B5Tz^5 + B6 Tz^6 + B7Tz^7 \end{pmatrix} \tag{3.30}$$

where $T_z = (T_3 + T_4)/1000$, and the values of $A0$-$A8$ and $B0$-$B7$ are give in Table 3.3.

Solving the exact exit temperature with an assumed initial value at the given ambient conditions and power output, results in a non linear equation. The formulated equation is solved numerically for FAR using Newton Raphson's method and the detail solution procedure is shown in Section 3.5.3.3. Once the FAR is determined, the characteristic gas constant can be obtained using the following expression [29]:

$$R = 287.05 + 212.85\ FAR - 197.89\ FAR^2 \tag{3.31}$$

3.3.4 Turbine Modelling and Analysis

The turbine model is needed to simulate overall power developed by the gas turbine. The performance characteristics of a turbine, like that of a compressor, are described mathematically by a number of fully dimensionless parameters or normalized parameters [37]. Equation (3.32) is in complete dimensionless form. Whereas Eq. (3.33) is in the general function form.

$$\frac{\tau_t}{\delta} = f\left(\eta_t, \frac{N}{\sqrt{\theta}}, \frac{\dot{m}_g\sqrt{\theta}}{\delta}, \frac{p_4}{p_5}\right) \tag{3.32}$$

$$\frac{\tau_t}{d^2 p_4} = \frac{1}{2\pi} \eta_t \left(\frac{dN}{\sqrt{c_p T_4}} \right)^{-1} \frac{m_g \sqrt{c_{pg} T_3}}{d^2 p_3} \left[1 - \left(\frac{p_5}{p_4} \right)^{(\gamma_g - 1)/\gamma_g} \right] \qquad (3.33)$$

The power developed by the turbine is calculated using the change in enthalpy in the working fluid. This enthalpy change is replaced by the exit properties of the combustor chamber and the turbine pressure ratio. The turbine power, $\dot{W}_t$ and its exit temperature, T_5 in the expansion process are calculated as follows:

$$\dot{W}_t = \dot{m}_g (\Delta h) = d^2 p_4 \sqrt{c_{pg} T_4} \frac{\dot{m}_g \sqrt{c_{pg} T_4}}{d^2 p_4} \eta_t \left[1 - \left(\frac{p_5}{p_4} \right)^{(\gamma_g - 1)/\gamma_g} \right] \qquad (3.34)$$

$$T_5 = T_4 - T_4 \eta_t \left[1 - \left(\frac{p_5}{p_4} \right)^{(\gamma_g - 1)/\gamma_g} \right] \qquad (3.35)$$

If any two dimensionless parameters are known, the rest of the parameters can be easily determined with the help of performance maps indicated in Figure 3.8 and Figure 3.9 and Eqs. (3.32) to (3.35).

The net electrical power output of the system is given by

$$\dot{W}_{net,term} = (\dot{W}_t - \dot{W}_c) \eta_{gb} \eta_{gen} \qquad (3.36)$$

where η_{gb} and η_{gen} are the gearbox coupling and the generator efficiencies, respectively.

3.3.5 Exhaust Duct Pressure Drop

Flue gas side pressure drop in the HRSG is an important design criterion as any additional pressure drop will cause a decline in the power output of the gas turbine. For the cogeneration considered that utilizes heat recovery steam generator the typical pressure drops are 127-254 mm of water [74] and for this study 3 bar was used. Hence the turbine exit pressure is:

$$p_5 = p_a(1 + \pi_e)$$

(3.37)

where π_e is the fraction of exhaust duct pressure drop.

Furthermore, in order to control the exhaust gas flow the exhaust system has diverter and guillotine dampers. The diverter and guillotine dampers are valves that are installed between the gas turbine and the HRSG. They are used when one or more of the following functions are required:

- Connection of the turbine exhaust to a bypass stack during start-up of the turbine.

- Turbine exhaust gas flow regulation to control the steam production.

- Thermal isolation of the HRSG during turbine operation when steam is not required or the exhaust gas is not required.

Generally, the end users steam demands vary for different reasons and hence the HRSG runs at part load in its considerable life time. Consequently, all the gas turbine exhaust gas is not admitted to the HSRG and only the amount of exhaust gas that is just enough to produce the steam demand is provided. The mass flow rate is proportional to the diverter damper opening. The stack gas temperature leaving to the environment is kept at $135 \pm 5°C$ [78] depending on the feedwater inlet temperature. However, the stack gas can leave the HRSG at the low temperature of 96°C, which is permissible for the natural gas fuel with low sulphur content [79].

3.3.6 Heat Recovery Steam Generator Model and Analysis

The HRSG in this study is a natural circulation water tube type [80]. In natural circulation HRSG risers and downcomers form a flow circuit by connecting the steam drum at the top and a mud drum at the bottom as shown in Figure 3.12. Conventional, vertical tube boilers are generally designed for natural circulation. During operation, the steam/water circuits are arranged so that the two phase mixture in the steam generating tubes (risers) rises to the steam drum by thermal lift of differential density and is replaced by water from the drum by gravity flow [81].

Flow occurs within the circuit at a rate where the difference in static head between the risers and downcomers balance the resistance to flow.

The mud drum is a unit which is located beneath the boiler drum to collect the solid materials which precipitate out of the boiler feedwater due to the high pressure and temperature conditions of the boiler. The mud drum stores these materials for later disposal. There are two types of blowdown used under such circumstances, intermittent manual blowdown and continuous blowdown [82]. Manual blowdown or sludge blowdown is necessary for the operation of boilers regardless of the type of blowdown. In order to illustrate and also as a help in calculations, it is common to describe the HRSG process using the so called temperature energy diagram.
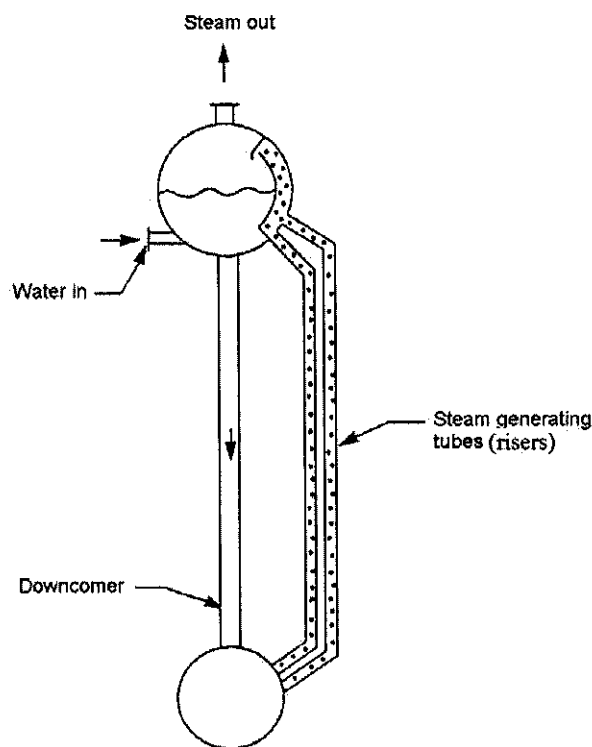
Figure 3.12 Natural circulation water tube HRSG [83]

3.3.6.1 Temperature Energy Diagram

Temperature energy diagram shows profiles for the heat transfer process between exhaust gas and water/steam, using temperature on the ordinate axis and heat transferred on the abscissa as indicated in Figure 3.13. For the water/steam, there are

two different zones. Starting from the lowest temperature, the first zone is heating of the liquid water close to the boiling temperature. The second zone is horizontal, and is water boiling at constant temperature. The two zones are commonly described as "economizer" and "evaporator" (or boiler), respectively. The GT exhaust gases are supplied to the gas-side of the evaporator at temperature T_{g5}. GT exhaust gas leaves the evaporator at T_{g6} and enters at the same temperature to the economizer. The exhaust gases exit the economizer at a temperature T_{g7} and is rejected to the atmosphere.
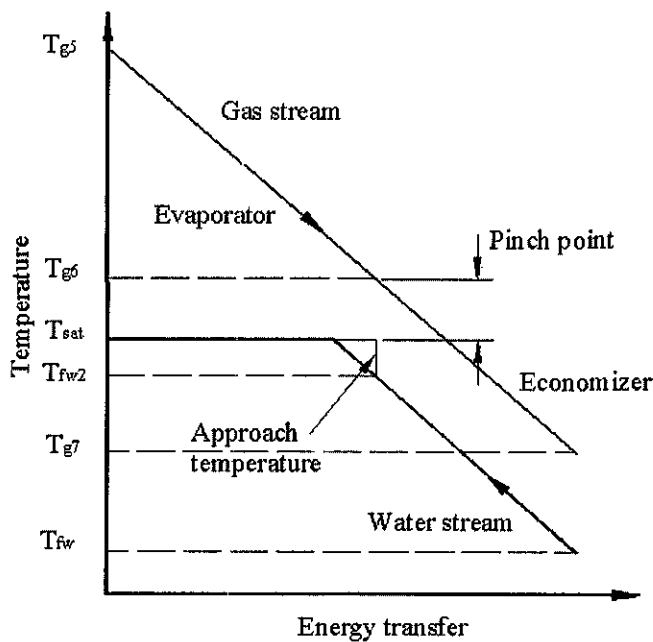
Figure 3.13 Temperature energy diagram, showing the heat transfer process between exhaust gas and water/steam for a single-pressure HRSG [84]

There are two important terms that determine the design of HRSG. These are the pinch and approach point temperatures.

3.3.6.2 Pinch Point and Approach Point

Pinch point analysis is employed for the calculation of thermal energy transfer in the HRSG itself. The pinch point is the temperature difference between the exhaust gas, T_{g6} and saturation temperature of water/steam, T_{sat}. Low pinch point yields a higher

54

rate of steam production but requires greater heat transfer surface areas. Therefore, determination of the pinch point gap would dictate the amount of thermal energy available in the evaporator. The approach point is the temperature difference between the saturation temperature and the water temperature at the economizer outlet, T_{fw2}.

Using literature recommendation and available experimental information the pinch and approach point temperatures are fixed. The temperature of the exhaust gas stream may be cooled in the evaporator above the water saturation temperature about, 8-20°C [31]. This temperature is given by:

$$T_{g6} = T_{sat} + \Delta T_p \tag{3.38}$$

where T_{sat} and T_{g6} are the evaporator steam saturation and exhaust gas stream at the evaporator exit temperatures, respectively. A further constraint to be considered is the temperature of the water leaving the economizer, T_{fw2}. This is 5.5–11°C below the saturation temperature in the boiler this is being the approach temperature [31]. This helps in avoiding the problems like erosion, water hammer etc., in relation to two phase flow [85].

$$T_{fw2} = T_{sat} - \Delta T_{app} \tag{3.39}$$

3.3.6.3 Heat Recovery Steam Production Model and Analysis

Schematic diagram of the HRSG is shown in Figure 3.14. Applying energy balance on the evaporator section between the steam and the exhaust gas streams, for $T_{sat} = T_{fw2}$, gives:

$$\dot{Q}_{ev} = \dot{m}_g c_{pgev} \left(T_{g5} - T_{g6} \right) = \frac{UA(T_{g5} - T_{g6})}{\ln\left[\left(T_{g5} - T_{sat} \right) / \left(T_{g6} - T_{sat} \right) \right]} \tag{3.40}$$

Simplifying the above equation:

$$\ln \frac{T_{g5} - T_{sat}}{T_{g6} - T_{sat}} = \frac{UA}{\dot{m}_g c_{pgev}} \tag{3.41}$$

55

where UA and c_{pgev} are the product of the evaporator overall heat transfer coefficient and the surface area, and the gas specific heat in the evaporator, respectively.
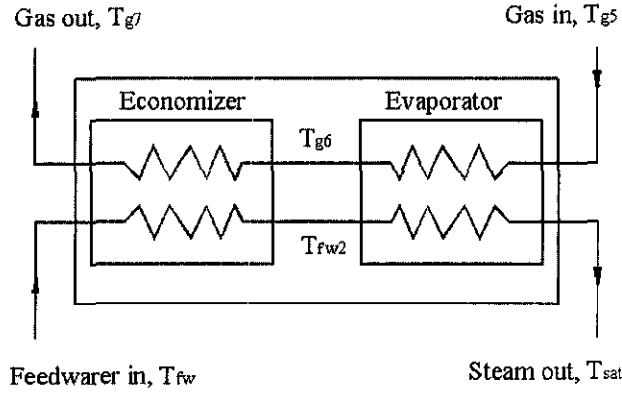
Figure 3.14 Schematic diagram of HRSG and its main parameters

Equation (3.41) indicates that the overall heat transfer coefficient is dependent on the mass flow rate outside the tube, that is, U is proportional to $\dot{m}_g^{0.6}$ provided that fouling is not severe [84]. Substituting this into Eq. (3.42), simplifying and solving for exhaust gas temperature at the exit of the evaporator gives:

$$T_{g6} = T_{sat} + \frac{(T_{g5} - T_{sat})}{e^{K(m_g)^{-0.4}}} \qquad (3.42)$$

where $K = \dfrac{A}{c_{pgev}}$ is determined at the design point.

Once the evaporator exit gas temperature is calculated, the evaporated duty is calculated from the exhaust gas stream as:

$$\dot{Q}_{ev} = \dot{m}_g c_{pgev} \left(T_{g5} - T_{g6} \right) \qquad (3.43)$$

In order to estimate the steam flow, the feedwater temperature leaving the economizer, T_{fw2}, must be known. Assuming T_{fw2} and applying energy balance on the evaporator section between the two streams, mass flow rate of the steam can be calculated by:

$$\dot{m}_s = \frac{\dot{Q}_{ev}}{\left(h_v - h_{fw2} \right) + x_{bd} \left(h_f - h_{fw2} \right)} \qquad (3.44)$$

56

where x_{bd}, h_f and h_v are the fraction of steam blowdown, saturated liquid enthalpy and the saturated vapour enthalpy of the steam, respectively.

However, the actual steam produced is arrived at through series of iteration. The economizer assumed duty for a given blowdown mass flow rate is calculated by:

$$\dot{Q}_{eca} = \dot{m}_s\left(1 + x_{bd}\right)\left(h_{fw2} - h_{fv}\right)$$ (3.45)

To make sure that T_{fw2} is a valid value, the value of *(UA)* for the economizer at design conditions is computed using the following expression:

$$(UA)_{design} = \frac{\dot{Q}_{ec,design}}{LMTD_{ec,design}}$$ (3.46)

The relationship between *(UA)$_{design}$* and *(UA)$_{off-design}$* is given by V. Ganapathy [84] as follows:

$$(UA)_{off-design} = (UA)_{design}\left(\frac{\dot{m}_{g,off-design}}{\dot{m}_{g,design}}\right)^{0.65}$$ (3.47)

From the economizer duty that is obtained with the assumed T_{fw2} and T_{g6} values, the economizer exhaust gas temperature is calculated by:

$$T_{g7} = T_{g6} - \frac{\dot{Q}_{eca}}{\dot{m}_g c_{pgec}}$$ (3.48)

Hence, the new economizer log mean temperature difference (LMTD) at off-design taking in to consideration the heat flows along the heat exchanger length is:

$$LMTD = \frac{\Delta T_1 - \Delta T_2}{\ln\left[\frac{\Delta T_1}{\Delta T_2}\right]} = \frac{\Delta T_2 - \Delta T_1}{\ln\left[\frac{\Delta T_2}{\Delta T_1}\right]} \cdot$$ (3.49)

The LMTD of the economizer according to the given designations of the temperatures in Figure 3.15 is given by:

$$LMTD_{off-design} = \frac{\left(T_{g7} - T_{fw}\right) - \left(T_{g6} - T_{fw2}\right)}{\ln\left[\frac{T_{g7} - T_{fw}}{T_{g6} - T_{fw2}}\right]}$$ (3.50)

57

Once the *UA* and *LMTD* of economizer are known at off-design conditions, the economizer duty can be calculated as follows:

$$\dot{Q}_{ecc} = (UA \times LMTD)_{off-design} \tag{3.51}$$
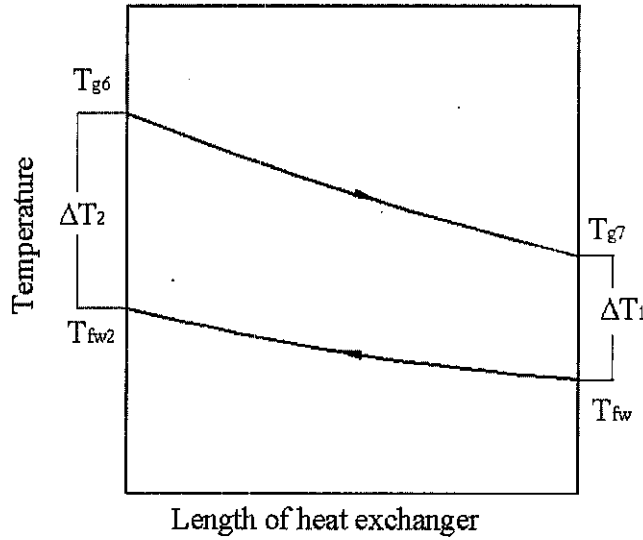
Figure 3.15 Temperature profiles of the economizer adopted form [86]

If the economizer's calculated duty is the same as its duty with the assumed T_{fw2} value, then the assumed economizer exit temperature and the other parameters are valid, otherwise the procedure needs to be repeated with new T_{fw2} value. The following equations are used to calculate the saturated liquid and vapour enthalpies at the saturated temperature [87]:

$$h_f(T) = 2099.3(a_1 + \sum_{i=2}^{8} a_i T_R^{i-1}) \tag{3.52}$$

$$h_v(T) = 2099.3(1 + b_1 T_R^{1/3} + b_2 T_R^{5/6} + b_3 T_R^{7/8} + \sum_{i=4}^{8} b_i T_R^{i-3}) \tag{3.53}$$

where $T_R = \dfrac{647.3 - T}{647.3}$ $\quad\quad$ (3.54)

The values of coefficients a_i and b_i are given in

Table 3.4

58

Table 3.4 Coefficients used to calculate saturated vapour and liquid enthalpies [86]

i	a_i	b_i
1	0.8839230108	0.457874342
2	-2.67172935	5.08441288
3	6.22640035	-1.48513244
4	-13.1789573	-4.81351884
5	-1.91322436	2.69411792
6	68.7937653	-7.39064542
7	-124.819906	10.4961689
8	72.1435404	-5.46840036

The program contains thermodynamic data for air, exhaust gases and water so that it can predict the specific heats of air and exhaust gases at different temperatures. Table 3.5 Evaluation of the specific heats of the exhaust gas may require interpolation.

Table 3.5 Specific heats of turbine exhaust gases at various temperatures [84]

Temperature[°C]	c_{pg} [kJ/kgK]
93.3	1.0588923
204.4	1.0819208
315.6	1.1042454
426.7	1.1321648
537.8	1.1589616

The water vapour saturation temperature of the drum is obtained at its corresponding drum pressure by interpolating saturated steam data that are taken from Steam Table from Reference [88]. The data within the drum pressure operating range is stored in the computer simulation program.

3.3.7 Efficiency, Heat Rate and Specific Fuel Consumption

The thermal efficiency of the gas turbine has been defined as the work done per unit input of heat. Furthermore, the following equations are used to evaluate the gas turbine thermal, HRSG efficiency and cogeneration efficiency, respectively.

$$\eta_{thermal} = \frac{Net\ power\ produced}{\dot{Q}_{in}} = \frac{\dot{W}_{net,term}}{\dot{m}_f\ LHV} \tag{3.55}$$

$$\eta_{HRSG} = \frac{Heat\ recovered}{\dot{Q}_{in}} = \frac{\dot{Q}_{ec} + \dot{Q}_{ev}}{\dot{m}_f\ LHV} \tag{3.56}$$

$$\eta_{total} = \frac{Power + Heat\ recovred}{\dot{Q}_{in}} = \frac{\dot{W}_{net} + \dot{Q}_{ec} + \dot{Q}_{ev}}{\dot{m}_f\ LHV} \tag{3.57}$$

However, operators on occasions require the amount of heat per unit of work done and this is referred to as the heat rate of the engine. The heat rate is simply the reciprocal or the inverse of the thermal efficiency and is usually quoted in kJ of heat per kW hour. Thus the heat rate (HR) is given by:

$$HR = \frac{3600}{\eta_t} \tag{3.58}$$

An alternative means to determine the heat input per unit of work done is to express the heat input in terms of fuel consumption. This is referred to as the specific fuel consumption (SFC). It is usually quoted as kg of fuel per kW hour and is given by:

$$SFC = \frac{3600}{\eta_t LHV} \tag{3.59}$$

60

It is evident from Eqs. 3.58 and 3.59 that the heat rate and specific fuel consumption are related via the *LHV* of the fuel. Thus the heat rate can be expressed as:

$$HR = LHV(SFC) \tag{3.60}$$

3.4 Exergy Model and Analysis

Exergy can be transferred between systems and destroyed by irreversibilities within systems and accounted for by exergy balance. Consider an arbitrary control volume shown in Figure 3.16 experiencing heat, exergy transfers accompanying mass flow, and flow work at the inlets and exits.
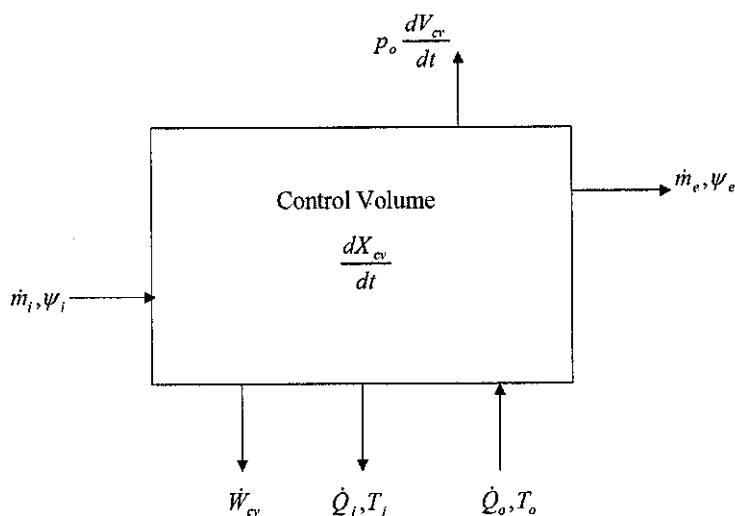
Figure 3.16 Schematic representation of an arbitrary control volume experiencing work, heat and mass flow interactions with the surroundings

Assuming one-dimensional flow at locations where mass enters and exits the unsteady exergy rate balance for a system interacting with the surrounding temperature T_o is given by [50] as:

$$\frac{dX_{cv}}{dt} = \sum_j \left(1 - \frac{T_o}{T_j}\right)\dot{Q}_j - \left(\dot{W}_{cv} - p_o \frac{dV_{cv}}{dt}\right) + \sum_i \dot{m}_i \psi_i - \sum_e \dot{m}_e \psi_e - \dot{I} \tag{3.61}$$

where:

- dX_{cv}/dt is the time rate of change of the exergy of the control volume;

61

- the term $\dot{Q}_j$ is the time rate of heat transfer at the location on the boundary where the instantaneous temperature is T_j;

- $(1 - T_o / T_j)\dot{Q}_j$ is exergy transfer rate by the heat transfer;

- the term $\dot{W}_{cv}$ is the time rate of energy transfer by work other than flow work;

- $((\dot{W}_{cv} - p_o dV_{cv} / dt)\ )$ is the exergy transfer rate by work and dV_{cv} / dt is the time rate of change of volume;

- $\dot{m}_i \psi_i$ and $\dot{m}_e \psi_e$ are the time rate of exergy transfer accompanying mass flow and flow work at inlet i and exit e, respectively; and

- $\dot{I}$ is the time rate of exergy destruction due to irreversibilities within the control volume.

For this particular study steady state condition is assumed hence the steady state exergy rate balance form is particularly important. At steady state, $dX_{cv} / dt = dV_{cv} / dt = 0$, so Eq. 3.61 reduces to the steady state exergy rate balance as:

$$\sum_j \left(1 - \frac{T_o}{T_j}\right)\dot{Q}_j - \dot{W}_{cv} + \sum_i \dot{m}_i \psi_i - \sum_e \dot{m}_e \psi_e - \dot{I} = 0 \tag{3.62}$$

If there is a single inlet and a single outlet, Eq. 3.62 reduces to:

$$\sum_j \left(1 - \frac{T_o}{T_j}\right)\dot{Q}_j - \dot{W}_{cv} + \dot{m}(\psi_i - \psi_e) - \dot{I} = 0 \tag{3.63}$$

The exergy destroyed in the rate form is proportional to the rate of entropy generated, and can be expressed as:

$$\dot{I} = T_o \dot{S}_{genrated} \tag{3.64}$$

For a general steady state single stream flow process the rate of entropy generated is

$$\dot{S}_{generated} = \dot{m}(s_e - s_i) - \frac{\dot{Q}_j}{T_j} \tag{3.65}$$

The corresponding change in the flow exergy based on a unit mass is given by:

$$\psi_e - \psi_i = (h_e - h_i) - T_o(s_e - s_i) + \frac{V_e^2 - V_i^2}{2} + g(z_e - z_i) \tag{3.66}$$

Once the exergy change is formulated, the exergy destruction or exergy loss within a particular component can be determined by applying the exergy rate balance Eq. 3.63. In general, irreversibilities are caused by frictional processes and property gradients within systems. All real processes are irreversible due to effects such as chemical reaction, heat transfer through a finite temperature difference, mixing of matter at different compositions or states, unrestrained expansion and friction [89].

3.4.1 Compressor Exergy Destruction

Applying exergy destruction rate Eq. 3.64 to the compressor where the compression process is shown in Figure 3.17 and assuming the gas perfect gas; the exergy destruction rate is given as:

$$\dot{I}_c = T_o \dot{m}_a (s_3 - s_2) = T_o \dot{m}_a \left(c_{p2\text{-}3} \ln\frac{T_3}{T_2} - R_a \ln\frac{p_3}{p_2} \right) \tag{3.67}$$

where $c_{p2\text{-}3}$ is the specific heat at the average temperature of state 2 and state 3.
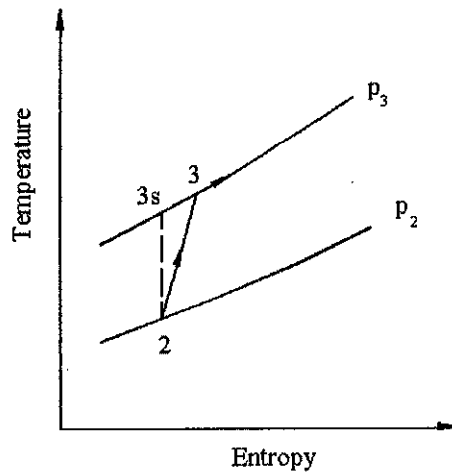
Figure 3.17 Compressor isentropic and actual compression processes on a T-s diagram

63

The compressor second law efficiency is given as:

$$\eta_{II,c} = \frac{w_{rev,in}}{w_{act,in}} = \frac{\psi_3 - \psi_2}{h_3 - h_2} = 1 - \frac{i_c}{h_3 - h_2}$$

(3.68)

The isentropic or adiabatic efficiency, which is a measure of the deviation of actual processes from the corresponding idealized ones, is given by:

$$\eta_{i,c} = \frac{w_{is,in}}{w_{act,in}} = \frac{h_{3s} - h_2}{h_3 - h_2}$$

(3.69)

3.4.2 Combustion Chamber Exergy Destruction

The exergy destruction in the combustion chamber is largely due to the chemical reaction taking place during the combustion process. However, other significant contributors to the exergy destruction include the initial mixing of the air and fuel at different temperatures and the mixing of the excess air and the gas formed at the end of the combustion process. Applying the exergy destruction rate Eq. 3.64 results in the following expression for the rate of exergy destruction in the combustor:

$$\dot{I}_{cc} = T_o \dot{m}_g (s_4 - s_3) = T_o \dot{m}_g \left(c_{p3-4} \ln \frac{T_4}{T_3} - R_g \ln \frac{p_4}{p_3} \right)$$

(3.70)

The second law efficiency of the combustion chamber is the ratio of exergy gain to the fuel chemical exergy value and approximately the same as its lower heating value.

$$\eta_{II,cc} = \frac{\dot{m}_g (\psi_4 - \psi_3)}{\dot{m}_f LHV}$$

(3.71)

3.4.3 Turbine Exergy Destruction

Applying Eq. 3.64 to the turbine where the expansion process is shown in Figure 3.18 and assuming the combustion products perfect gas, the exergy destruction rate in the turbine is:

$$\dot{I}_c = T_o \dot{m}_g (s_5 - s_4) = T_o \dot{m}_a \left(c_{p5-4} \ln\frac{T_5}{T_4} - R_g \ln\frac{p_5}{p_4} \right)$$ (3.72)

Its exergetic efficiency is given as the ratio of actual useful work output to the reversible work output.

$$\eta_{II,t} = \frac{w_{act}}{w_{rev,out}} = \frac{h_4 - h_5}{\psi_4 - \psi_5} = 1 - \frac{i_t}{(h_4 - h_5) - T_o(s_4 - s_5)}$$ (3.73)

The isentropic or adiabatic efficiency, of the turbine which is a measure of the deviation of actual processes from the corresponding idealized ones, is given as the ratio of actual useful work output to the isentropic work out put.

$$\eta_{I,t} = \frac{w_{ac,out}}{w_{is,out}} = \frac{h_4 - h_5}{h_4 - h_{5s}}$$ (3.74)
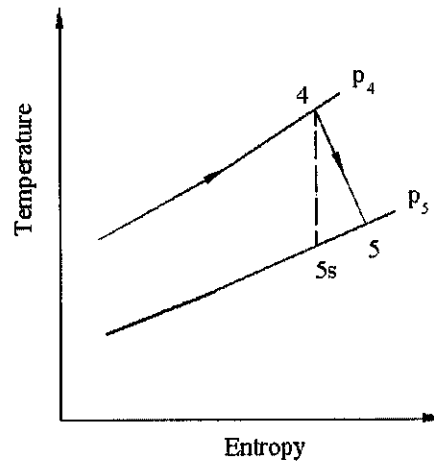
Figure 3.18 Turbine isentropic and actual expansion processes on a T-s diagram

3.4.4 Heat Exchanger Exergy Destruction

The irreversibilities that occur in the HRSG is due to finite temperature differences heat transfer, pressure loss, and thermal interactions with the environment. Furthermore, for an adiabatic heat exchanger with two unmixed fluid streams the exergy supplied is the decrease in the exergy of the hot stream, and the exergy recovered is the increase in the exergy of the cold stream. Applying exergy rate

balance equation to the heat exchanger control volume shown in Figure 3.19, gives exergy destruction rate as:

$$\dot{I}_{HRSG} = T_o\left[\dot{m}_{fw}\left(s_v - s_{fw}\right) + \dot{m}_g\left(s_7 - s_5\right)\right]$$ (3.75)

Gas out, T_{g7}, s_7 Gas in, T_{g5}, s_5

Feedwater in, T_{fw}, s_{fw} Steam out, T_{sat}, s_v
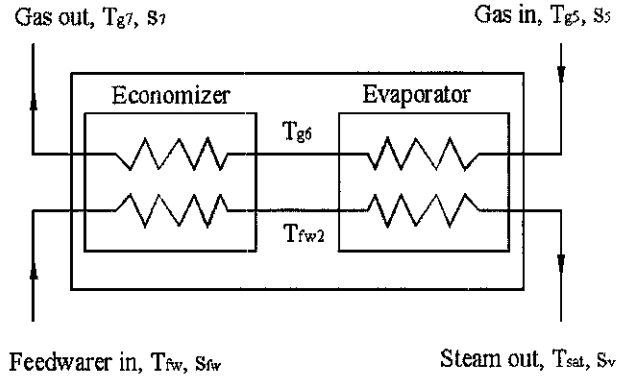
Figure 3.19 Schematic diagram of the HRSG model showing entropy at various points

The purpose of the HRSG is to supply heat to the cold stream. Thus the second law efficiency of the HRSG is calculated as the ratio of the change in exergy of the water/steam to the fuel exergy value.

$$\eta_{II,HRSG} = \frac{\dot{m}_s\left(\psi_{sat} - \psi_{fw}\right)}{\dot{m}_f LHV} = 1 - \frac{\dot{I}_{HRSG}}{\dot{m}_f LHV}$$ (3.76)

On the other hand the first law HRSG efficiency is given as the ratio of the heat recovered rate to the heating value of the fuel.

$$\eta_{I,HRSG} = \frac{\dot{Q}_{rec}}{\dot{m}_f LHV}$$ (3.77)

3.4.5 Stack Gas Exergy Loss

The rate of exergy loss with the stack gas to the surroundings is given by:

$$Stack_{exergy,loss} = \dot{m}_g T_o\left(\left(h_7 - h_o\right) - T_o\left(s_7 - s_o\right)\right)$$ (3.78)

Assuming the gas perfect gas and applying the perfect gas behaviour for the change in enthalpy and specific entropy from the exhaust state to the surroundings the rate of exergy loss with the exhaust gas is written as:

$$Stack_{exergy,loss} = \dot{m}_g T_o [c_{p,sg}(T_5 - T_o) - (c_{p,sg} \ln\frac{T_5}{T_o} - R_{sg} \ln\frac{p_5}{p_o})], \text{ for load} \leq 50\% \qquad (3.79)$$

$$Stack_{exergy,loss} = \dot{m}_g T_o [c_{p,sg}(T_7 - T_o) - (c_{p,sg} \ln\frac{T_7}{T_o} - R_{sg} \ln\frac{p_7}{p_o})], \text{ for load} > 50\% \qquad (3.80)$$

For comparison purpose each component exergy destruction rate is compared to the total exergy destruction rate of the gas turbine or cogeneration. This is given as:

$$\bar{I}_{dest,comp} = \frac{\dot{I}_{comp}}{\dot{I}_{total}} \qquad (3.81)$$

3.4.6 The Cogeneration Second Law Efficiency

Exergy efficiency is evaluated as ratio of outputs to input exergies. For the cogeneration plant, the exergetic efficiency is evaluated as:

$$\eta_{II,cogen} = \frac{\dot{W}_{net,term} + Exergy \ gained \ by \ the \ cold \ stream}{\dot{m}_f LHV} = \frac{\dot{W}_{net,term} + \dot{m}_s(\psi_{sat} - \psi_{fw})}{\dot{m}_f LHV} \qquad (3.82)$$

3.5 Numerical Solution Method

The purpose of modeling is to formulate the essential features of a real problem in mathematical form and to obtain practical results from out of it. The reduction of reality to model, which can be treated mathematically followed by a comparison of the predictions with actual plant data, is the essence of mathematical modeling. However, solving all the mathematical equations that are formulated to represent the cogeneration process manually is very difficult. Furthermore, a few equations are non-linear and need numerical solution method. To overcome these, a computer program is developed in MATLAB environment that can be used to simulate the cogeneration plant process at given conditions. Thus, this section focus on how these

67

mathematical equations that make up the individual models are incorporated in the computer simulation including the subroutines. The program performs design analysis, map scaling based on the design data, off-design calculations, and parametric and exergy analyses.

A computer program for simulating a cogeneration plant should basically satisfy matching conditions between the various components to produce a valid point. This simulation program is a component based modeling subroutine suitable for steady state modeling of a single shaft gas turbine for cogeneration application. The externally applied conditions are load and the surrounding ambient temperature and pressure. With these inputs the simulation model would enable the operating point of each cogeneration component inlet and outlet properties to be found with one pass through the cogeneration calculation. However, a valid point is obtained after a number of iterations. Once gas turbine valid point is obtained, HRSG and cogeneration performance could be predicted. The matching conditions at steady state conditions for constant shaft speed are the laws of conservation of mass and energy. To satisfy this all the components in series must have the same mass flow, and the mass flow into a given gas turbine section must be equal to the flow out. The flow of energy in and out of the gas turbine, or a particular section, must also be equal.

$$\dot{W}_{net,term} = (\dot{W}_t - \dot{W}_c)\eta_{gb}\eta_{gen} \tag{3.83}$$

$$\dot{m}_t = \dot{m}_g + \dot{m}_f - \dot{m}_b \tag{3.84}$$

3.5.1 Program Hierarchy and Modular Structure of the Main Program

The program is written in modular form, with each module carrying out some specific operation. The program starts by reading data either from stored input file or it could collect data interactively.

First it calculates the design point performance values and scale the maps and then the off-design and exergy analyses are carried out. The operational flow and

module hierarchy of the programs are shown in Figure 3.20 and Figure 3.21, respectively.
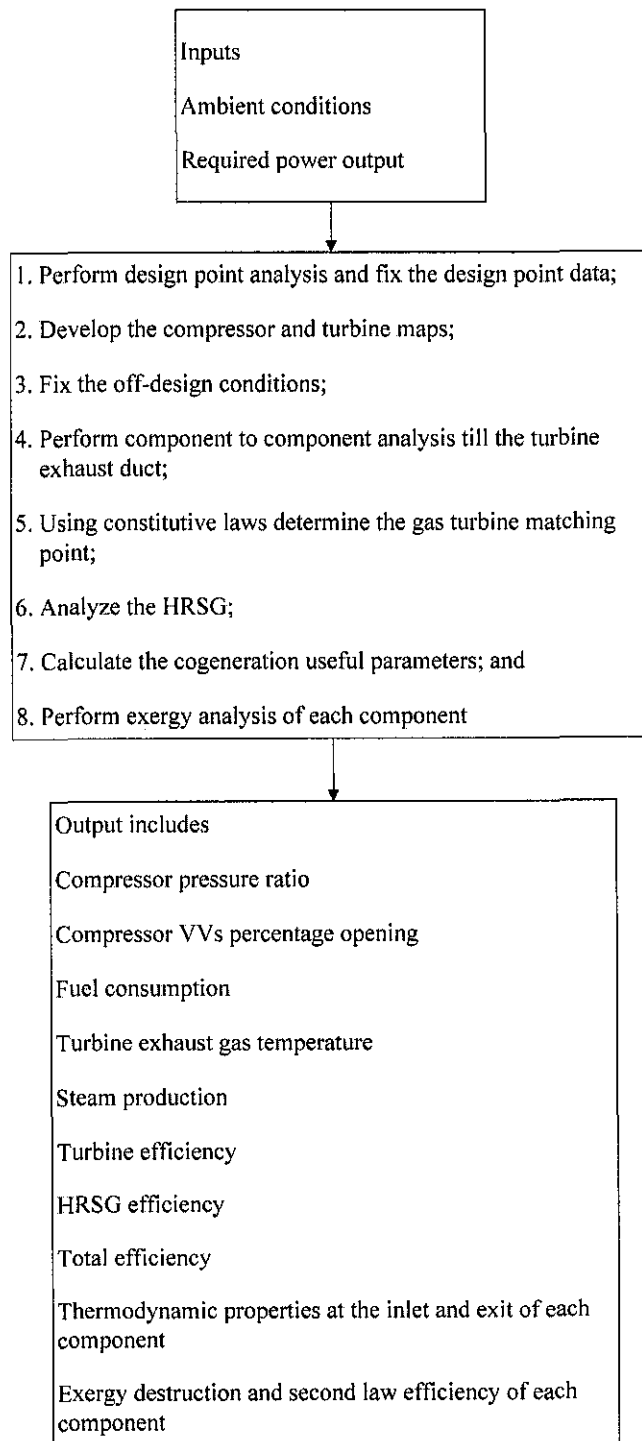
Figure 3.20 Operational computer simulation order for single shaft based cogeneration plant
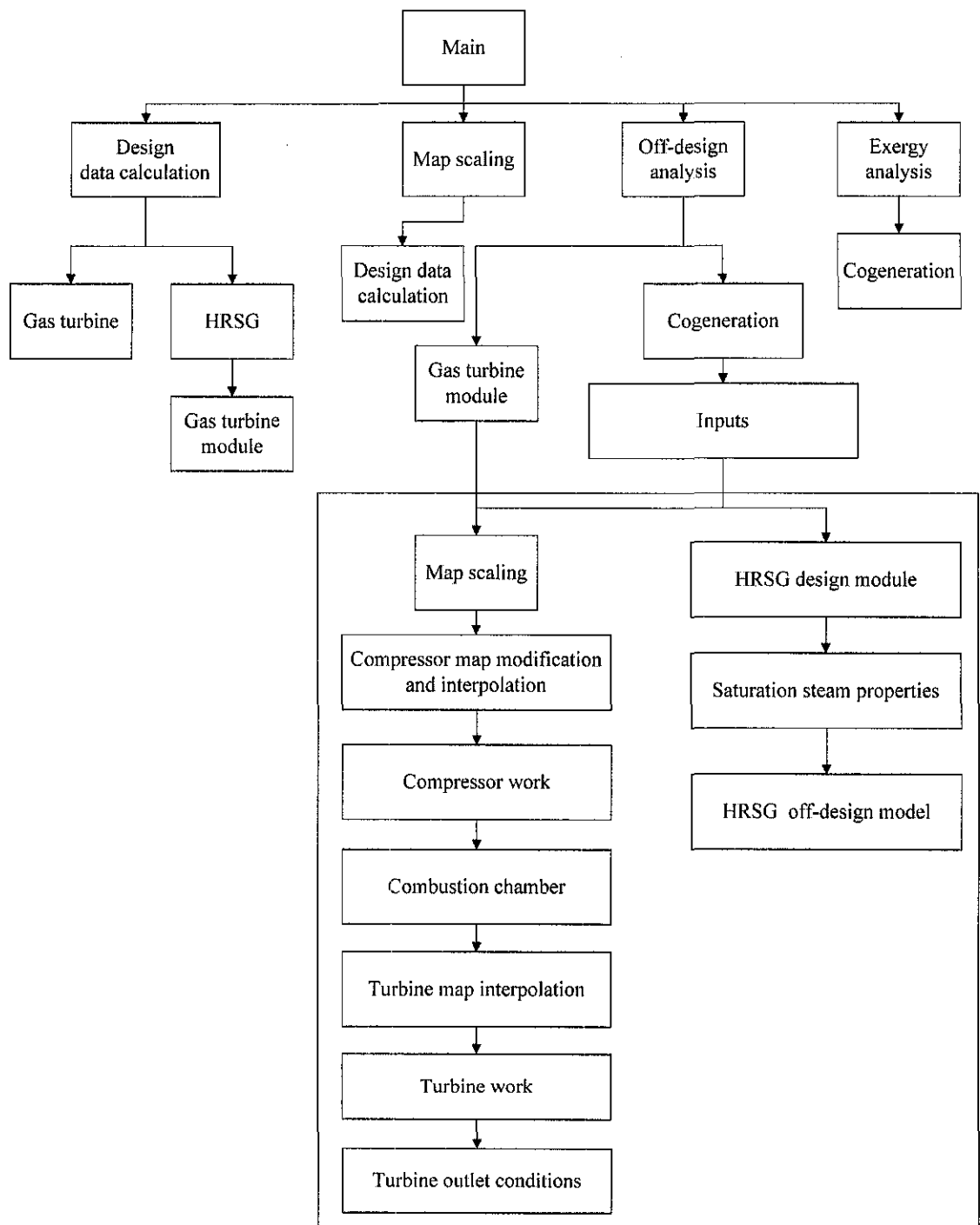
Figure 3.21 Module hierarchy of the numerical solution method for single shaft
gas turbine based cogeneration plant

The main program is divided into four sections:

1)   Design point data and performance calculations.

2)   Scaling the performance maps.

3)   Off-design performance analysis.

4)   Exergy analysis

The detail techniques of how the design point data determined and maps scaled are explained in Section 3.2. The off-design performance calculation comprises the largest portion of the main program. Furthermore, the exergy analysis is based on the first law results; therefore the exergy analysis is included in the off-design analysis. The subroutines design and scaling method are called to perform the design point calculations and scale maps, respectively. The modules that are used in the programming are described below.

3.5.2 Design Module

This subroutine is part of the main program that performs the design point calculations. First, it calculates the gas turbine design point parameters and then analyse each component performance until the calculation reaches the HRSG stack. The pinch and approach point temperatures are selected within the literature recommended values so that the predicted HRSG steam production rate would be the same as the known design value. The flowchart shown in Figure 3.22 is used to examine the design point performance of the cogeneration.

```
                    ┌─────────────┐
                    │    Start    │
                    └──────┬──────┘
                           │
        ┌──────────────────▼──────────────────┐
        │ Inputs                              │
        │ Inlet conditions                    │
        │ Compressor exit temperature         │
        │ Fuel air ratio                      │
        │ Generator terminal power output     │
        │ Component polytropic efficiencies   │
        │ Other efficiencies                  │
        │ Turbine exhaust gas temperature     │
        └──────────────────┬──────────────────┘
                           │
     ┌─────────────────────▼──────────────────────┐
     │ Perform gas turbine design point analysis based on │
     │ property ratio relationships, conservation laws and │
     │ matching concepts                          │
     └─────────────────────┬──────────────────────┘
                           │
  ┌────────────────────────▼────────────────────────────┐
  │ Gas turbine outputs                                  │
  │ Compressor pressure ratio, isentropic efficiency and air mass flow rate │
  │ turbine pressure ratio, isentropic efficiency, air mass flow rate and │
  │ inter-component temperatures and pressures           │
  └────────────────────────┬────────────────────────────┘
                           │
     ┌─────────────────────▼──────────────────────┐
     │ Get the values of the following parameters at │
     │ design point: $\dot{m}_g, T_{g5}, P_{drum}, T_{fw}, \dot{m}_{fw}, x_{bd}, \dot{m}_s$ │
     └─────────────────────┬──────────────────────┘
                           │
     ┌─────────────────────▼──────────────────────┐
     │ Assume the following parameters within the │◄──────┐
     │ literature recommended values: $\Delta T_{pinch}, \Delta T_{app}$ │      │
     └─────────────────────┬──────────────────────┘      │
                           │                              │
        ┌──────────────────▼──────────────────┐          │
        │ Get the saturated temperature at the │          │
        │ drum pressure and calculate $T_{g6}$ and $T_{fw2}$ │          │
        └──────────────────┬──────────────────┘          │
                           │                              │
        ┌──────────────────▼──────────────────┐          │
        │ Calculate evaporator and economizer duty from │   │
        │ the gas and feedwater streams respectively │   │
        └──────────────────┬──────────────────┘          │
                           │                              │
        ┌──────────────────▼──────────────────┐          │
        │ Apply energy balance on the evaporator between │  │
        │ the streams and calculate $\dot{m}_s$ │          │
        └──────────────────┬──────────────────┘          │
                           │                              │
                     ◇─────▼──────◇                 No    │
                    Does $\dot{m}_s$ close to the steam production ──┘
                    rate at the design value?
                     ◇─────┬──────◇
                        Yes │
        ┌──────────────────▼──────────────────┐
        │ Calculate $T_{g7}$, $K = A/c_p$ and UA │
        └──────────────────┬──────────────────┘
                           │
                    ┌──────▼──────┐
                    │     End     │
                    └─────────────┘
```

Figure 3.22 Cogeneration design point analysis subroutine flowchart

3.5.3 Off-design Module and Matching Procedure

The subroutine flowchart used in the off-design analysis of the cogeneration plant is shown in Figure 3.23. Its main purpose is to find the matching point of all the components specially the compressor and turbine for different off-design conditions. In actual situations, the net power and turbine exhaust gas temperature of an engine are controlled by regulating fuel flow rate and VVs angle, respectively. Similarly in the simulation, the VVs percentage opening and fuel injected into the combustion chamber are regulated to maintain the set value of exhaust gas temperature and load, respectively. Since both the inlet and outlet of the cogeneration are at atmospheric pressure the overall change in pressure must be zero. At the beginning of the simulation the compressor flow rate, *FAR* and VVs percentage opening are not known. Hence they are assumed initially in order to run the system model. A valid matching point is obtained after a number of iterations. The flow rate, FAR and VVs percentage opening at this point are actual values. Once gas turbine valid point is obtained, its cogeneration performance could be predicted.

The gas turbine components matching procedure can be described as follows:

1. Select any point on the compressor characteristic by specifying VVs percentage opening and two parameters. The two parameters could be mass flow and corrected speed, pressure ratio and corrected speed or compressor efficiency and corrected speed.

2. Having specified a point on the compressor performance map, the program searches in the look-up tables for values of the other parameters. If the specified parameters are not the table values the program will follow an interpolation routine to provide the values of the other parameters.

3. Then by satisfying flow and speed compatibility the corresponding turbine inlet conditions will be calculated. Having found this input the program will search for the values of other parameters by following the same procedure as that of the compressor.

4. The program would compare if the calculated net power output, turbine exhaust gas temperature and pressure are the same as their corresponding set values. If they do not match then assume another FAR, VVs percentage

73

opening and two compressor parameters and the procedure repeated again until a valid matching point is obtained. The detail procedure is shown in Figure 3.23.

Start

Assume variable vanes percentage opening

Fixed geometry compressor maps → Modify compressor maps

If T exhaust simulated $< T$ set then
$VVs = VVs_{old} - \Delta VVs$, else
$VVs = VVs_{old} + \Delta VVs$

Assume compressor air flow $\dot{m}_a$

Assume the fuel flow injected to the combustor

$\dot{m}_a = \dot{m}_{a,old} \pm \Delta \dot{m}$

Solve the set of equations that represent the gas turbine component process

If Power simulated $<$ Power set then $\dot{m}_f = \dot{m}_{f,old} + \Delta \dot{m}$, else
$\dot{m}_f = \dot{m}_{f,old} - \Delta \dot{m}$

Is the power produced =part load demand ? — No

Yes

Is the simulated turbine pressure the same as the set value? — No

Yes

Is the air flow within the surge and choke margin and/or the exhaust temperature equal to the set value? — No

Yes

Assume T_{fw2} call saturated vapor and liquid enthalpy subroutiens and get h_g, h_f, h_{fw2}, h_{fw}

Apply energy balance on the evaporator and find the steam generated

Calculate economizer duty from the feedwater stream $(\dot{Q}_{ec,a})$

Apply energy balance on the economizer between the two streams and find T_{g7}

$T_{fw2} = T_{fw2,old} + \Delta T, if \, \dot{Q}_{ec,c} > \dot{Q}_{ec,a}$
$T_{fw2} = T_{fw2,old} - \Delta T, if \, \dot{Q}_{ec,c} < \dot{Q}_{ec,a}$

Calculate the economizer off design duty using the LMTD $(\dot{Q}_{ec,c})$

$\dfrac{\dot{Q}_{ec,a} - \dot{Q}_{ec,c}}{\dot{Q}_{ec,c}} < \varepsilon_{ter}$ — No

Yes

Calculate all useful parameters

End

Figure 3.23 Cogeneration plant off-design simulation model flowchart

The program contains thermodynamic data for air, steam/water and combustion products so that it can predict the specific heats of air and combustion products, enthalpy, and entropy of steam/water at different temperatures. The detail of the sub modules that were used in the off-design modular program is included in the following sections.

3.5.3.1 Compressor Performance Map Interpolation Module

Although performance maps are drawn in two-dimensions, they actually represent a three-dimensional relationship. They relate corrected shaft speed and mass flow, to pressure ratio or efficiency. Given the data for a particular speed a linear interpolation, using the two closest points to the required value on that speed curve, is used to determine the unknown value. Equation 3.85 is used to achieve this.

$$f(x_o) = [f(x_2) - f(x_1)] \frac{(x_o - x_1)}{(x_2 - x_1)} + f(x_1)$$

(3.85)

where: $\{(x_1, f(x_1)), (x_2, f(x_2))\}$ are a set of known points and xo is given value that lies between x2 and x1 at the required corrected speed and f(xo) is the unknown. Furthermore, if that particular corrected speed does not coincide with the existing discrete corrected speed data, then its corresponding performance parameters are first obtained by linear interpolation of the two closest speed values. The two closest corrected speed curves must sandwich the particular speed.

Once the corrected speed is specified, the purpose of this subroutine is to obtain the compressor working point assuming the mass flow at a given corrected speed. If the assumed mass flow does not coincide with the discrete data then the corresponding efficiency and pressure ratio values are obtained by linear interpolation. This is done iteratively until the compressor load match with the turbine. Figure 3.24 shows the flowchart for interpolating of any point on the map.
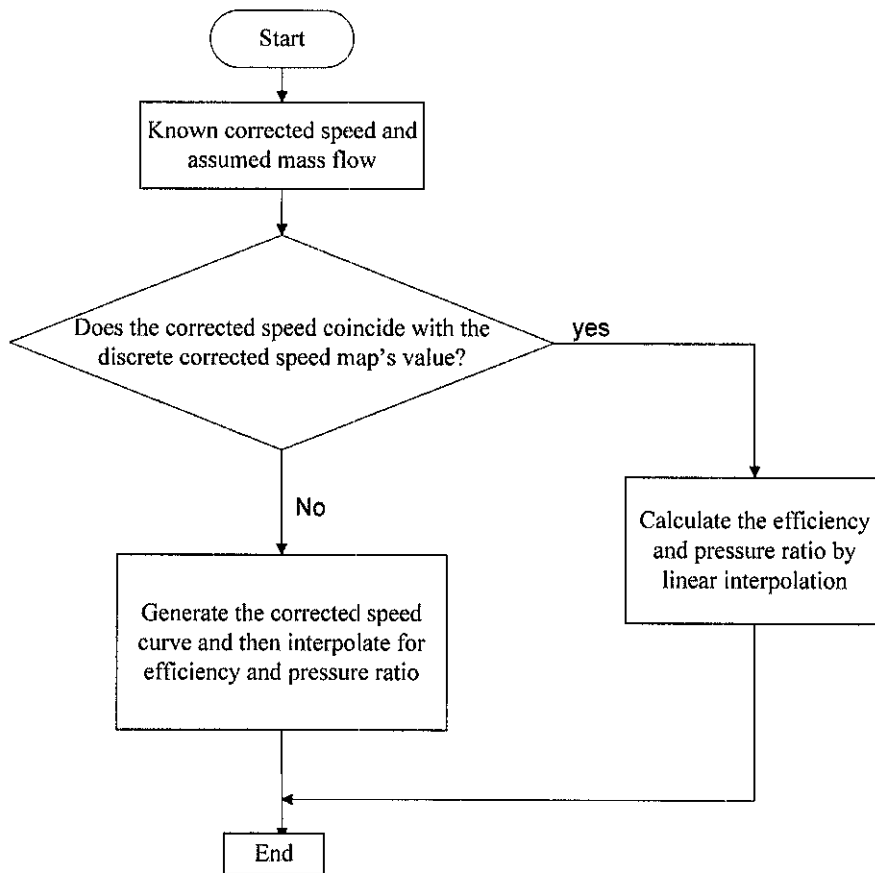
Figure 3.24 Compressor performance map interpolation flowchart

3.5.3.2 Compressor Work Module

This subroutine calculates the compressor outlet temperature, work consumption, exergy destruction, and exergetic efficiency at a given ambient temperature and part load demand. The flowchart used for this subroutine is shown in Figure 3.25.
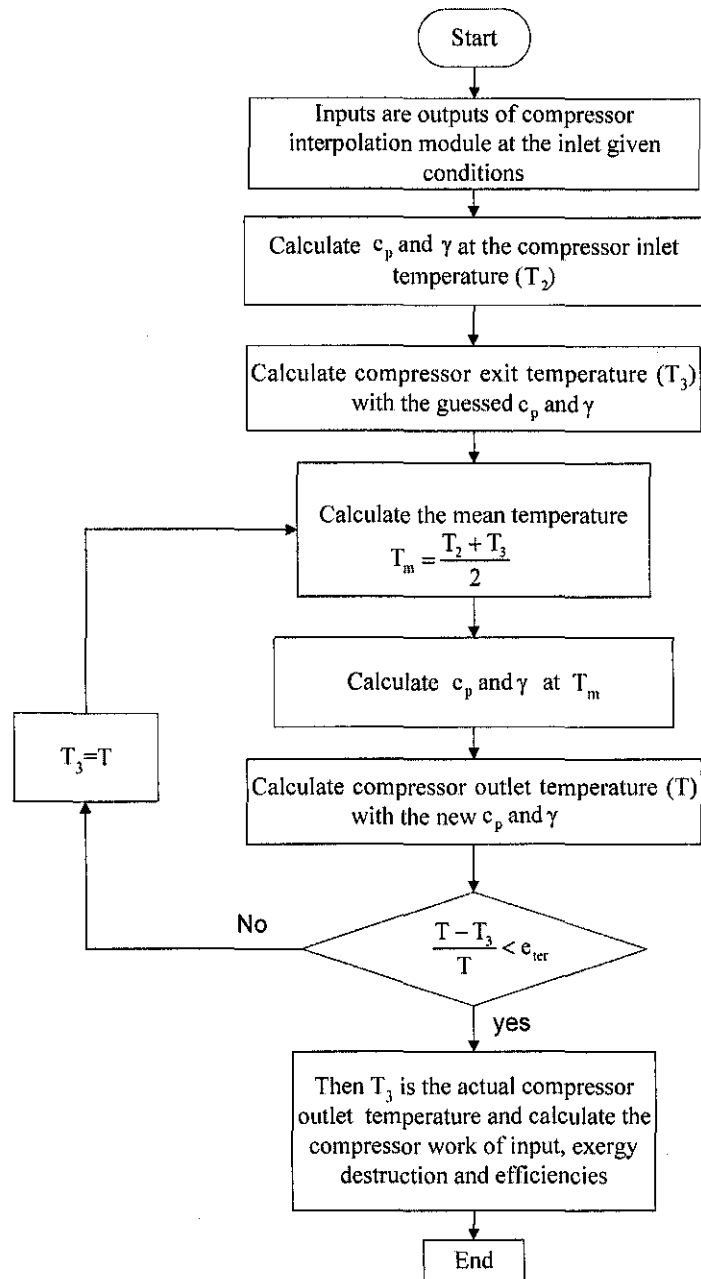
Figure 3.25 Flowchart that is used in the compressor work module to calculate compressor work input, outlet temperature, exergy destruction and efficiencies

3.5.3.3 Combustion Chamber Module

The purpose of this subroutine is to solve non-linear equation using Newton Raphson's numerical solution method. Here at a given power output it calculates the corresponding *FAR* and combustion outlet temperature iteratively. Once the fuel amount is known the characteristic gas constant, the specific heat, the combustion

77

exergy destruction and exergetic efficiency are calculated. The combustor module with assumed initial combustor outlet temperature and *FAR* could call the Newton Raphson module to find the formulated non-linear function solution. The Newton Raphson module in turn uses the Newton Raphson function (fcn_nr) module to formulate the function while the *FAR* is being made the independent parameter. The combustor module flowchart is shown in Figure 3.26.
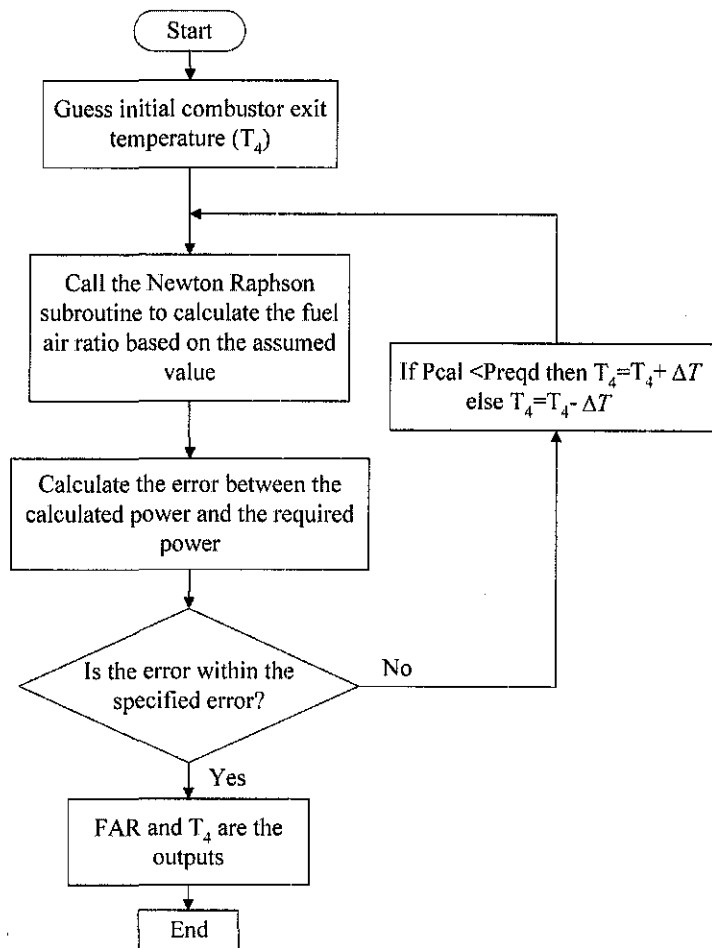
Figure 3.26 Overall flowchart of the combustion chamber module program

Newton's method (also called Newton Raphson method) for solving nonlinear equations is one of the most well-known and powerful method for numerical analysis. It always converges if the initial approximation is sufficiently close to the root, and it converges quadratically (the error is the square of the error in the previous step) [90]. Its only disadvantage is that the derivative $f'(x)$ of the nonlinear function $f(x)$ must be evaluated. This iterative flowchart used to calculate the FAR is shown in Figure 3.27, where ε_{ter} is the error tolerance.
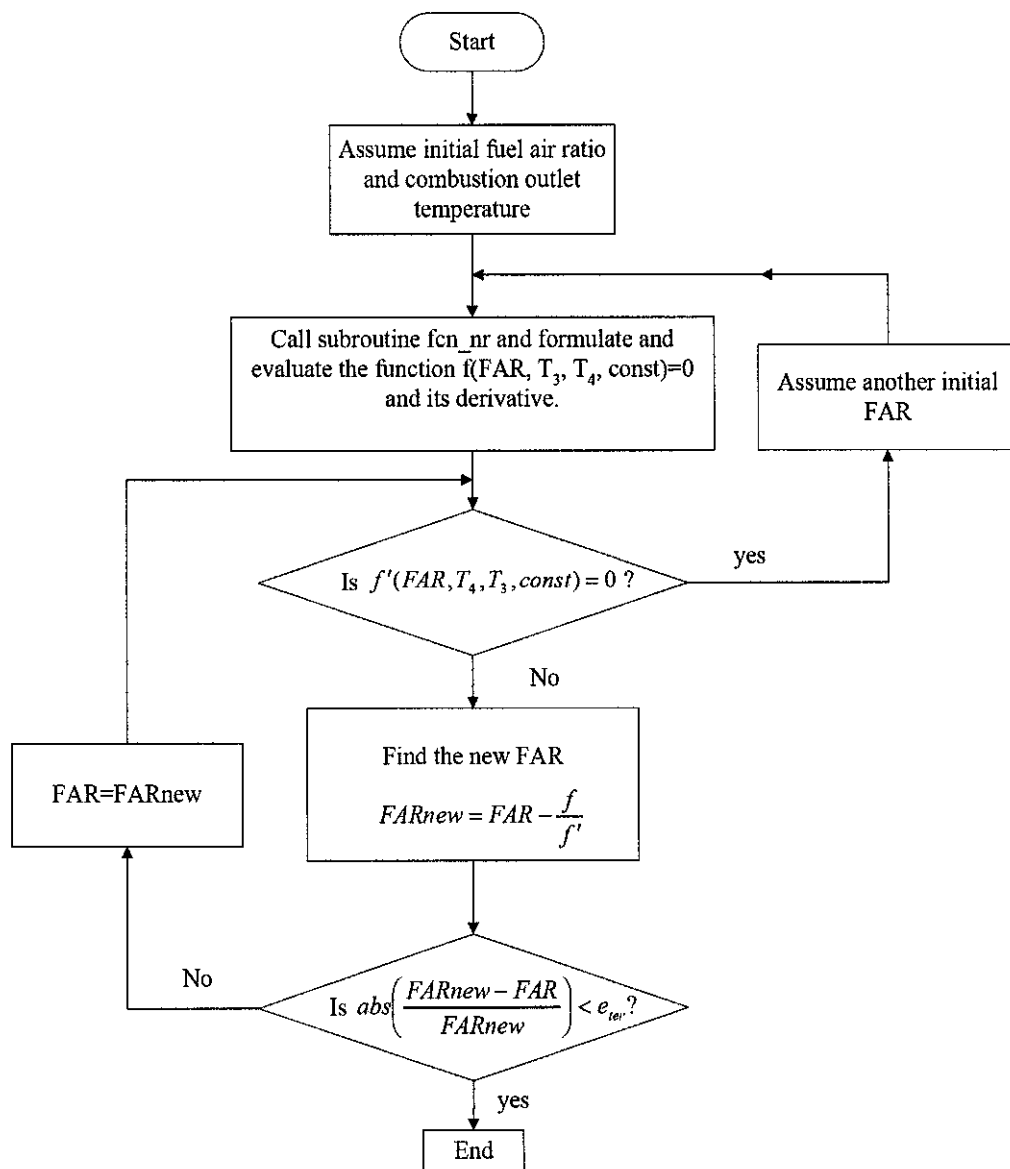
Figure 3.27 Newton Raphson's flowchart used to find the solution of non-linear equation

3.5.3.4 Specific Heat Module

This is the subroutine that is used to calculate the values of the specific heat at constant pressure (c_p), specific heat ratio (γ) and characteristics gas constant at a particular temperature. These values are required by various equipments and this module would be used when ever required. This subroutine uses polynomial expressions for the aforementioned properties. The flowchart used to find these properties at the average value is shown in Figure 3.28.

79
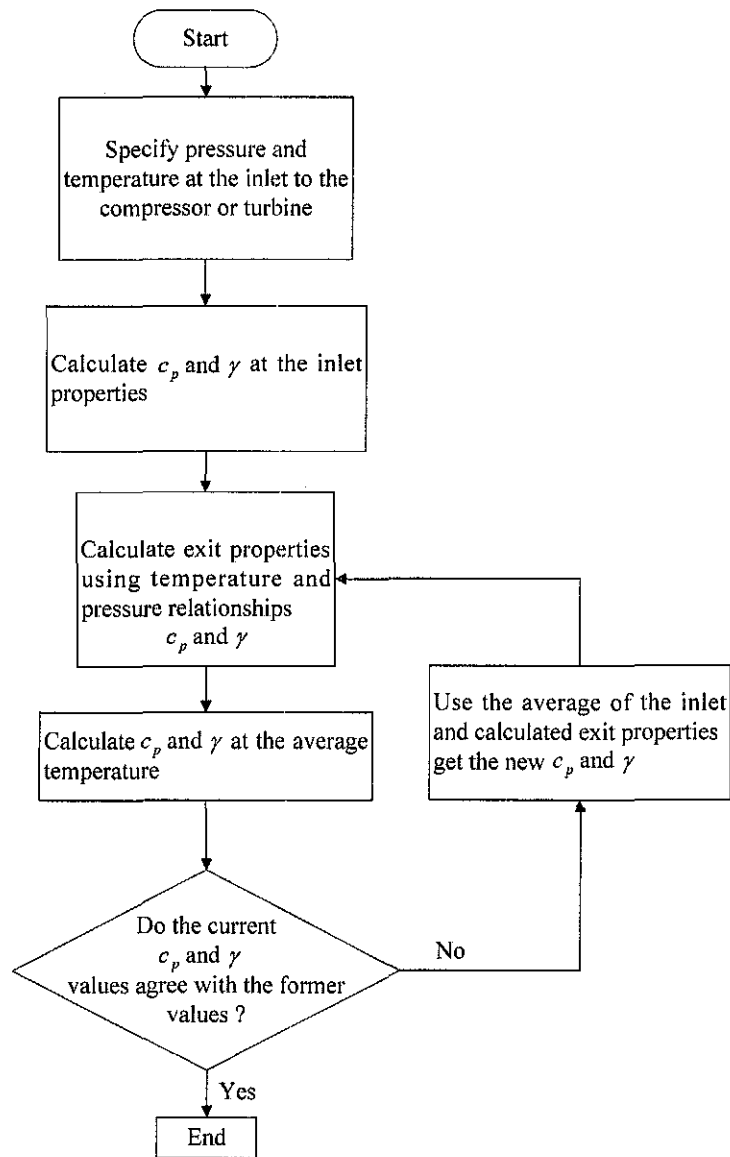
Figure 3.28 A flowchart used to find specific heat, characteristic gas constant and specific heat ratio at the average temperature value

3.5.3.5 Turbine Interpolation Module

This subroutine is used to calculate the turbine characteristics, i.e., the turbine pressure ratio and efficiency at given corrected speed and mass flow rate. Any value other than the discrete data is obtained by linear interpolation. The flowchart for turbine interpolation is similar as that of the compressor performance map interpolation, shown in Figure 3.24.

3.5.3.6 Turbine Work Module

This subroutine calculates the power developed by the turbine at the given off-design conditions. In addition to the turbine work output it calculates the turbine exit temperature, pressure, exergy destruction, and exergetic efficiency. The flowchart used for this purpose is similar as that of the compressor work flowchart, shown in Figure 3.25.

3.5.3.7 HRSG Module

The two important parameters that determine the design of an HRSG are: pinch and approach point temperatures. Based on literature recommendation and available experimental information the pinch and approach point temperatures are determined. The flowchart used for the analysis is indicated in Figure 3.29. Once the design parameters are fixed they would be used to model the off-design performance of the HRSG. For the off-design analysis of HRSG, the computer flowchart indicated in Figure 3.30 is used.
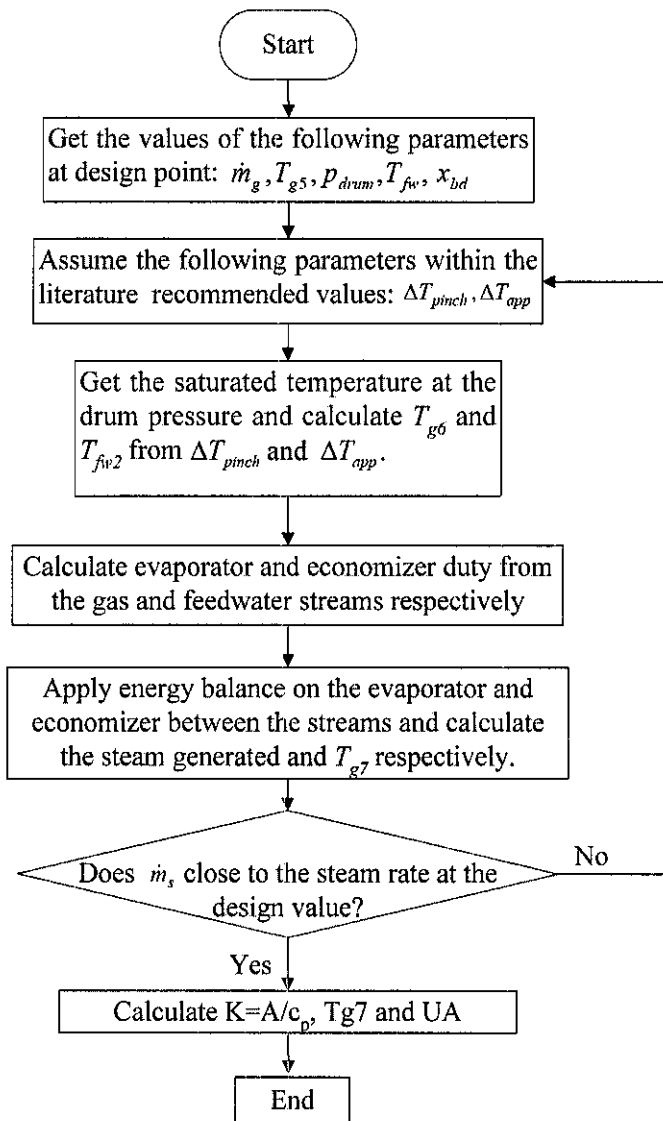
Figure 3.29 Flowchart for design point analysis of the HRSG

```
                              ┌─────────┐
                              │  Start  │
                              └─────────┘
                                   │
          ┌────────────────────────────────────────────────┐
          │  Call gas turbine off design module to get      │
          │  ṁ_g and T_g5, and fix the parameters           │
          │           P_drum, T_fw, x_bd                    │
          └────────────────────────────────────────────────┘
                                   │
          ┌────────────────────────────────────────────────┐
          │  Get saturated temperature at the given drum pressure │
          └────────────────────────────────────────────────┘
                                   │
          ┌────────────────────────────────────────────────┐
          │  Call HRSG design subroutine to get K and UA at the design point │
          └────────────────────────────────────────────────┘
                                   │
          ┌────────────────────────────────────────────────┐
          │  Calculate T_g6 using K at the design point      │
          └────────────────────────────────────────────────┘
                                   │
          ┌────────────────────────────────────────────────┐
          │  Estimate c_pgev and c_pgec at their respective temperature │
          │  from the discrete exhaust gas data which may need │
          │                interpolation                     │
          └────────────────────────────────────────────────┘
                                   │
          ┌────────────────────────────────────────────────┐
          │  Calculate evaporator duty from the gas stream   │
          └────────────────────────────────────────────────┘
                                   │
          ┌────────────────────────────────────────────────┐
          │  Assume T_fw2 call saturated vapor and liquid enthalpy │
          │  subroutines and get h_g, h_f, h_fw2, h_fw at their respective │
          │                temperature                       │
          └────────────────────────────────────────────────┘
                                   │
          ┌────────────────────────────────────────────────┐
          │  Calculate evaporator duty per unit mass         │
          │         from the steam stream                    │
          └────────────────────────────────────────────────┘
                                   │
          ┌────────────────────────────────────────────────┐
          │  Apply energy balance on the evaporator and      │
          │         find the steam generated                 │
          └────────────────────────────────────────────────┘
                                   │
          ┌────────────────────────────────────────────────┐
          │  Calculate economizer assumed duty from          │
          │       the feedwater stream (Q̇_ec,a)             │
          └────────────────────────────────────────────────┘
                                   │
          ┌────────────────────────────────────────────────┐
          │  Calculate UA of economizer at off-design        │
          └────────────────────────────────────────────────┘
                                   │
          ┌────────────────────────────────────────────────┐
          │  Apply energy balance on the economizer between the two │
          │            streams and find T_g7                 │
          └────────────────────────────────────────────────┘
                                   │
          ┌────────────────────────────────────────────────┐
          │  Calculate LMTD_ec at off-design condition       │
          └────────────────────────────────────────────────┘
                                   │
          ┌────────────────────────────────────────────────┐
          │  Calculate the economizer off-design duty (Q̇_ec,c) using │
          │                the LMTD_ec                       │
          └────────────────────────────────────────────────┘
```

$$T_{fw2} = T_{fw2,old} + \Delta T, \text{if } \dot{Q}_{ec.o} > \dot{Q}_{ec.a}$$
$$T_{fw2} = T_{fw2,old} - \Delta T, \text{if } \dot{Q}_{ec.o} < \dot{Q}_{ec.a}$$

No — decision: $\left| \dfrac{\dot{Q}_{ec.a} - \dot{Q}_{ec.c}}{\dot{Q}_{ec.c}} \right| < \varepsilon_{ter}$ — Yes

Store the final values of $\dot{m}_s, T_{g6}, T_{g7}$ and T_{fw2}

End

Figure 3.30 A flowchart used to analyse the HRSG off-design performance

3.6 Summary

Using partial data obtained from manufacturer's maps, basic conservation laws and thermodynamics property ratio relationships the design point data of the compressor and the turbine are calculated. The characteristics maps of the compressor and turbine are developed. Scaling method is used to develop existing compressor and turbine maps from known maps with their design data. Once the design data of both the gas turbine and HRSG are determined each component of the cogeneration off-design model is developed. To address the effect of the compressor air bleeding and VVs modulation in the first and second mode of operations correction coefficients are developed. In the second mode of operation as the VVs opening change the performance maps change. To overcome this, the developed correction coefficients are used to modify the compressor maps at a given VVs percentage opening. The exergetic model of each cogeneration component is also developed. All the relevant equations, numerical simulation flowcharts including all detail logics that are implemented in the computer programming are presented in this chapter.

CHAPTER 4

RESULTS AND DISCUSSION

4.1 Introduction

In this chapter, the Taurus 60S single shaft gas turbine based cogeneration plant simulation results are presented. The performance predictions are the result of both the mathematical model and the subroutines described in Chapters 3. First, the simulation output of each component is compared to its corresponding actual data whenever available. After that each compared parameter's error is calculated and statistically evaluated and validated. Once the statistical evaluation is done, the simulation model is used to carry out the effect of ambient temperature on the cogeneration performance. Finally the cogeneration exergy analysis is carried out to identify the component that contributes to the major exergy destruction.

4.2 Experimental Configuration and Assumptions

Universiti Teknologi PETRONAS (UTP) has Taurus 60S gas turbine based cogeneration plant. The Taurus 60S has an ISO rating power production capacity of 5.3 MW (5MW generator terminal power) with a maximum rotational speed of approximately 14,944 rpm. However, it produces a maximum of around 4.2MW generator terminal power. This is because the power output is a function of the ambient temperature and the tropical region ambient temperature is higher than the ISO rating temperature of 15°C. The Taurus 60S gas turbine's operation has been recorded using Turbotronic Control System monitoring and reception of data at the UTP's control room. To determine the status of the cogeneration operation the monitored parameters include system temperatures, pressures, vibration levels, VVs

percentage opening, power output and fuel flow rate etc. The external view of the gas turbines is shown in Figure 4.1.
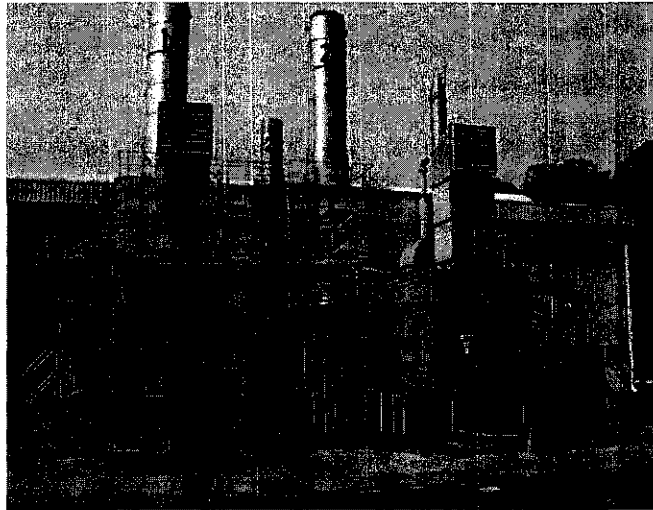
Figure 4.1 Two gas turbine generators (External view captured photo)

The assumptions that are used in the simulation are summarized as follows, whereas the typical values of the parameters are already described in Chapter 3.

Table 4.1: Shows the parameters assumed values to simulate the cogeneration plant

Parameters	Assumed values
The pressure drop in the inlet duct	3% [74]
Combustion chamber efficiency	99% [18]
Combustion chamber pressure drop	3% [18]
HRSG gas side pressure drop	3% [74]
Kinetic energy and potential energy effects	neglected
LHV of the fuel	50016 kJ/kg [68]
Feedwater inlet temperature	90°C [78]
The HRSG is producing saturated steam [80]	
Drum pressure	9.00 bar [80]
For exergy analysis	
Effect of blowdown	neglected
Dead state ambient pressure and temperature conditions	101.32 kPa and 303.15 K
Diverter damper opening	100%

4.3 Validation of the Results

The purpose of the validation effort is to demonstrate that the developed mathematical model simulation results can match actual running engine data over the wide range of operational conditions. Furthermore, to ensure the conclusions drawn from the simulation are reasonable, the validation is carried out based on actual measured data. As the measurable data are limited, a complete validation of the various components and parameters are not made. For example, there are no data measuring device for the air flow and turbine inlet temperature and pressure ratio. However, sufficient data are collected to demonstrate the process of validation and that the simulation can be matched to the representative data sets. A change in the gas turbine operation was done by varying the turbine power output, which in actual operation of the gas turbine causes a reduction in the fuel flow rate to the combustor. Hence, the power output and ambient temperature are used as input for simulation.

4.3.1 Effect of Variation of Part Load

In order not to disturb the operation of the plant during actual data collection varying one parameter while keeping the others constant like experimental rig input variable manipulation could not be done. Moreover, the ambient temperature is an independent variable that cannot be controlled. Therefore, during the part load variation, the ambient temperature was varying between 27.3 to 35°C.

As mentioned in Section 3.3.2.2 of the compressor model, the gas turbine in its full range operation has shown two modes of operation, that is, for less than and greater than 50% load. Its parameter variations during the simulation for both modes of operation are examined. In each mode the target of the operation is different. The first one involves compressed air bleeding control at the downstream of the compressor while the VVs are fully opened to meet the power demand. In the second mode, the VVs and fuel mass flow are regulated to maintain the exhaust gas temperature at the set value and minimize emission while the bleed valve is closed. As these two modes of operation targets are different when the load reaches 50%, there is a sudden change of parameters that is manifested. When the load reaches

50% and above the combustion chamber SoLoNOx low emission operation begins. The turbine exit temperature (T_5) set point is ramped up and variable vanes modulated as necessary to maintain T_5 set value. This set value will vary slightly depending on the emission requirement.

Figure 4.2 indicates the variation of the compressor VVs percentage opening with respect to relative load. In the first mode, both the actual and the simulated VVs are fully opened. However, for load above 50% in the low emissions range as the load increases, the VVs are allowed to open to the required value so that the turbine exhaust gas temperature would be maintained at the set value. For comparison purpose the actual VVs percentage openings are included and it shows that the actual values are replicated by the simulation model with good agreement.
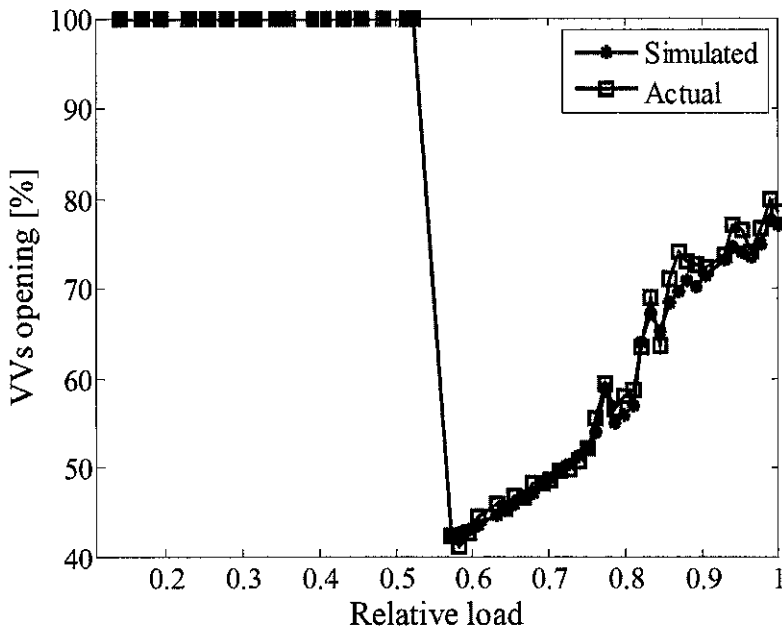
Figure 4.2 Variation of percentage VVs opening with respect to relative load

The turbine inlet and outlet temperatures variation with respect to part load is shown in Figure 4.3. In the first mode of operation, both temperatures keep on increasing as the load increases. For part load greater than 50%, as the load increases the inlet temperature keeps on increasing while the outlet temperature is maintained constant. The outlet temperature that is maintained at the set value would be used to recover saturated steam in the HRSG. The engine is running mostly in the second mode, hence it delivers low emission and high exhaust gas temperature.
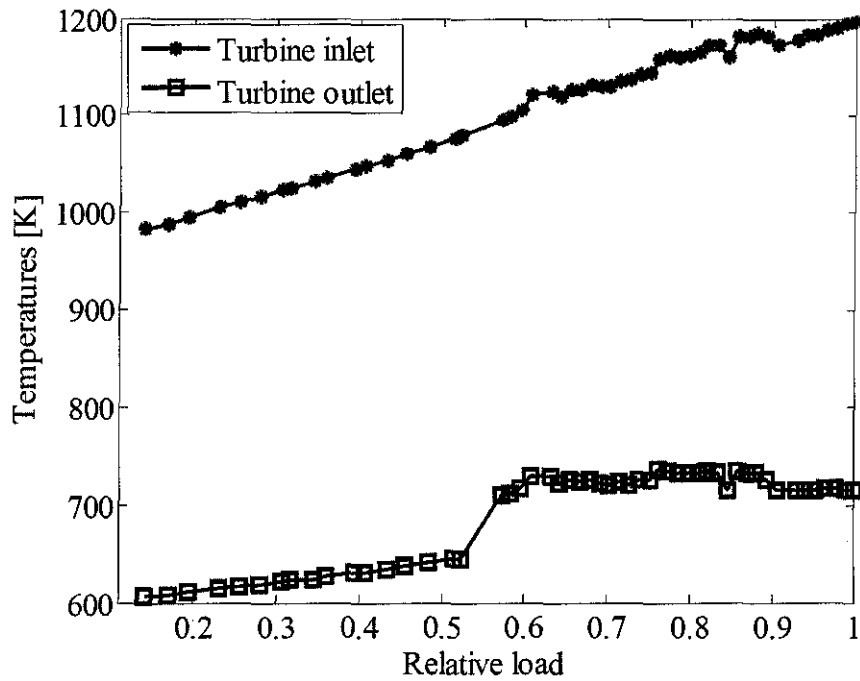
Figure 4.3 Variation of turbine temperatures with respect to load

The compressor pressure ratio variation with respect to part load is depicted in Figure 4.4. Both in the first and second modes the pressure ratio is increasing as the load increases. In general for a single shaft gas turbine rotating at constant speed the pressure ratio is the same as the load increases. However, in this case, there is air bleed at the down stream of the compressor that decreases as the load increases. Consequently, the pressure ratio is increasing as load increases. Furthermore, exhaust gas temperature is essentially a result of the pressure ratio and firing temperature. A higher pressure ratio will tend to decreases the exhaust temperature for a given firing temperature. Hence, at 50% load the pressure ratio drops and from that onward keeps on increasing so that both the load and exhaust gas set value temperature are achieved. Actual value is included for comparison and shows a good agreement with the simulated pressure ratio. The possible causes for the small discrepancies are the constants in the quadratic air bleed assumption and the bleed may be dependent on other factors than the load.
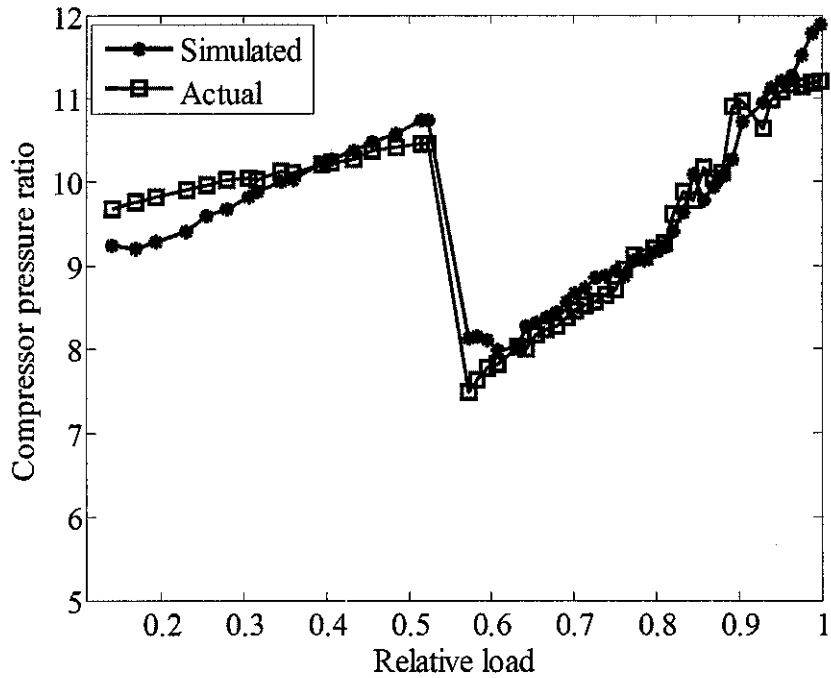
Figure 4.4 Variation of compressor pressure ratio with respect to relative load

Figure 4.5 shows comparison of the simulated and actual fuel consumption. In general, the trends are replicated by the simulation. As expected, the fuel consumption increases as the load increases. Since the flow rate is reduced the fuel required to achieve the turbine inlet temperature requires less fuel consumption hence there is a slight fuel consumption drops at 50% load and then keep on increasing. The matching between the simulation and the actual data in the first mode is good but in the second mode there is a small discrepancy. The cause for the discrepancy could be the possible differences in the specific heat capacity used in the calculation of the combustion chamber and turbine or compressor.
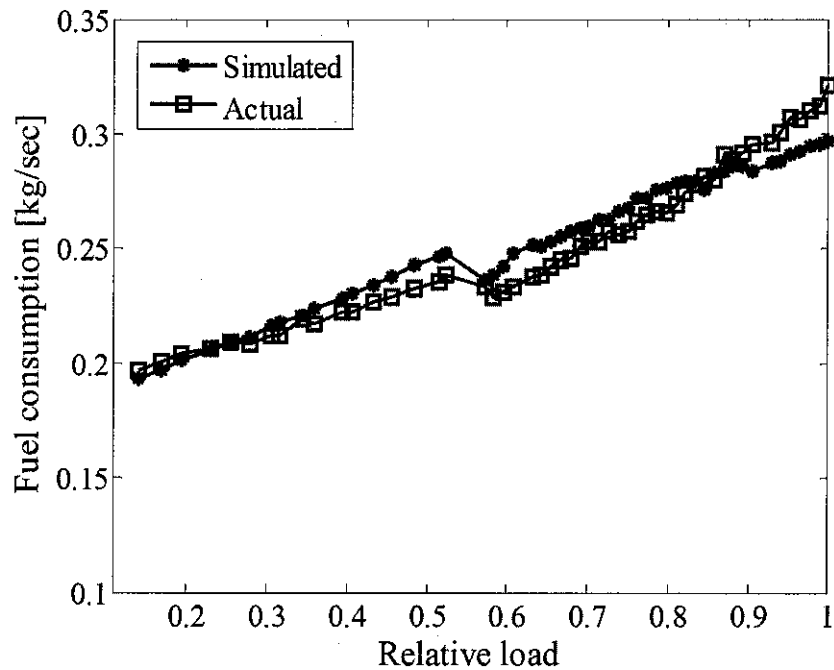
Figure 4.5 Variation of fuel consumption with respect to relative load

The variation of gas turbine inlet and outlet flow (inlet of the compressor and exit of the turbine) with respect to part load is indicated in Figure 4.6. In the first mode, the gas turbine inlet mass flow is constant as the compressor is running at constant speed and its VVs are fully opened whereas the outlet mass flow is increasing the discrepancy is the bleed mass flow at the down stream of the compressor. In the second mode, both the inlet and the outlet mass flows increase as the load increases. Noting that there is no bleeding in this mode the outlet is grater than the inlet mass flow. The mass flow difference is the contribution of the fuel injected in the combustion chamber. The abrupt jump happened due to change of operation mode at 50% load.
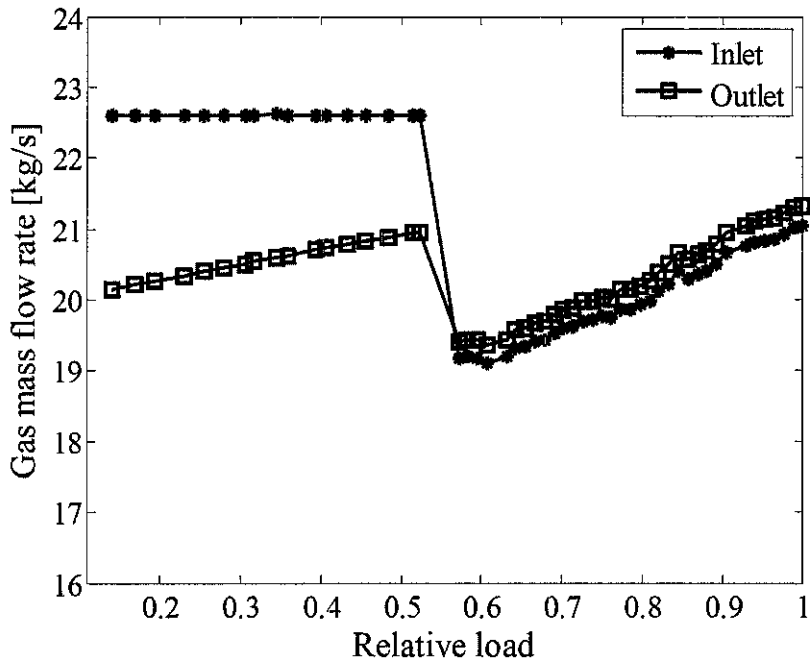
Figure 4.6 Variation of gas turbine mass flow rate with respect to relative load

The gas turbine efficiency increases with respect to part load as shown in Figure 4.7. This is expected and the maximum efficiency is approximately 0.29. Since the specific fuel consumption (sfc) is inversely proportional to efficiency, it decreases as the part load increases.
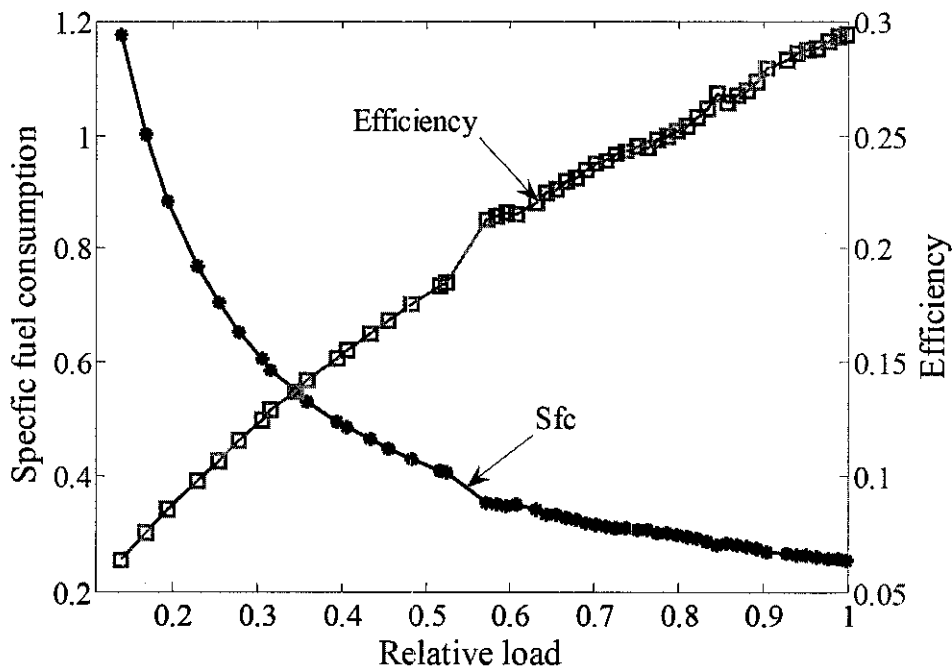
Figure 4.7 Variation of specific fuel consumption and efficiency with respect to load

The input to the HRSG is the exhaust gas temperature at a certain flow rate that varies with the part load. The HRSG starts to work at 50% and above load. When it is not operating at full load the exhaust gas mass flow entering the HRSG is controlled by the diverter damper. Hence, the other parameter that controls the amount of steam production rate other than the part load is the diverter damper opening. Figure 4.8 shows as the turbine relative part load and diverter damper opening increase the steam production rate increases at a given constant exhaust gas temperature. For comparison the actual steam production rate is included and the agreement is good. The increase in both load and diverter damper opening will also increases the HRSG efficiency and correspondingly the total cogeneration efficiency as indicated in Figure 4.9. The result shows that the plant thermal load demand is not high; as a result the diverter damper is usually not fully opened. This condition results in some unrecovered turbine exhaust energy, thereby causing a reduction in overall system energy efficiency.
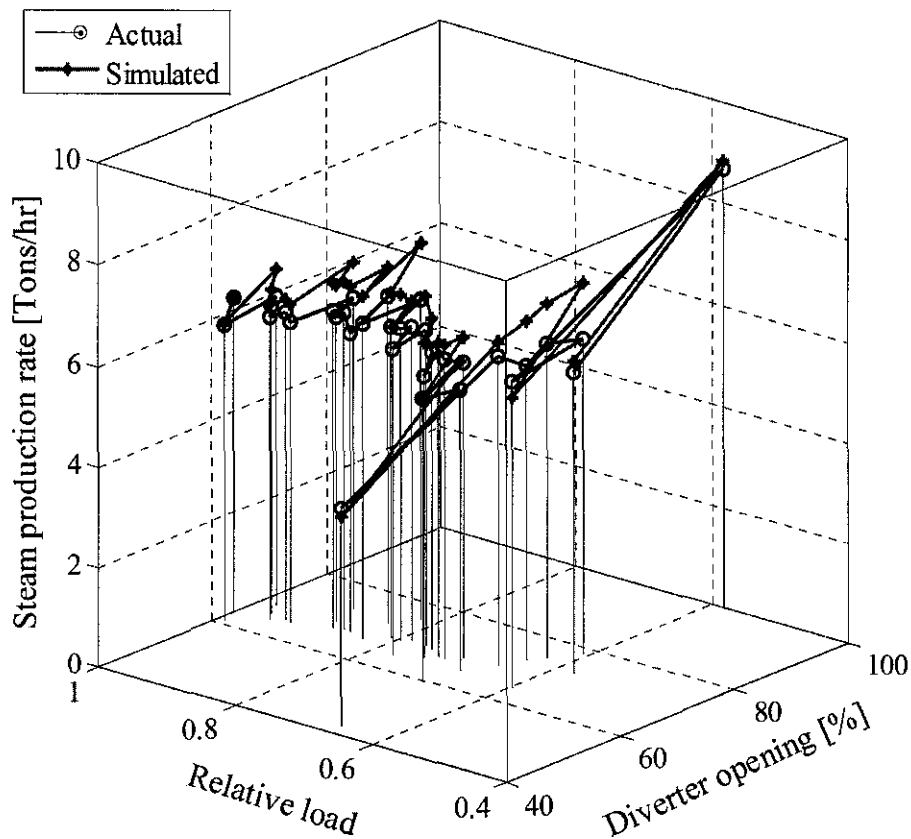
Figure 4.8 Variation of steam production rate with respect to load and diverter damper opening

93
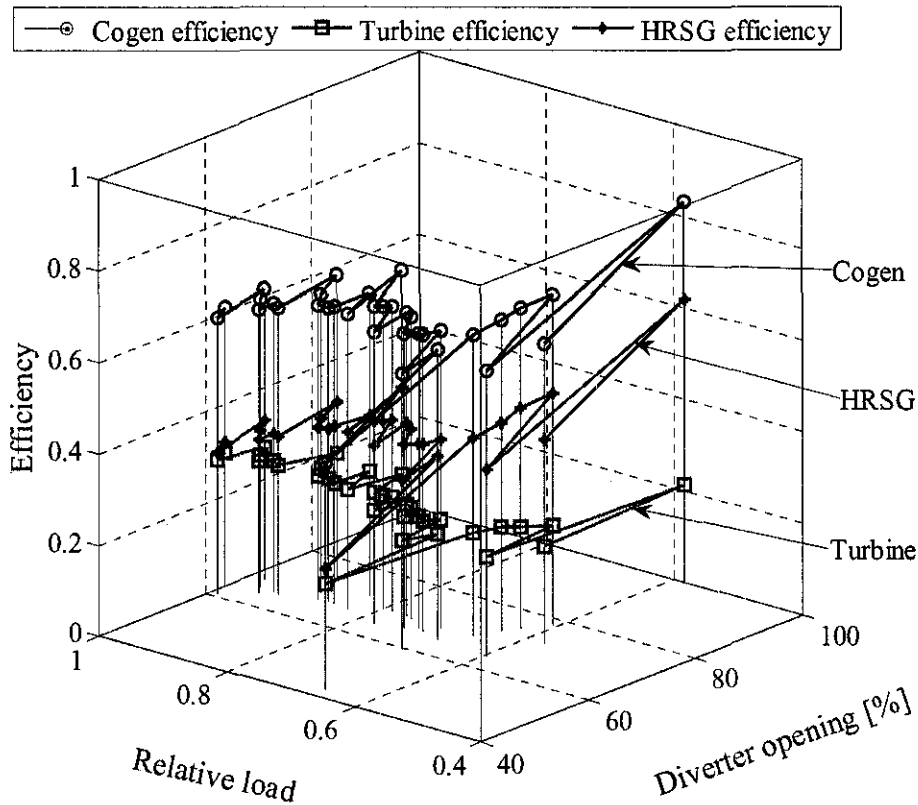
Figure 4.9 Variation of efficiencies with respect to load and diverter damper opening

4.3.2 Statistical Evaluation

The reliability of a physical system's simulation is dependent on the accuracy of the mathematical model. The quantitative modeling of a component requires knowledge of the process and ability to mathematically represent it. Replacing an equipment or process by mathematical model can never exactly represent the process. Validation, which requires information from actual tests, must show that the mathematical model is a reasonable representation of the real process. Therefore, the errors of the cogeneration model simulation results relative to the actual data are statistically evaluated to investigate the variations of the model results with their corresponding actual values.

Based on the defined test and statistical parameters in Appendix C, the results of the statistical analysis of each parameter error using Minitab statistical software are summarized in graph form. The graphical summary includes four graphs: histogram

of data with an overlaid normal curve, boxplot, 95% confidence intervals for mean, and 95% confidence intervals for the median.

4.3.2.1 Interpreting the Results

Ideally, the mean error and the standard deviation would be zero. Generally, it is said that there is a 95 percent probability of the error values falling within two standard deviations of the mean. The larger the standard deviation, the greater the range of error would be.

If the standard deviation of the entire normal distribution curve is known, then the result of the error analysis could be explained as follows. Consider the compressor pressure ratio error analysis, as shown in Figure 4.10, an individual model prediction error lies within 2s = 0.6066 and the mean value of 0.03392. If the model is used for prediction of the compressor pressure ratio 95 % of the error compared to the measured value will fall in the range of 0.03392± 0.3033. This statement determines the confidence interval of model error. Using a significance level of 0.05, the Anderson-Darling Normality Test (A-Squared = 0.3800, P-Value = 0.3810) indicates that the resulting pressure ratio error data follow a normal distribution as the P-Value is greater than 0.05.

On the other hand, the mean and standard deviation are not true values. Therefore, the uncertainty of the mean and the standard deviation values should be defined. Using the 95 % confidence interval, the mean value should then be reported as $\bar{x} \pm 2s_{\bar{x}}$. For the case of compressor pressure ratio error, the mean is 0.03392 (95% confidence intervals of -0.05052 and 0.1184). The standard deviation is 0.3033 (95% confidence intervals of 0.2542 and 0.3761). In the same way, the other parameters' error results can be explained. The error evaluation summary for VVs percentage opening, fuel flow rate and steam production rate are indicated in Figure 4.11 to Figure 4.13.

Anderson-Darling Normality Test		
A-Squared	0.38	
P-Value	0.381	
Mean	0.033920	
StDev	0.303293	
Variance	0.091987	
Skewness	-0.190496	
Kurtosis	-0.203188	
N	52	
Minimum	-0.634921	
1st Quartile	-0.139143	
Median	0.089031	
3rd Quartile	0.212868	
Maximum	0.666463	
95% Confidence Interval for Mean		
-0.050518	0.118357	
95% Confidence Interval for Median		
-0.045488	0.158097	
95% Confidence Interval for StDev		
0.254174	0.376122	

Figure 4.10 Summary of the statistical evaluation for the compressor pressure ratio prediction model error

Anderson-Darling Normality Test		
A-Squared	0.26	
P-Value	0.694	
Mean	-0.93355	
StDev	1.27830	
Variance	1.63406	
Skewness	-0.243671	
Kurtosis	0.243697	
N	35	
Minimum	-4.34210	
1st Quartile	-1.79850	
Median	-0.85160	
3rd Quartile	-0.06780	
Maximum	1.58270	
95% Confidence Interval for Mean		
-1.37267	-0.49444	
95% Confidence Interval for Median		
-1.55494	-0.22132	
95% Confidence Interval for StDev		
1.03398	1.67483	

Figure 4.11 Summary of the statistical evaluation for the compressor variable vanes percentage opening prediction model error

96
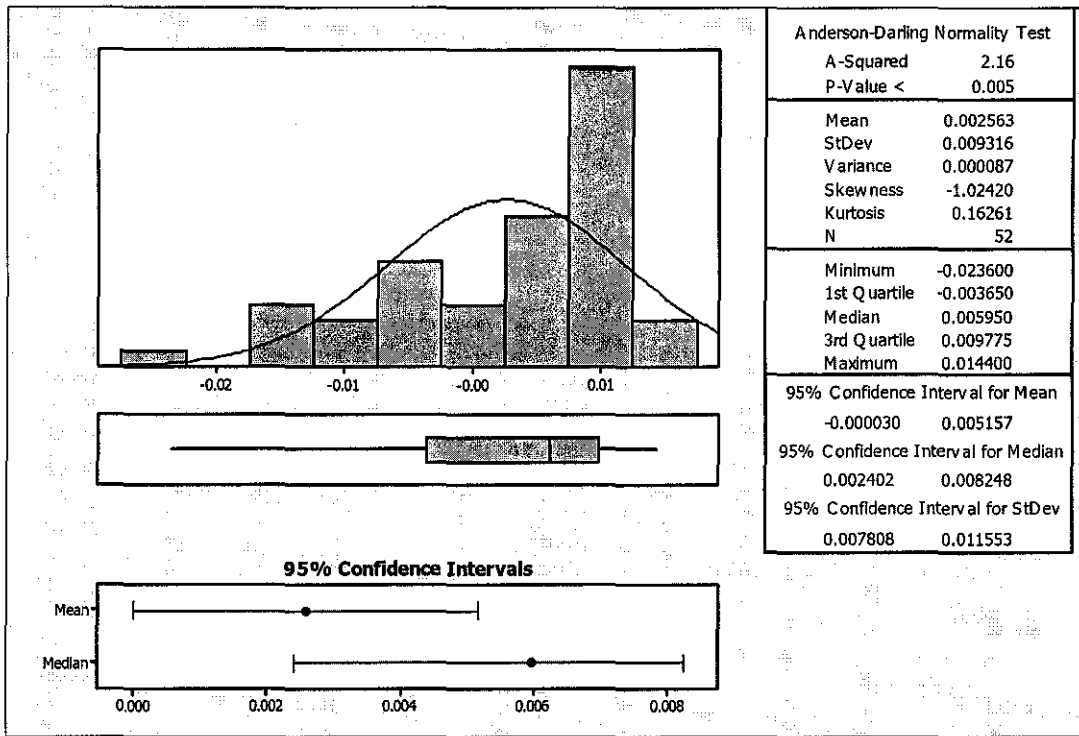
Figure 4.12 Summary of the statistical evaluation for the gas turbine fuel
consumption prediction model error
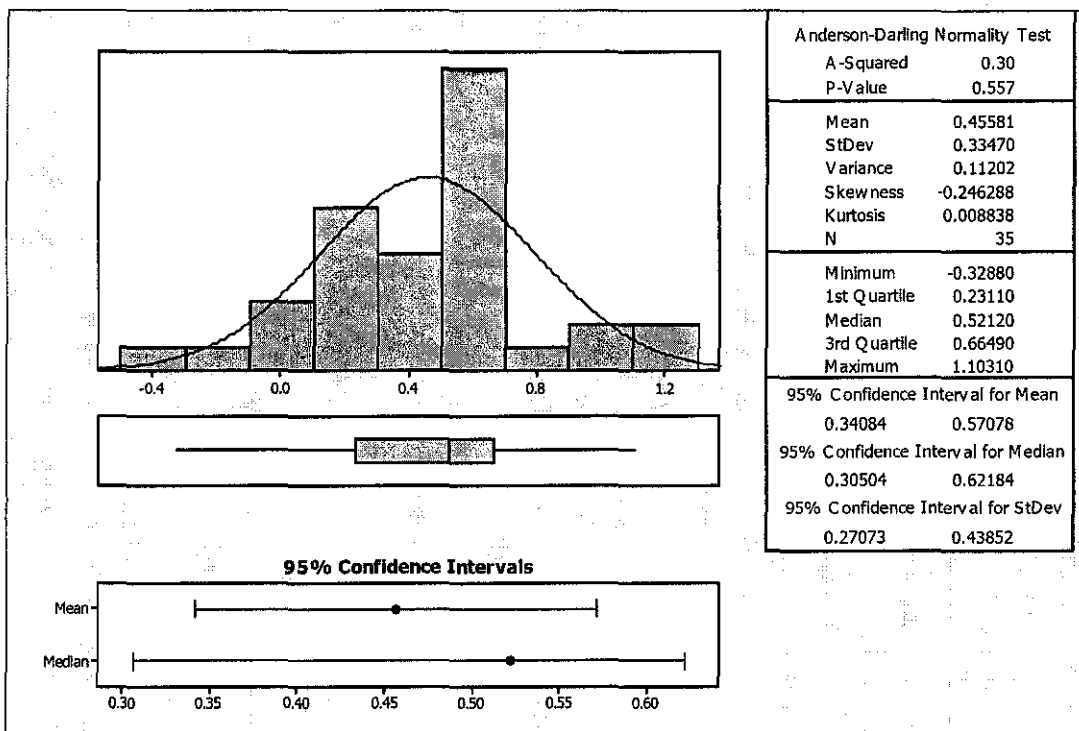
Figure 4.13 Summary of the statistical evaluation for the cogeneration steam
production rate prediction model error

97

As indicated in Table 4.2 each mean is centred close to zero and their mean standard deviations are small. Furthermore, no minimum error requirements are established as the necessary prediction accuracy varies greatly with the particular interest the data might be used for. This suggests that the cogeneration component model is reasonably predicting its performance parameters within acceptable degree of error.

Table 4.2 Summary of the statistical evaluation of the cogeneration plant model errors

Model parameter	Anderson Darling Normality test		Mean of error	Standard deviation	95% confidence interval	
	A-squared	P-Value			Mean	Standard deviation
Pressure ratio	0.38	0.381	0.0339	0.3033	-0.05052	0.2542
					0.11836	0.3762
VVs percentage opening	0.26	0.694	-0.9335	1.2783	-1.3727	1.03398
					-0.4944	1.6748
Fuel consumption	2.16	0.005	0.00256	0.00932	-0.00003	0.00781
					0.00516	0.01155
Steam produced	0.3	0.557	0.4558	0.3347	0.3408	0.2707
					0.5708	0.4385

4.4 Effect of Ambient Temperature Change on the Cogeneration Performance

The cogeneration performance is affected by anything that changes the density and or mass flow of the air intake to the compressor. The air density is a function of ambient temperature, pressure and humidity. The air density increases as the ambient temperature decreases, and it reduces as the site elevation increases. As a result,

these factors have impact on the gas turbine performance. The ambient parameters also affect the mass flow rate of the exhaust gas from the turbine and hence they influence the HRSG steam production rate. Therefore, once the model is validated it is used to examine the effect of ambient temperature on the gas turbine and its cogeneration performance. Simulation is done for a hypothetical case, that is, full diverter damper opening and a given inlet temperature. The cogeneration is simulated at three ambient temperatures, i.e., 15, 25, and 35°C for a wide range of part load while keeping the ambient pressure 1 atm. The results of the simulation are included with discussion as follows.

4.4.1 Effects on the components' performance parameter(s)

Figure 4.14 shows variation of turbine inlet temperature with respect to load. As the ambient temperature decreases, the specific volume of the air decreases and the work input to the compressor is proportional to the specific volume. Consequently, in the first mode of operation as the ambient temperature decreases, the compressor work input decreases. Thus, for a given turbine net power output, the turbine would require less additional power to drive the compressor. Therefore, at a given load the lower the ambient temperature, the lower will be the turbine inlet temperature.
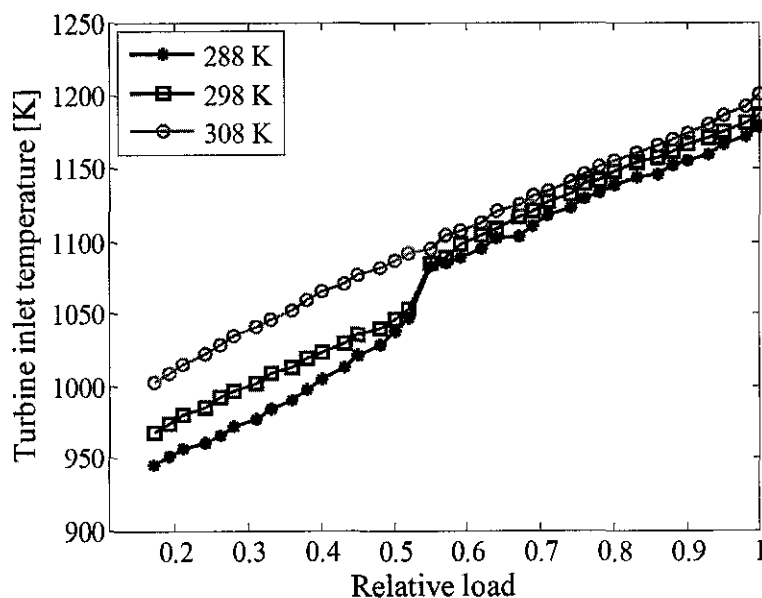
Figure 4.14 Variation of turbine inlet temperature with relative load for different ambient temperatures

In the second mode of operation, the objective is to maintain the turbine exhaust gas temperature at the set value. Therefore, given any ambient temperature the turbine inlet temperature has to be increased to high value by regulating both the VVs opening and the fuel consumption rate. Furthermore, the higher the ambient temperature, the higher will be the turbine inlet temperature but the difference among the turbine inlet temperatures is not as large as the first mode of operation.

The variation of the fuel consumption with respect to load is shown in Figure 4.15. In the first mode of operation the lower the ambient temperature, the lower will be fuel consumption at a given load as the work input to the compressor is lower. In both mode of operation the fuel consumptions increase as the load increases. However, at 50% load the one that has the highest ambient inlet temperature fuel consumption drops. This is because in the second mode the combustion is in SoLoNOx mode where the mixture has to be lean mixture to minimize emissions. Moreover, in this mode the VVs is modulated to reduce the air mass flow rate entering into the compressor and hence to make the mixture lean the injected fuel into the combustor decreases for ambient temperature greater than 15°C.]
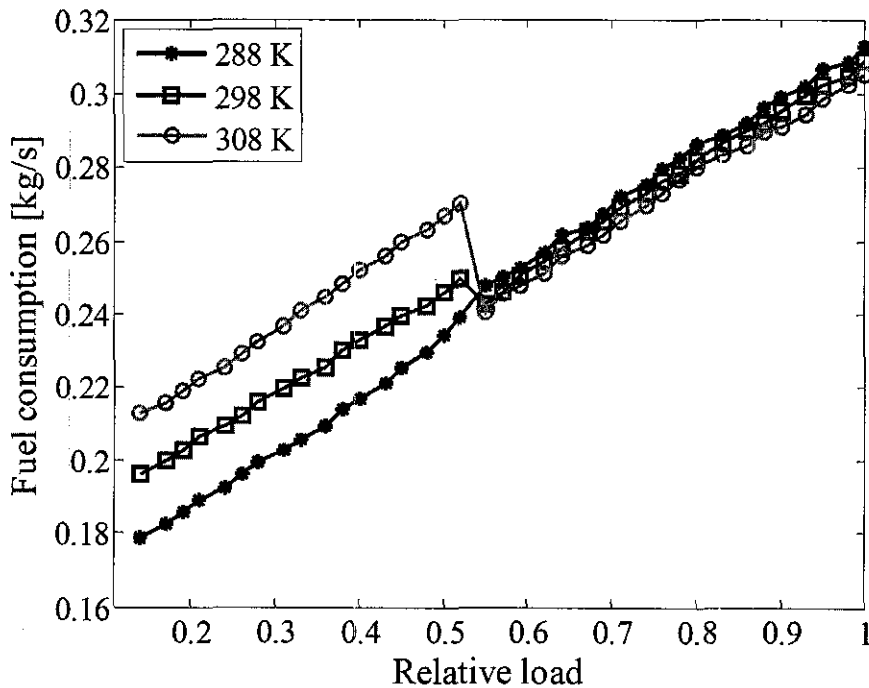
Figure 4.15 Variation of fuel consumption with relative load for different ambient temperatures

The variation of the VVs percentage opening with load for different ambient temperatures is indicated in Figure 4.16. In the first mode the turbine is running as a fixed geometry gas turbine while the VVs are fully opened. On the other hand, in the second mode the VVs are modulated to control the flow entering into the turbine so that at a given ambient temperature the gas turbine can maintain its set value exhaust gas temperature. Moreover, at high ambient temperature the air density is small. Thus to achieve a reasonable air flow rate the highest the ambient temperature, the highest will be the VVs opening at a given load.
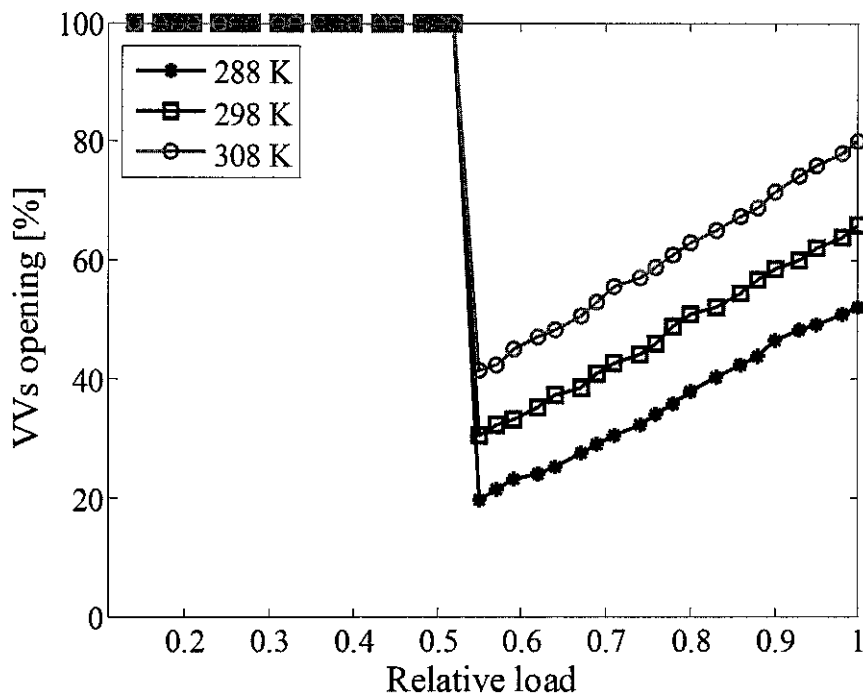
Figure 4.16 Variation of compressor VVs percentage opening with relative load for different ambient temperatures

Compressor pressure ratio variation with load for different ambient temperatures is indicated in Figure 4.17. In general for a constant speed shaft as ambient temperature decreases the corrected speed ($N/\sqrt{T}$) increases and the compressor will run in the high performance region. Thus, in the first mode of operation the one with the lowest ambient temperature will have the highest compressor pressure ratio as shown in Figure 4.17. But, in the second mode of operation to increase the turbine inlet temperature the VVs are closed partly depending on the load and the ambient temperature. This will force the compressor to operate in its low pressure ratio characteristic at low ambient temperature. Moreover, the gas turbine exhaust gas

101

temperature is dependent on the turbine inlet temperature and pressure ratio. The higher the pressure ratio, the smaller will be the exhaust gas temperature. Therefore, the lowest ambient temperature has the lowest pressure ratio at a given load as its turbine inlet temperature is the lowest.
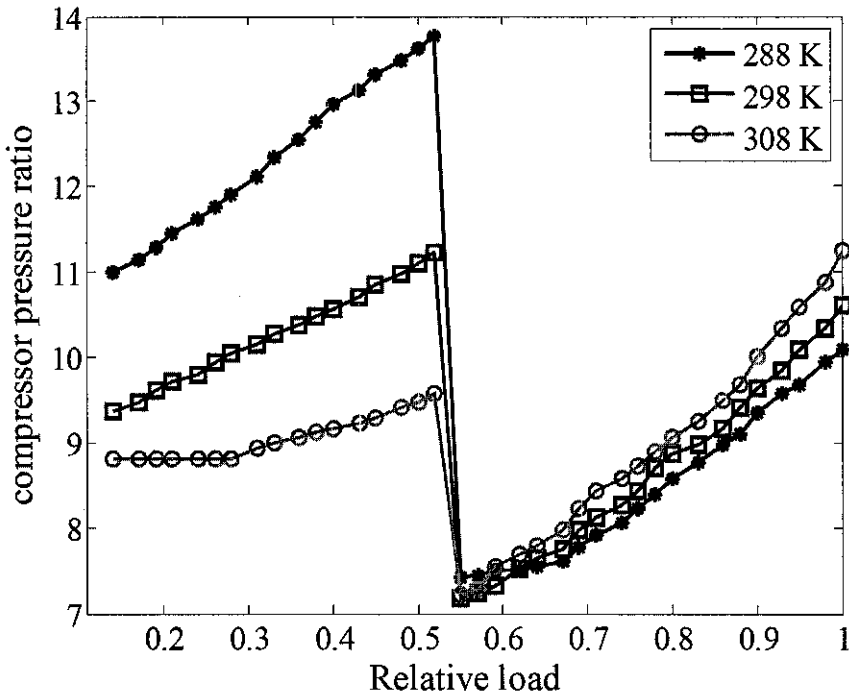
Figure 4.17 Variation of compressor pressure ratio with relative load for different ambient temperatures

The exhaust gas temperature variation for different ambient temperatures with respect to load is shown in Figure 4.18. In the first mode the gas turbine is running like a fixed geometry gas turbine hence the exhaust gas temperatures are increasing as the load increases. The higher the ambient temperature, the higher will be the corresponding exhaust gas temperature as its pressure is smaller at a given load. However, in the second mode the exhaust gas temperature is maintained at the set value by regulating the VVs closure.
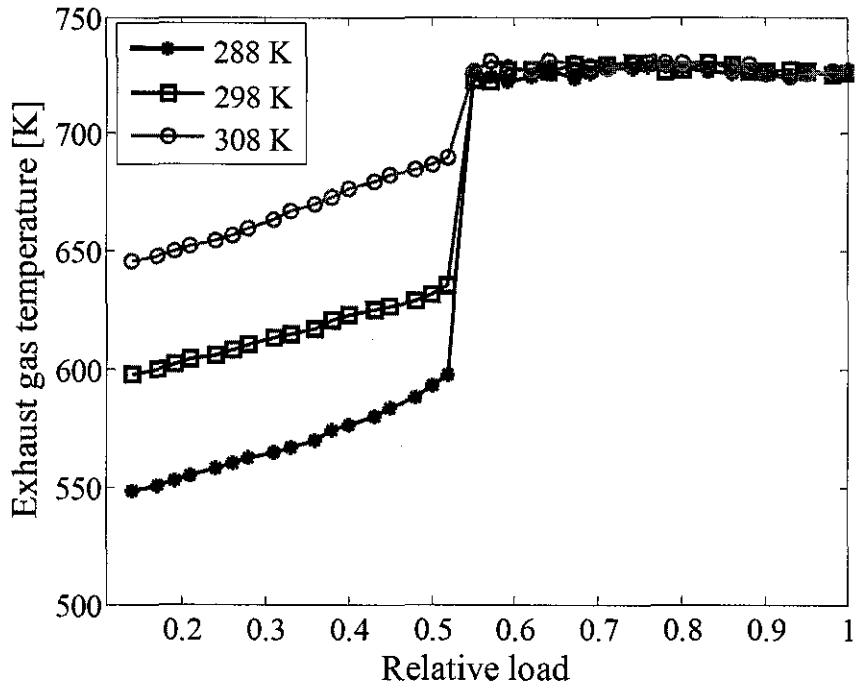
Figure 4.18 Variation of turbine exhaust gas temperatures with relative load for different ambient temperatures

The variation of the exhaust gas flow is shown in Figure 4.19. In general, the reduction in ambient temperature will result in an increase in the compressor corrected speed ($N/\sqrt{T}$). This in turn will increase the compressor inlet mass flow. In the first mode, the exhaust mass flow increases as the ambient temperature decreases at a given load. However, in the second mode since the flow is modulated using VVs the compressor is forced to run in the low performance region and hence the compressor flow rate is small even at the lowest ambient temperature. Furthermore, the lower the ambient temperature, the higher will be the VVs closure as justified in Figure 4.16. Consequently, the exhaust gas flow decreases as the ambient temperature decreases.
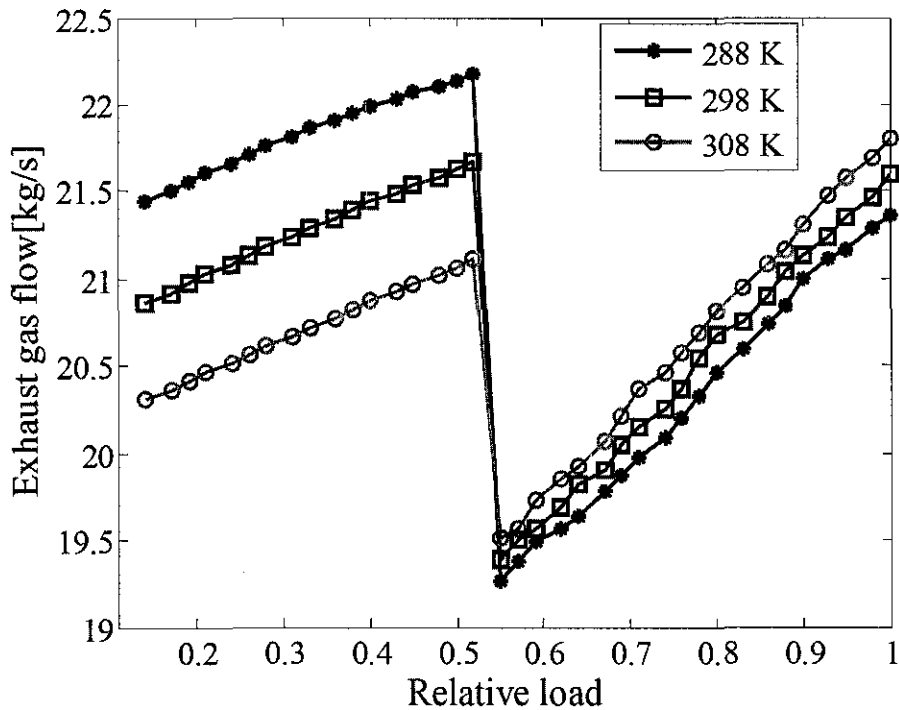
Figure 4.19 Variation of exhaust gas flow with relative load for different ambient temperatures

4.4.2 Effects on the gas turbine and its cogeneration performance

Figure 4.20 shows the thermal efficiency variation with respect to load for different ambient temperatures. As can be seen, in the first mode of operation the lower the ambient temperature, the higher will be the thermal efficiency at a given load. This is because the thermal efficiency is inversely proportional to compressor temperature ratio (for ideal Brayton cycle, $\eta_t = 1 - T_1/T_2$). In the second mode, the thermal efficiency of the highest ambient temperature is on the upper side and the one with the lowest temperature is on the bottom side at a given load. This is because the thermal efficiency is directly proportional to the pressure ratio and specific heat ratio of the compressor (for ideal Brayton cycle, $\eta_t = 1 - 1/(p_2/p_1)^{(\gamma-1)/\gamma}$). However, the efficiency variations are very small, as the compressor pressure ratios at a given load do show big differences.

104
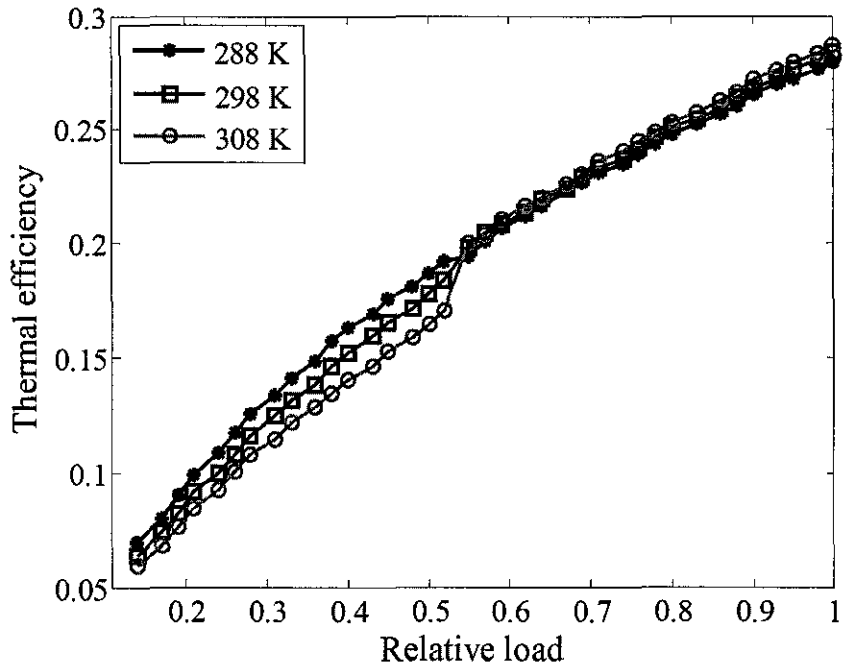
Figure 4.20 Gas turbine thermal efficiencies variation with relative load for different ambient temperatures

The effect of ambient temperatures on heat rate is indicated in Figure 4.21. The result is strongly influenced by the gas turbine operation. In order to reduce the gas turbine
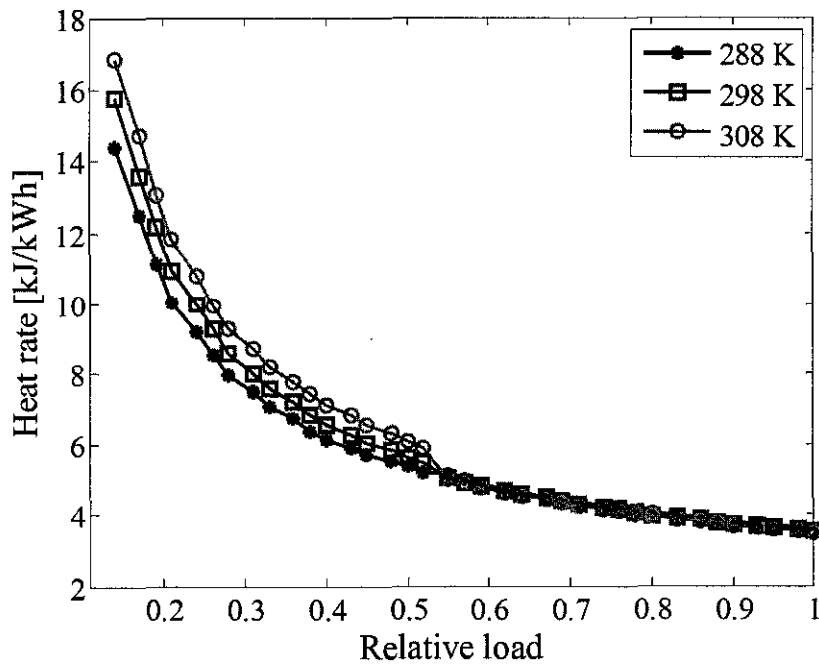
Figure 4.21 Variation of the cogeneration heat rate with relative load operation for different ambient temperatures

105

output below 50% load the fuel flow is regulated while VVs are fully opened. In this mode (Figure 4.15), the lower the ambient temperature, the lower will be the fuel consumption. Consequently the heat rate will be lower at lower ambient temperature at a given load. Whereas in the second mode both the fuel and mass flows are regulated accordingly to maintain turbine set value exhaust gas temperature. Therefore, the heat rate is almost the same at all ambient temperatures at a given load.

The gas turbine is operating in two modes. In the first mode, that is for load less than 50%, the exhaust gas temperature is not high enough for heat recovery. Therefore, the gas is diverted to the atmosphere through a by-pass chimney. Whereas in the second mode, that is for load greater than 50%, the diverter damper is regulated to control the exhaust gas flow entering into the HRSG according to the steam demand. Moreover, usually the engine is operated in the second mode. In order to examine the effect of ambient temperature on the HRSG performance the diverter damper is assumed fully opened. In addition to that, the design point data are used. These are 9 bar drum pressure, 90°C inlet temperature and 3% steam blowdown. Consequently, the total steam production rate and the efficiencies would vary only with part load and the variation is indicated in Figure 4.22. The lower the ambient temperature, the lower will be the exhaust gas flow rate, lowering the steam production rate at a given load.
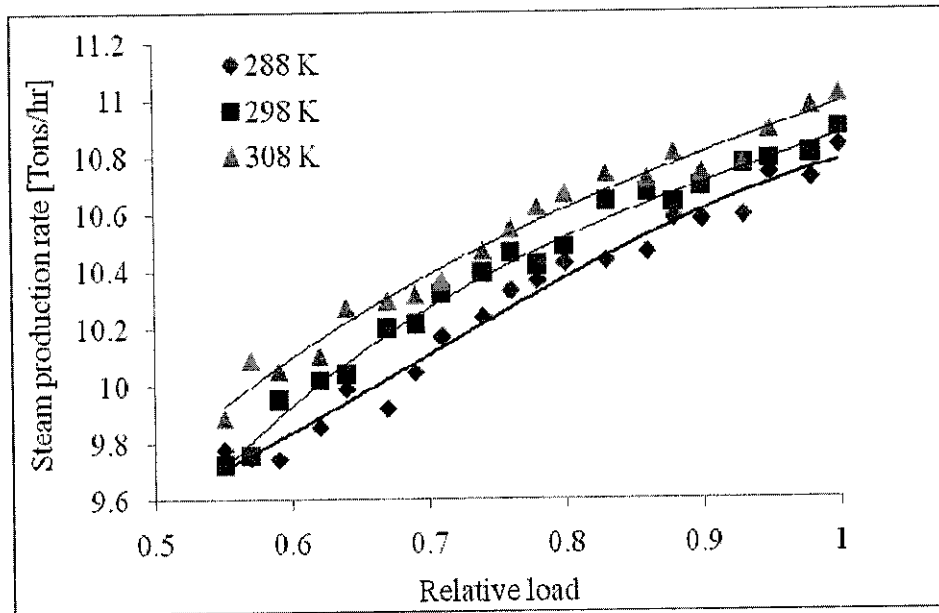
Figure 4.22 Variation of steam production rate with respect to relative load for different ambient temperatures

Hence, the higher ambient temperature will produce more steam than the lower ambient temperature. The higher ambient temperature gives higher HRSG efficiency at a given load as indicated in Figure 4.23, although the efficiency is decreasing with the increased part load.
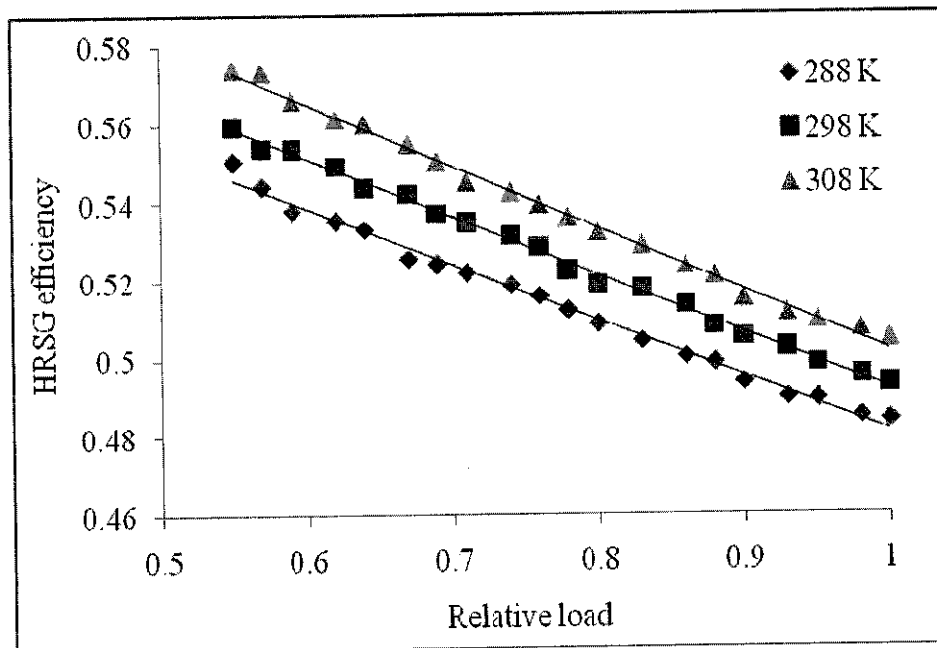
Figure 4.23 Variation of HRSG efficiency with respect to relative load for different ambient temperatures

The cogeneration performance with respect to part load for different ambient temperatures is indicated in Figure 4.24. The total cogeneration efficiency is a combined effect of the gas turbine and the HRSG efficiencies. In the second mode of operation, the thermal efficiency of the gas turbine is increasing whereas the HRSG efficiency is decreasing. Their combined effect would be almost constant total cogeneration efficiency. The HRSG performance is significant in the cogeneration total efficiency. Moreover, the lower the ambient temperature, the lower would be the total efficiency.
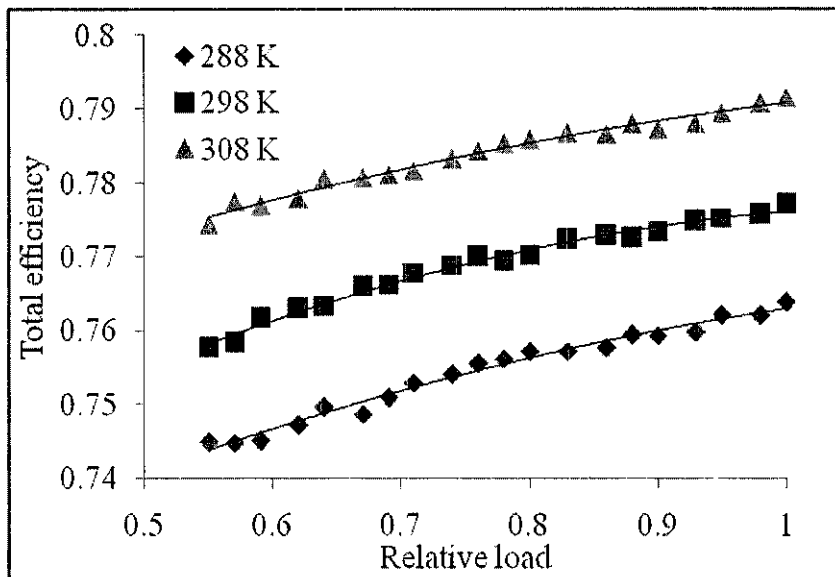
Figure 4.24 Variation of total efficiency with relative load for different ambient temperatures

How the cogeneration total efficiency related to the variation of the gas turbine thermal efficiency and HRSG efficiency at 308K ambient temperature is shown in Figure 4.25. The simulation shows that gas turbine thermal efficiency increases as the load increases whereas the HRSG efficiency declines. This is because higher heat input is used in the gas turbine to meet the power demand while the exhaust gas temperature remains constant. However, the total efficiency with respect to load almost remains constant.
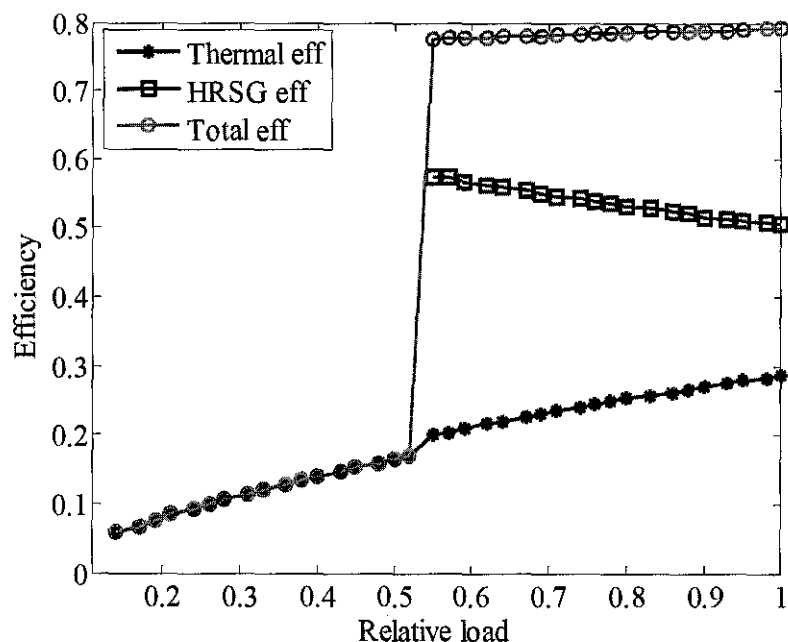
Figure 4.25 The variations of efficiencies with relative load at 308K

In general the aforementioned results trend comply with the results that are produced by the simulation and compared with actual data of Taurus 60S gas turbine based cogeneration plant in Section 4.3.1. In addition to that, the trends can be compared with published works. In the first mode of operation the likes of pressure ratio, fuel mass flow rate, and turbine exhaust gas temperature have similar trends with the fixed geometry gas turbine analytical model solution by Zhang and Cai [38] as shown in Figure 2.3. In the second mode of operation where the part load is greater than 50% and the VVs are modulated. The simulation results of the compressor pressure ratio, turbine inlet and exhaust temperatures, exhaust gas flow and thermal efficiency have similar trends with the results obtained experimentally by Jansen, et al. [47] that is shown in Figure 2.4.

4.5 Exergy Analysis of the Cogeneration Plant

Using the equations that are formulated in Section 3.4, the cogeneration plant as a whole and its components exergy destruction and second-law efficiency are evaluated. The analysis is useful to identify the system components that have high exergy destruction and its reasons. This would be helpful to improve plant's component efficiencies by reducing the exergy destruction within the component. In

the following discussion the first law efficiency is included for comparison purpose. An average tropical region restricted dead state reference condition of 30°C and 1 atm was used for the exergy analysis.

The variation of exergy destruction or the lost work rate in the compressor with respect to load is shown in Figure 4.26. In both modes of operation the exergy destruction rate is inversely proportional to the load. However, the exergy destruction rate at the beginning of the second mode increases as the VVs is repositioned to control the flow rate.
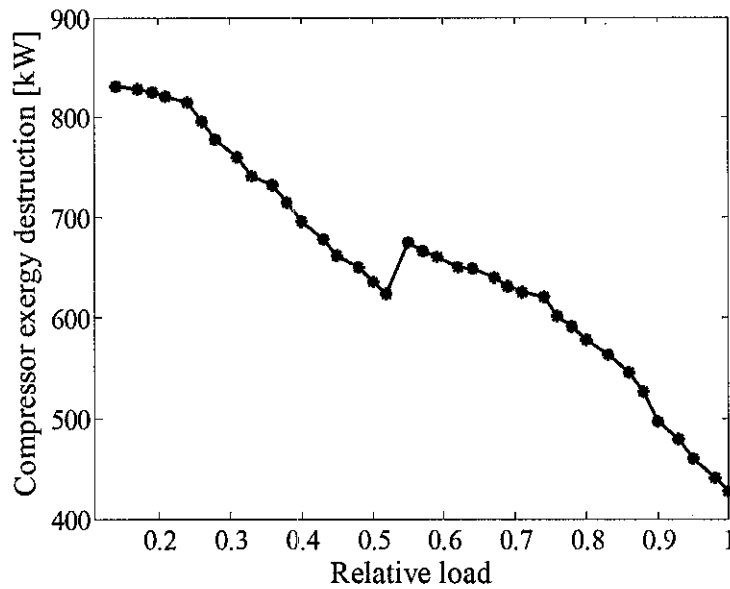
Figure 4.26 The variation of exergy destruction rate in the compressor versus relative load

As shown in Figure 4.27 both the isentropic and second law efficiencies of the compressor follow the same profile with respect to load. In the first mode of operation the efficiencies increase with load and around 50% load they drop suddenly. The reason is associated with the exergy destruction when VVs are modulated to maintain the exhaust gas temperature set value, after that again the efficiencies go on increasing. In general, VVs are useful to control the flow so that the exhaust gas temperature is maintained at the set value and the cogeneration plant performance is enhanced. However, they have also negative effect on the compressor efficiency which would also affect the subsequent components performance.

Figure 4.27 also shows that the second law efficiency is greater than the isentropic efficiency. This is because in the isentropic efficiency the useful minimum work input is calculated based on reversible and adiabatic compression that leads to another final state condition, whereas the second law efficiency calculation considers the actual initial and final states and assumes reversible compression. The useful minimum compression work input of the second law analysis is higher than the corresponding isentropic work input hence the second law efficiency is higher than its corresponding isentropic efficiency.
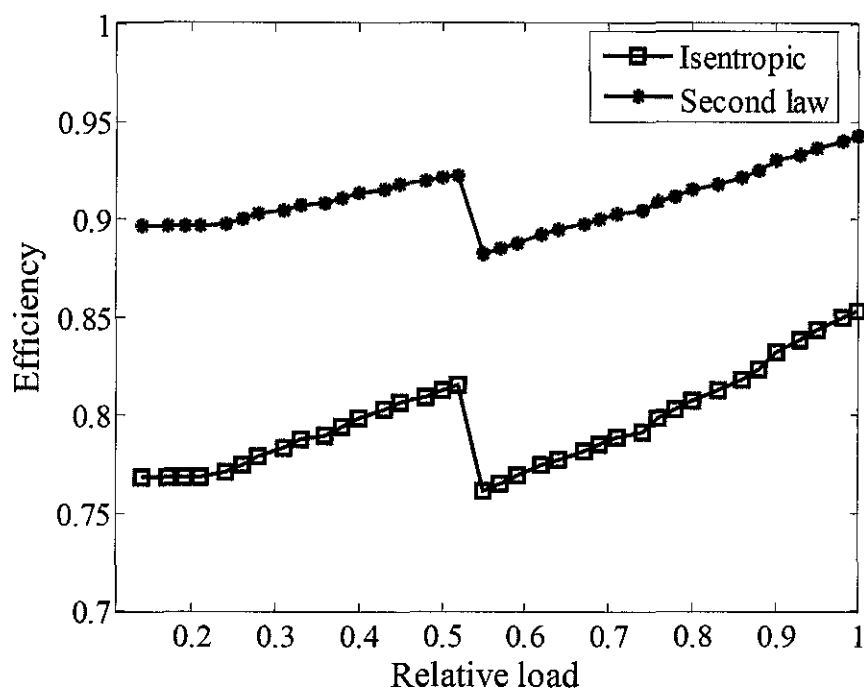
Figure 4.27 Variation of compressor isentropic and second law efficiencies with respect to relative load

The exergy destruction rate variation with respect to load is indicated in Figure 4.28. In general, the exergy destruction rate in the combustion chamber increases with load in the range of 50.6 to 63.7% of the overall system destruction rate, except the small variation during change of mode. The main causes for the exergy destruction are the chemical reaction and mixing of fluids at different temperatures. These are the mixing of the compressed air with fuel, and the burned gas with the excess air at the downstream of the combustor.
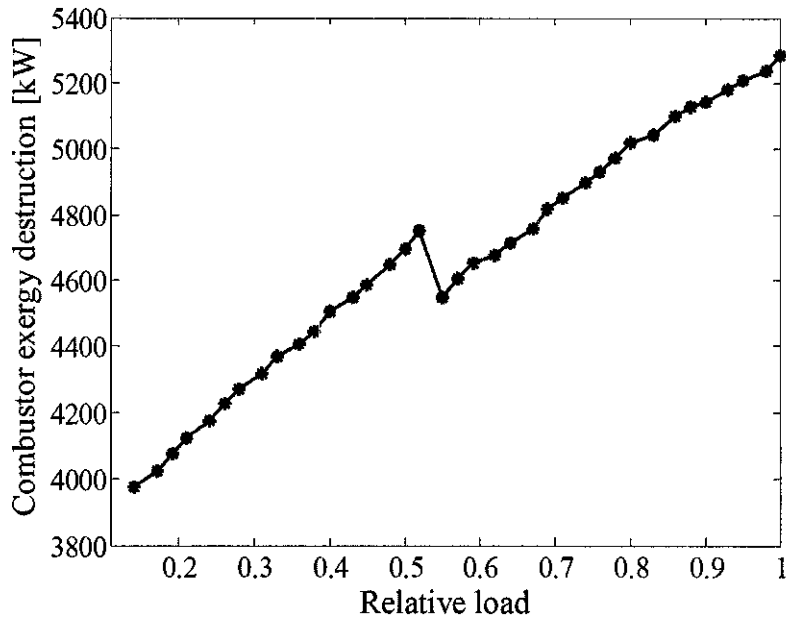
Figure 4.28 Combustion chamber exergy destruction variation with respect to relative load

As shown in Figure 4.29, the combustion chamber exergetic efficiency is increases as the load increases except for very small variation at 50% load. This variation is the consequence of the compressor VVs repositioning to control the air flow.
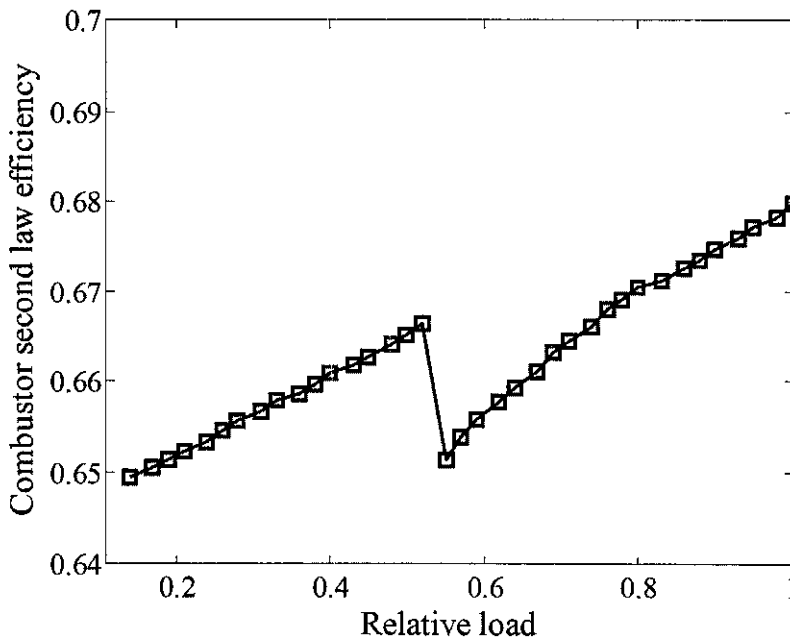
Figure 4.29 Variation of combustion exergetic efficiency with respect to relative load

As indicated in Figure 4.30 the turbine exergy destruction rate increases in both the first and second mode of operations but the rate of increment is slightly different. At the point where the mode of operation changes the exergy destruction rate decreases suddenly. The reason is the exergy destruction rate is proportional to the flow rate that is reduced in the compressor.
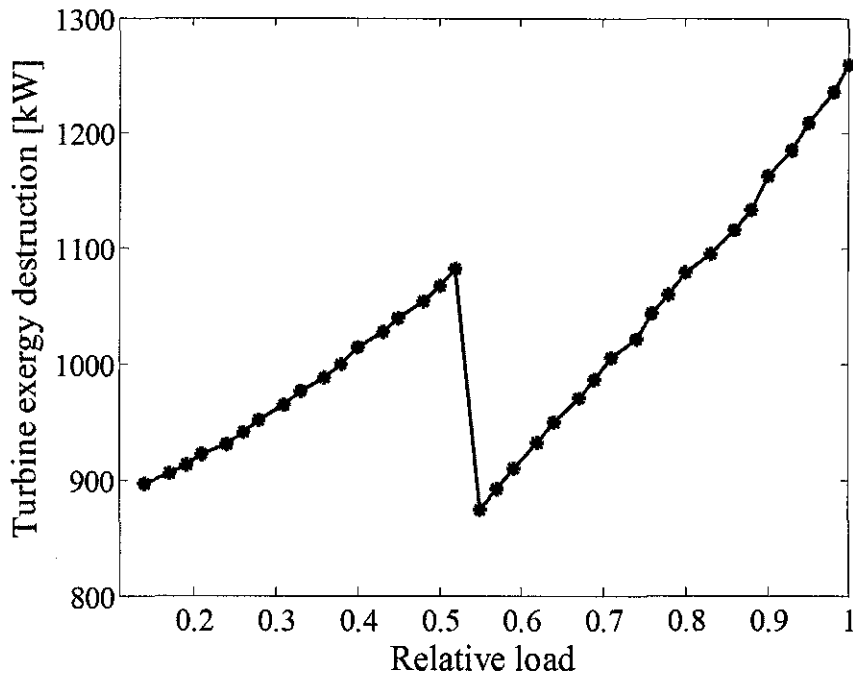
Figure 4.30 Variation of turbine exergy destruction with respect to relative load

The variation of the second law and first law efficiencies of the turbine is indicated in Figure 4.31. Almost both efficiencies have similar profile with respect to load. However, the second law efficiency is higher than the first law efficiency. The reason is in the isentropic expansion process the maximum useful work output is calculated assuming the process is reversible adiabatic that leads to another final state point that very much deviates from the real process. However, in the second law efficiency calculation, the assumption is reversible process with the same actual initial and final state points. In other words the optimum expansion work obtained using the second law analysis is less than the isentropic work output; hence the turbine second law efficiency is greater than its isentropic efficiency. Furthermore, the efficiencies are increasing in the first mode of operation but when the load is around 50% the efficiencies drop and then again start to increase. The efficiencies drop is the consequence of reduced mass flow rate in the compressor.

113
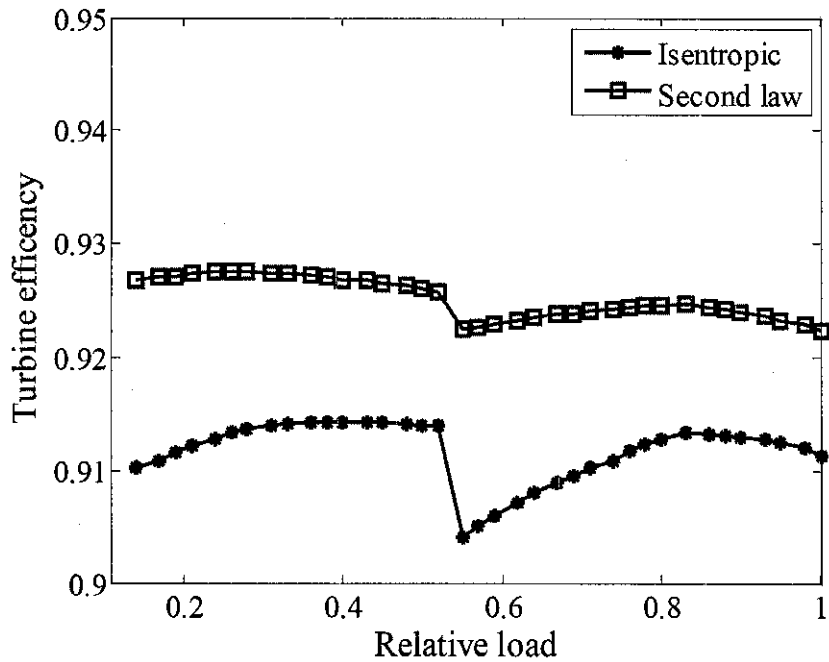
Figure 4.31 The variation of turbine efficiencies with respect to relative load

Figure 4.32 shows the exergy destruction rate variation in the HRSG with respect to load. It is clear that the exergy destruction rate is proportional to both exhaust gas flow and steam production rates. Moreover, these flows are increasing with load and hence the exergy destruction rate increases as the load increases. The HRSG exergy destruction rate shows some kind of fluctuation. This is because simulated exhaust gas temperatures are within the given error tolerance.
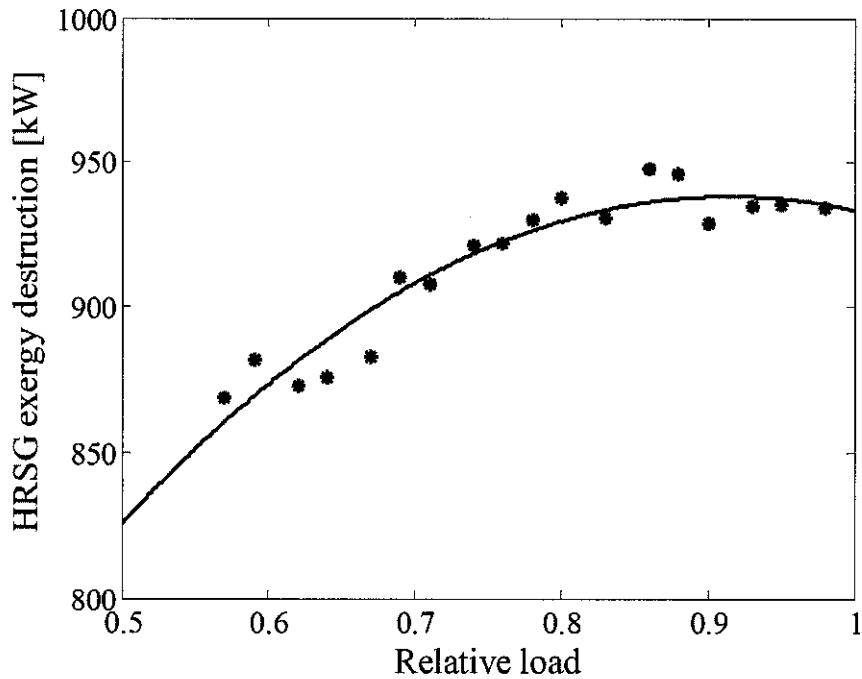
Figure 4.32 Variation of exergy destruction rate in the HRSG versus relative load

Figure 4.33 shows the performance of the HRSG. Its performance appears significantly more efficient based on the first law (energy) basis than on exergy basis. For example at full load 50% of the gas turbine exhaust heat content is transferred to the water/steam. However, the exergy analysis shows that the useful recovered exergy is only 16%, physically this discrepancy implies that the energy is degraded as it is transferred due to irreversibilities. An exergy analysis highlights this degradation and it complies with the second law of thermodynamics work is the valuable commodity of a power plant. Work can be completely and continuously converted to heat. However, heat cannot be completely converted to work in a thermodynamics cycle.
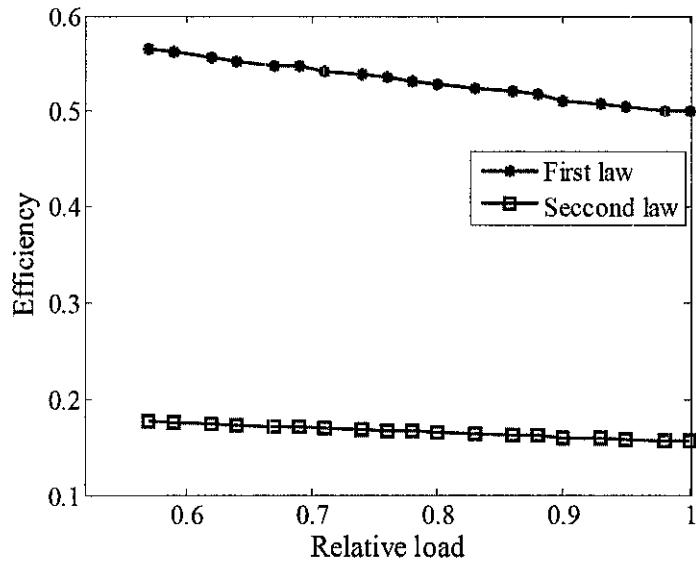
Figure 4.33 Variation of the HRSG first and second law efficiencies with respect to load

Figure 4.34 shows the exergy loss rate with the stack gas. The exergy loss rate with the stack gas is high in the first mode of operation. However, in the second mode of operation this loss rate dramatically decreases as the HRSG is used to recover heat from the exhaust gas before being rejected to the surroundings.
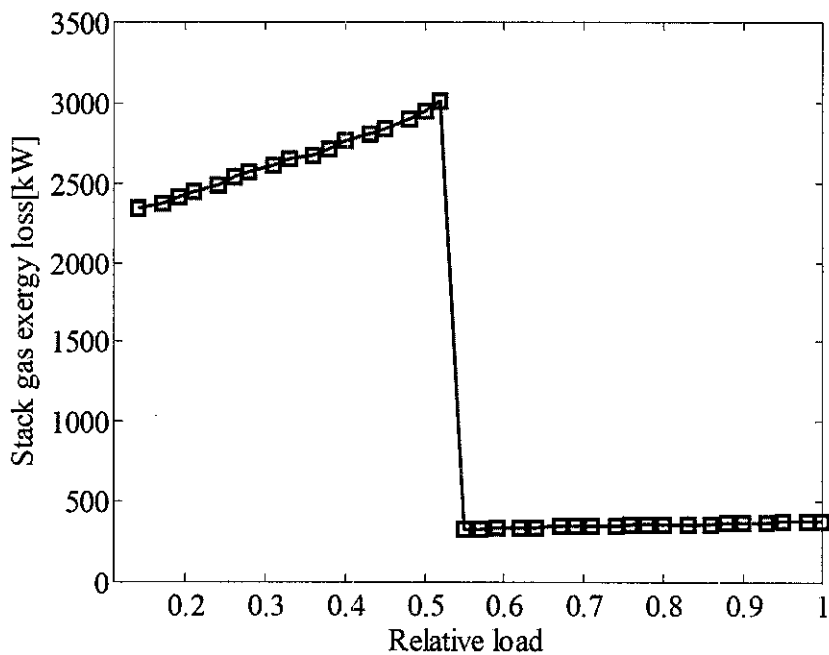
Figure 4.34 Variation of the stack gas exergy loss with respect to load

The cogeneration first and second law efficiencies are indicated in Figure 4.35. For above 50% load the first law efficiency almost remain constant at round 78.5%; whereas the second law efficiency keeps on increasing and reach around 45% at full load. These efficiencies are the sum of the gas turbine thermal efficiency and HRSG efficiency. However, the second-law efficiency of the cogeneration plant is less than its first-law efficiency for a given load.
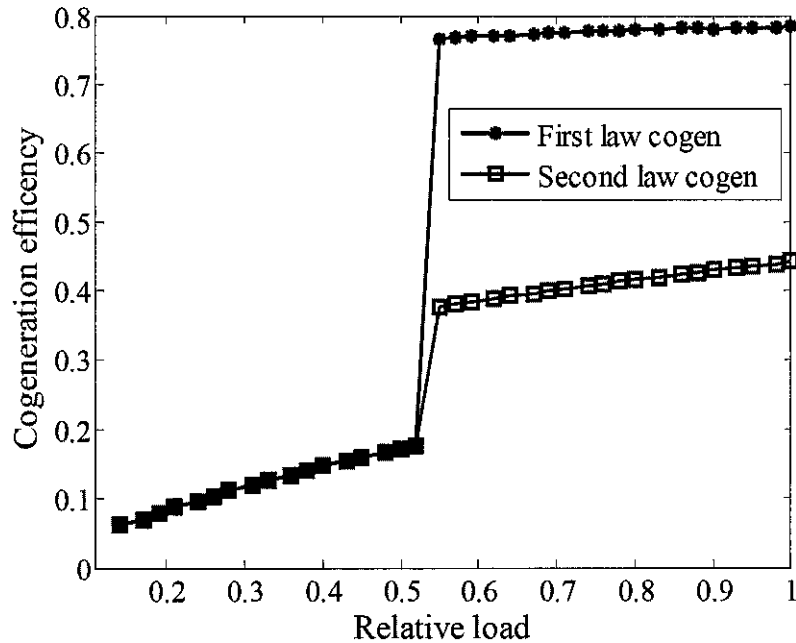
Figure 4.35 Variation of the cogeneration total efficiencies with respect to turbine load

This big discrepancy is mainly due to the difference in the evaluation method of the heat recovered from the HRSG. Furthermore, in the second law analysis the rate of heat recovered does not have the same value as the power. Since its equivalent exergy value is used which is much smaller than the heat value, the plant second law based efficiency is smaller than the first law based efficiency at a given load.

When the plant act as a simple gas turbine, the overall exergy destruction rate is shown in Figure 4.36. In both mode of operations the exergy destruction rate in the combustion chamber and the exhaust gas are responsible for the major exergy losses. For example at full load, the relative percentage exergy destruction in the combustion chamber is 47.9% and the loss with the exhaust gas is 36.7%. The remainder is being destroyed in the turbine and the compressor at 11.4% and 3.9%, respectively.

117
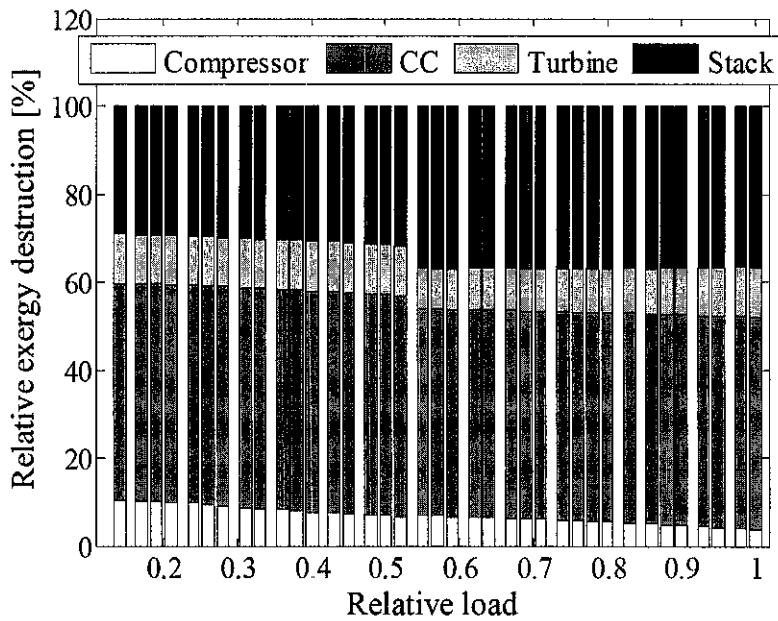
Figure 4.36 Variation of gas turbine components' relative percentage exergy destruction with respect to load

When the plant act as a cogeneration plant, in the first mode of operation the combustion chamber and the stack gas exergy destruction rates still remain the major contributors. While in the second mode of operation as indicated in Figure 4.37 the exergy destruction in the combustion chamber is the highest and the stack exergy loss is the smallest. The turbine, HRSG and compressor exergy destruction are being the second, the third and the fourth, respectively. For example at full load the exergy destructions in the combustion chamber, turbine, heat recovery, compressor and stack loss are 63.7, 15.2, 11.5, 5.2, and 4.5 %, respectively. In a nut shell, in the first mode of operation where the heat is not recovered the exergy loss with the stack gas is the second maximum. However, this loss drastically decreases in the second mode of operation because heat is recovered in the HRSG before rejected to the surroundings. Hence, this is the advantage of implementing a cogeneration plant that uses the waste heat to produce steam that would otherwise be rejected to the surroundings.
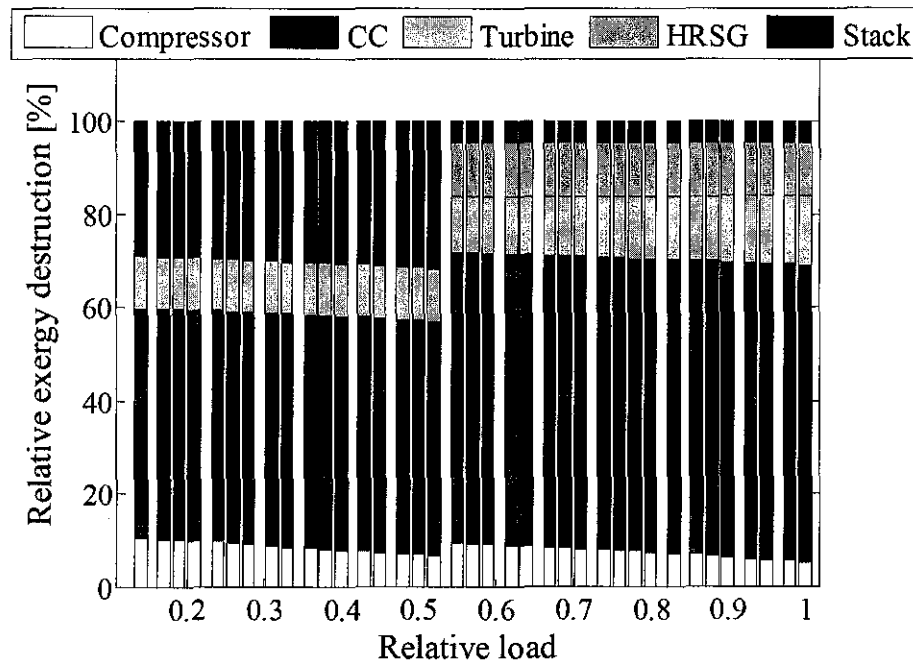
Figure 4.37 Variation of cogeneration components' relative percentage exergy destructions with respect to load

4.6 Summary

Computer simulation program based on mathematical model has been developed in MATLAB environment and used to study the performance of a cogeneration plant. The results of the developed mathematical model are compared with actual plant data. The discrepancies are quantified as errors and their statistical evaluation were carried out with Minitab software and found valid. The response of the cogeneration to different ambient temperatures is presented. The exergy destruction rate and second law efficiency of each component and the cogeneration itself were evaluated. From this study the following conclusions are drawn:

- Energy analyses do not thoroughly identify the location and cause of process inefficiencies, but exergy analyses could do.

- The major exergy destruction rate contributors are primarily high exergy consumptions in the combustion chamber and exhaust gas loss when there is no heat recovery.

- Efforts to increase the efficiency of the combustor and to recover the stack gas loss should be made to improve the overall performance of the plant.

CHAPTER 5

CONCLUSIONS AND RECOMMENDATIONS

5.1 Conclusions

A detail literature review is conducted on the general issues of a cogeneration plant in Chapter 2. It showed that there is a need to determine the performance of a cogeneration/gas turbine for different purposes. For instance, to predict the cogeneration plant or its components performance at the early development stage, or to examine in detail their off-design performance as they usually operate at part load conditions for a considerable part of their life time. Efforts are also continually required in order to improve the plant performance and increase both the power generation and fuel efficiency of the cogeneration plant. Hence, to identify where the major losses are occurring in the system and the equipments that have the potential for performance improvement and trends which may aid in the design of future plants, exergy analysis is useful. One method to solve the aforementioned issues is experimental; however, this method is expensive and time consuming. Another option is mathematical modeling using computational techniques that is considered to be the most economical solution. Other uses of mathematical modeling of the cogeneration plant are:

- To check and confirm projected engine performance data provided by the engine manufacturer while the engine is still in the design and test phase.
- To assess the effect of climate conditions on the plant performance before installation.
- Sensitivity analyses for change of parameters.
- To assess engine performance for healthy monitoring purpose.

The methodology used for mathematical modeling depends on the availability of components data. The methods that have been used to predict the performance of variable geometry gas turbine engine are stage by stage and row by row. However, these methods require intensive stage performance data or geometric characteristics of the components which are proprietary of the manufacturers. If the component maps are known it is possible to use component map matching method. However, again detailed performance maps are not usually available and this method is useful only for fixed geometry gas turbine based cogeneration plant. Therefore, a new methodology is developed that require minimum input data that accommodate compressor bleeding and VVs repositioning. The method is based on modified component map matching method. The developed model is used for performance prediction, ambient temperature effect, and exergetic analyses of the cogeneration plant working under tropical climate conditions.

Modeling of a cogeneration plant depends on its component model. The most difficult component is the compressor as it consists of variable geometry vanes and modulates the air flow to achieve the required turbine exhaust gas temperature. In order to accommodate this effect correlations in Section 3.3.2.2 are developed and at any VVs percentage opening the nominal map parameters are multiplied by their respective correction coefficients. During low part load operation air is bled at the downstream of the compressor to avoid surge formation. To determine the amount of air bleed at a given part load a correlation is developed in the same Section 3.3.2.2 and evaluated in Section 4.3.1.

Using the simulation model performance prediction is carried out and compared with the available actual data in Section 4.3.1. Comparison of each simulation output is not shown due to unavailability of complete data however those compared have shown good agreement. This is because the error statistical evaluation has shown that the values of the errors (difference between the actual and simulated data) mean and standard deviation of the pressure ratio, fuel consumption rate, VVs percentage opening, and steam generation rate are (0.03392, 0.30329), (0.00256, 0.00932), (-0.9335, 1.27830) and (0.4558, 0.3347), respectively. The detail is included in Section 4.3.2.

The effect of ambient temperature analysis on the cogeneration plant is shown in Section 4.4.2. In general, it is found that the smaller the ambient temperature, the better is the gas turbine performance in the first mode of operation. For instance, at 50% load the thermal efficiencies of the gas turbine at 35°C, 25°C and 15°C are 0.171, 0.183 and 0.192, respectively. However, in the second mode of operation for the given ambient temperatures the gas turbine thermal efficiency is almost the same, whereas the HRSG performance is higher at higher ambient temperature. This is because in the second mode of operation the VVs is modulated to maintain the turbine exhaust gas temperature. Consequently, in this mode the overall performance of the cogeneration plant is higher at higher ambient temperature. For instance, at full load, the cogeneration efficiencies of the cogeneration plant at 35°C, 25°C and 15°C are 0.792, 0.777 and 0.764, respectively.

To identify the potential component/s that has/have high margin of performance improvement, exergy analysis is carried out in Section 4.5. It is found that the major exergy destruction rate contributors are primarily high exergy consumptions in the combustion chamber and exhaust gas loss at no heat recovery. At 50% load the percentage exergy destruction rates in the compressor, turbine and exergy loss with the stack gas are 6.98, 47.08, 9.05 and 36.89, respectively. At full load, the exergy destruction rates in the combustion chamber, turbine, heat recovery, compressor and stack gas loss are 63.7, 15.2, 11.5, 5.2, and 4.5 %, respectively. Thus, attention should be given to decrease the exergy destruction rate in the combustion chamber and to recover the energy loss with the stack gas in the first mode of operation.

Therefore, to address the objective of this research a mathematical model of a cogeneration plant is developed and validated using statistical techniques in a tropical region. Simulations are carried out to analyse its energy and exergy performance both at design and off-design points under steady state condition. Compared to the stage by stage and row by row methods, the developed method requires minimum inputs to model the plant. The desired model and simulation is capable of simulating engine operation over a wide range of operating conditions. The prediction of a cogeneration plant performance is advanced by developing a mathematical model and computer simulation. The development effort and results

are documented herein. This dissertation provided a description of the various components models required to describe the working principle of a cogeneration plant. Validation of the simulation model is conducted using available data sets obtained from Taurus 60S gas turbine based cogeneration plant.

5.2 Research Contributions

Based on these efforts and results, it is concluded that the model and simualtion methodology represents a new capablity in gas turbine/cogeneration plant modeling. The contributions of this research include:

- Determining the design point of the components of the gas turbine engine.
- Modeling the amount of air bleed at the down stream of the compressor in the first mode of operation,i.e., part load less than 50%.
- Modeling the compressor variable vanes effect using experimental and simulated data in the second mode of operation, i.e., above 50% part load.
- Assembling the components' models to a full plant model to get a simualtion model of a cogeneration plant that provides operational capablities for steady state gas turbine/cogeneration plant operation.
- The exergy analysis could contribute some original information on the role of part load operation which will be useful in the design of a cogeneration plant.

Previous researchers have focused their effort on developing mostly on fixed geometry compressor based gas turbine/cogeneration plant. There are also models that can accommodate variable geometry compressor effect. However, these methods require detailed geometric dimensions and stage characteristics which are not usually available. To overcome the unavailability of detailed data, this study has developed a new method that needs minimum input data. This is done by modifying the existing component matching method to accommodate variable geometry compressor. Hence it has introduced variable geometry compressor model simulation capability. The model and simulation can supplement experimental efforts and provides a test bed for what if studies that would not be economically affordable if done experimentally.

5.3 Recommendations

The gas turbine/cogeneration plant model and simulation are created and validated against actual data sets obtained from real plant. As with any modeling and simulation there are certain assumptions and limitations placed on the model and the resulting simulation that limits the capability of the prediction. These limitations could be removed and further improvements could be made to facilitate applications to future gas turbine/cogeneration plant. The following recommendations for future work are, therefore, listed as a mean to broaden the scope and viability of the model.

- Multiple configurations: the model should be extended to include twin shaft gas turbine based cogeneration plant.

- Additional component models: Second level component models should be incorporated into this model to enhance its usability. For example, heat transfer models for the compressor, the combustor and the turbine.

- Transient analysis: The model developed does not predict start up and shutdown scenarios. Therefore, noting steady state model is an input to the transient analysis, this study should be extended to the transient analyses.

REFERENCES

[1]   T. Korakianitis, J. Grantstrom, P. Wassingbo, and A. F. Massardo, "Parametric performance of combined-cogeneration power plants with various power and efficiency enhancements," *ASME Journal of Engineering for Gas Turbines and Power,* vol. 127, pp. 65-72, 2005.

[2]   C. Strickland and J. Nyboer, "A review of existing cogeneration facilities in Canada, Simon Fraser University," 2004.

[3]   "Combined heat and power: a federal manager's resource guide final report," Aspen Systems Corporation and Applied Management Sciences Group 2000.

[4]   I.P.Koronakis, "CO-GENERATION, in Air Conditioning - Energy Consumption and Environmental Quality, [Ed. Matheos Santamouris], in Encyclopedia of Life Support Systems (EOLSS), Developed under the Auspices of the UNESCO," Oxford, UK: Eolss Publishers, 2004.

[5]   N. C. S. John, "Cogeneration potential in Canada: phase two," MK Jaccard and Associates 2002.

[6]   "A guide to cogeneration," The European Association for the Promotion of Cogeneration 2001.

[7]   A. Martens, "The energetic feasibility of CHP compared to the separate production of heat and power," *Applied Thermal Engineering,* vol. 18, pp. 935-946, 1998.

[8]   "The World's first industrial gas turbine set," The American Society of Mechanical Engineers, Neuchatel, Switzerland 1988.

[9]   L. S. Langston and J. George Opdyke, "Introduction to gas turbines for non-engineers." vol. 37: Global Gas Turbine News, 1997.

[10]   "Thermal energy equipment: cogeneration," United Nations Environment Programme 2006.

[11]   F. Hou, "Development of a neural network fault diagnostic system for gas turbine engine," Cranfield university, 2007.

[12]   C. Bringhenti and J. R. Barbosa, "Methodology for gas turbine performance improvement using variable-geometry compressors and turbines," *Power and Energy Proc. Instn. Mechanical Engineers,* vol. 218, pp. 541-549, 2004.

[13]   H. Cohen, G. Rogers, and H. Saravanamuttoo, *Gas turbine theory,* 5th Edition ed. London: Longman, 2001.

[14]   Q. Z. Al-Hamadan and M. S. Y. Ebaid, "Modeling and simulation of a gas turbine engine for power generation," *ASME Journal of Engineering for Gas Turbines and Power,* vol. 128, 2006.

[15]   T. S. Kim and S. H. Hwang, "Part load performance analysis of recuperated gas turbines considering engine configuration and operation strategy," *Energy,* vol. 31, pp. 260-277, 2006.

[16]   R. F. Boehm, *Design analysis of thermal systems.* New York: John Wiley & Sons, Inc, 1987.

[17]   R. F. Boehm, *Developments in the design of thermal systems*: Cambridge University Press, 1997.

[18]   F. Haglind and B. Elmegaard, "Methodologies for predicting the part-load performance of aero-derivative gas turbines," *Energy,* vol. 34, pp. 1484–1492, 2009.

[19]   D. E. Muir, H. I. H. Saravanamuttoo, and D. J. Marshall, "Health monitoring of variable geometry gas turbines for the Canadian Navy," *ASME Journal of Engineering for Gas Turbines and Power,* vol. 111, pp. 244-250, 1989.

[20]   D. E. Muir, B. Eng., and P. Eng., "Axial flow compressor modeling for engine health monitoring studies," in *Department of Mechanical Engineering and Aeronautical Engineering* Ottawa, Ontario: Carleton University, 1988.

[21]   M. Schobeiri, *Turbomachinery flow physics and dynamic performance.* Berlin Springer, 2005.

[22]   L. H. Fishbach and R. W. Koenig, "GENENG II- A Program for calculating design and off-design performance of two- and three-spool turbofans with as many as three nozzles engines," NASA Lewis 1972.

[23]   R. W. Koenig and L. H. Fishbach, "GENENG - A program for calculating design and off-design performance for turbojet and turbofan engines," NASA Lewis 1972.

[24]   M. R. S. Okelah, "Optimization of the design parameters of a co-turboshaft gas turbine engine as a heavy equipment power plant," PhD thesis, Ottawa Ontario: Carleton University, 1980.

[25]   C. Riegler, M. Bauer, and J. Kurzke, "Some aspects of modeling compressor behavior in gas turbine performance calculations," *ASME Journal of Engineering for Gas Turbines and Power,* vol. 23 pp. 372-378, 2001.

[26]   R. J. Steinke, "STGSTK - A computer code for predicting multistage axial-flow compressor performance by meanline stage-stacking method," NASA Lewis 1982.

[27]   M. S. Attia, "Development of axial compressor and turbine simulation modules for integration into the dynamic simulation code GETRAN," PhD Thesis, Texas A&M University, 1995.

[28]   J. D. Mattingly, *Elements of propulsion: gas turbines and rockets.* Virginia: American Institute of Aeronautics and Astronautics, Inc., 2006.

[29]   P. P. Walsh and P. Fletcher, *Gas turbine performance,* 2nd ed. London: Blackwell Science Ltd., 2004.

[30]   J. H. Horlock, *Advanced gas turbine cycles.* Cambridge, UK: Pergamon, 2003.

[31]   M. P. Boyce, *Gas turbine engineering handbook*, 2nd ed.: Gulf Professional Publishing, 2002.

[32]   S. L. Dixons, *Fluid mechanics, thermodynamics of turbomachinery*, 5th ed. London: Elsevier Butterworth–Heinemann, 2004.

[33]   D. H. Frost, *A streamline curvature through flow computer program for analysing the flow-through axial flow turbomachines*: National Gas Turbine Establishment, 1970.

[34]   K. M. Boyer, "An improved streamline curvature approach for off-design analysis of transonic compression systems," in *Department of Mechanical Engineering*: Virginia Polytechnic Institute and State University, 2001.

[35]   M. W. McBride, "The design and analysis of turbomachinery in an incompressible, steady flow using the streamline curvature method," 1979.

[36]   V. Pachidis, P. Pilidis, I. Templalexis, T. Korakianitis, and P. Kotsiopoulos, "Prediction of engine performance under compressor inlet flow distortion using streamline curvature," *ASME Journal of Engineering for Gas Turbines and Power,* vol. 129, pp. 87-103, 2007.

[37]   Q. Z. Al-Hamadan and M. S. Y. Ebaid, "Modelling and simulation of a gas turbine engine for power generation," *ASME Journal of Engineering for Gas Turbines and Power,* vol. 128, pp. 302-310, 2006.

[38]   N. Zhang and R. Cai, "Analytical solutions and typical characteristics of part-load performances of a single shaft gas turbine and its cogeneration," *Energy Conversion and Management,* vol. 43, pp. 1323-1337, 2002.

[39]   W. Wang, R. Cai, and N. Zhang, "General characteristics of single shaft microturbine set at variable speed operation and its optimization," *Applied Thermal Engineering,* vol. 24, pp. 1851-1863, 2004.

[40] Y. S. H. Najjar, "Comparison of performance for cogeneration systems using single or twin shaft gas turbine engines," *Applied Thermal Engineering,* vol. 17, pp. 113-124, 1997.

[41] J. F. Sellers and C. J. Daniele, "DYNGEN - A program for calculating steady state and transient performance of turbojet and turbofan engines," NASA Lewis 1975.

[42] S. M. Jones, "An Introduction to thermodynamic performance analysis of aircraft gas turbine engine cycles using the numerical propulsion system simulation code," NASA/TM 2007.

[43] J. H. Kim, T. S. Kim, J. L. Sohn, and S. T. Ro, "Comparative analysis of off-design performance characteristics of single and two shaft industrial gas turbines," *ASME Journal of Engineering for Gas Turbines and Power,* vol. 125, pp. 954-960, 2003.

[44] N. WEI, "Significance of loss models in aerothermodynamic simulation for axial turbines," in *Department of Energy Technology Division of Heat and Power Technology.* vol. PhD: Royal Institute of Technology, 2000.

[45] D. G. Ainley and G. C. R. Mathieson, "A method of performance estimation for axial-flow turbines," Ministry of Supply, London 1957.

[46] T. S. Kim, "Comparative analysis on the part load performance of combined cycle plants considering design performance and power control strategy," *Energy,* vol. 29, pp. 71–85, 2004.

[47] M. Jansen, T. Schulenberg, and D. Waldinger, "Shop test result of the V64.3 gas turbine," *ASME Journal of Engineering for Gas Turbines and Power,* vol. 114, pp. 676–681, 1992.

[48] V. Dorer, "Review of existing residential cogeneration systems performance assessments and evaluations," The International Energy Agency 2007.

[49]   Y. A. Çengel and M. A. Boles, *Thermodynamics: An engineering approach*, 5th ed.: McGraw-Hill, 2006.

[50]   M. J. Moran and E. Sciubba, "Exergy analysis: principles and practice," *ASME Journal of Engineering for Gas Turbines and Power*, vol. 116, pp. 285-290, 1994.

[51]   M. J. Moran and H. N. Shapiro, *Fundamentals of engineering thermodynamics*, 3rd ed. New York: John Wiley and Sons, Inc., 2006.

[52]   A. Bejan, G. Tsatsaronis, and M. Moran, *Thermal design and optimization*: Wiley-IEEE, 1996.

[53]   K. Annamalai and I. K. Puri, *Advanced thermodynamics engineering*. New York: CRC PRESS, 2002.

[54]   I. Hussein, M. H. Mustaffa, M. Z. Yuoff, and M. H. Bosrooh, "Exergy coasting for thermal plant optimization," in *Proceedings of the 3rd Technical Conference* 6-8 August 2001, UNITEN, 2001.

[55]   F. F. Huang, "Performance evaluation of selected combustion gas turbine cogeneration systems based on first and second-law analysis," *ASME Journal of Engineering for Gas Turbines and Power*, vol. 112, pp. 117-21, 1990.

[56]   J. H. Horlock, J. B. Young, and G. Manfrida, "Exergy analysis of modern fossil-fuel power plants," *Journal of Engineering for Gas Turbines and Power*, vol. 122, pp. 1-7, 2000.

[57]   G. P. Verkhivker and B. V. Kosoy, "On the exergy analysis of power plants," *Energy Conversion and Management*, vol. 42, pp. 2053-2059, 2001.

[58]   J. Zheng, F. Sun, L. Chen, and C. Wu., "Exergy analysis for a Braysson cycle," *Exergy an International Journal*, vol. 1, pp. 41-45, 2001.

[59]   T. W. Song, J. L. Sohn, J. H. Kim, T.S.Kim, and S. T. Ro, "Exergy-based performance analysis of the heavy-duty gas turbine in part-load operating conditions," *Exergy an International Journal*, vol. 2, pp. 105-112, 2002.

[60] C. J. Butcher and B. V. Reddy, "Second law analysis of a waste heat recovery based power generation system," *International Journal of Heat and Mass Transfer*, vol. 50, pp. 2355–2363, 2007.

[61] S.-D. Oh, H.-S. Pang, S.-M. Kim, and H.-Y. Kwak, "Exergy analysis for a turbine cogeneration system," *ASME Journal of Engineering for Gas Turbines and Power*, vol. 118, pp. 782-791, 1996.

[62] B. Facchini, D. Fiaschi, and G. Manfrida, "Exergy analysis of combined cycles using latest generation gas turbines," *ASME Journal of Engineering for Gas Turbines and Power*, vol. 122 pp. 233- 238, 2000.

[63] D.-C. Sue and C.-C. Chuang, "Engineering design and exergy analyses for combustion gas turbine based power generation system," *Energy*, vol. 29, pp. 1183–1205, 2004.

[64] I. Hussein, M. Z. Yuoff, and M. H. Bosrooh, "Exergy analysis of a 120 MW thermal power plant," in *Proceedings of the BSME-ASME International Conference on thermal Engineering* 31st December 2001, Dhaka, Bangladesh.

[65] M. Kanoglu, I. Dincer, and M. A. Rosen, "Understanding energy and exergy efficiencies for improved energy management in power plants," *Energy Policy*, vol. 35, pp. 3967-3978, 2007.

[66] A. Abusoglu and M. Kanoglu, "First and second law analysis of diesel engine powered cogeneration systems," *Energy Conversion and Management*, vol. 49 pp. 2026–2031, 2008.

[67] M. Kanoglu and I. Dincer, "Performance assessment of cogeneration plants," *Energy Conversion and Management*, vol. 50, pp. 76–81, 2009.

[68] "Solar Technical Training, Engine performance curves," UTP Cogeneration/District Cooling Project 2001.

[69] F. J. Brooks, "GE Gas turbine performance characteristics " GE Power Systems, New York.

131

[70]   I. J. Nickerson, "A parametric study of gas turbine cycles for electrical power generation," Canada: Master thesis, Carleton University, 1991.

[71]   G. L. Converse and R. G. Giffin, "Extended parametric representation of compressor fans and turbines," NASA Lewis 1984.

[72]   G. L. Converse, "Extended parametric representation of compressor fans and turbines," NASA Lewis 1984.

[73]   A. M. Y. Razak, *Industrial gas turbines performance and operability*: Taylor & Francis Group, 2007.

[74]   F. M. Odom, "Performance evaluation of gas turbine engines," Solar Turbines 1993.

[75]   P. Wirkowski, "Modelling the characteristics of axial compressor of variable flow passage geometry working in the gas turbine engine system," *Polish Maritime Research 3 (53)*, vol. 14, pp. 27-32, 2007.

[76]   "Installation and maintenance instructions," UTP Cogeneration/District Cooling Project 2001.

[77]   "Illustrated Parts List power generation Taurus™ 60S gas turbine-driven generator set." vol. IV: GDC/Shinryo UTP Co-Generation Project, 2001.

[78]   "UTP GDC plant daily operation data for 2009 " UTP Gas District Cooling Plant

[79]   J. H. Horlock, "Combined power plants present, and future past," *ASME Journal of Engineering for Gas Turbines and Power,* vol. 117, pp. 608-616, 1995.

[80]   "General description of system plant," UTP Cogeneration/District Cooling Project 2001.

[81]   B. Olav, "Thermal power generation," Department of energy and process engineering-NTNU 2009.

[82] "Boiler steam and water systems, Available at http://canteach.candu.org/library/20051209.pdf.", Accessed 5th October 2009.

[83] "Heat recovery steam generators," American Petroleum Institute 2005.

[84] V. Ganapathy, *Industrial boilers and heat recovery steam generators design, applications and calculations*. New York: Marcel Dekker Inc., 2003.

[85] N. Subrahmanyam, S. Rajaram, and N. Kamalanathan, "HRSGs for combined cycle power plants," *Heat Recovery Systems & CHP,* vol. 15, pp. 155-161, 1995.

[86] F. P. Incropera and D. P. Dewitt, *Introduction to heat transfer*, 4th ed.: Mc Graw-Hill, 2006.

[87] D. W. Sun, "Thermodynamic design data and optimum design maps for absorption refrigeration systems," *Applied Thermal Engineering,* vol. 17, pp. 211-221, 1996.

[88] R. E. Sonntag, *Fundamentals of thermodynamics*. New York: John Wiley & Sons Inc., 1998.

[89] Potter, Merle, and Somerton, *Schaum's outline of thermodynamics for engineers*, 2nd ed.: McGraw-Hill, 2006.

[90] J. Kiusalaas, *Numerical methods in engineering with Python*. New York: Cambridge University Press, 2005.

[91] "Meet MINITAB for Windows® Release 14," 2003.

Appendix A: Basic Equations Derivation

A.1 Derivation of the First Law of Thermodynamics for a Control Volume

Consider an arbitrary control volume having single inlet and exit as shown in Figure A.1. It is interacting work and heat with the surroundings.

(a)   (b)
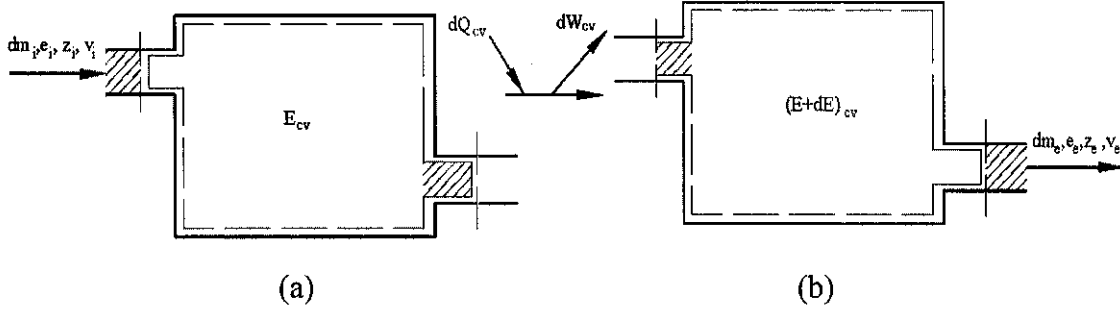
Figure A.1 Schematic representation of arbitrary control volume (a) at time t; and (b) at time $t+dt$

Applying the conservation of energy to the control volume, the change of total energy in the control volume between time t and $t+dt$ is equal to the energy in minus the energy out. This is mathematically represented as:

$$dE = [dQ + e_i dm_i + p_i v_i dm_i] - [dW + e_e dm_e + p_e v_e dm_e] \qquad \text{(A.1)}$$

where $e = u + \dfrac{V^2}{2} + z$.

Substituting this into Eq. (A.1) gives:

$$dE = [dQ + (u_i + V_i^2/2 + gz_i)dm_i + p_i v_i dm_i] - [dW + (u_e + V_2^2/2 + gz_e)dm_e + p_e v_e dm_e] \quad \text{(A.2)}$$

$$dE = [dQ + (h_i)dm_i + (V_i^2/2 + gz_i)dm_i] - [dW + (h_e)dm_e + (V_e^2/2 + gz_e)dm_e] \qquad \text{(A.3)}$$

where $h = u + pv$.

Rearranging gives:

$$dQ - dW = dE + (h_e + V_e^2/2 + gz_e)dm_e - (h_i + V_i^2/2 + gz_i)dm_i \qquad \text{(A.4)}$$

Dividing by dt both sides gives:

$$\dot{Q}_{cv} - \dot{W}_{cv} = \frac{dE}{dt} + \dot{m}_e(h_e + \frac{V_e^2}{2} + gz_e) - \dot{m}_i(h_i + \frac{V_i^2}{2} + gz_i) \tag{A.5}$$

For steady state condition there is no property change with time. In addition to that the change in kinetic and potential energies are small compare to the enthalpy change therefore these terms are neglected and the first law simplified as:

$$\dot{Q}_{cv} - \dot{W}_{cv} = \dot{m}_e h_e - \dot{m}_i h_i \tag{A.6}$$

A.2   Relationships for Isentropic Process

Consider a compression process shown in Figure A.2. The isentropic compression process follows path 1-2s while the polytropic compression process follows path 1-2.
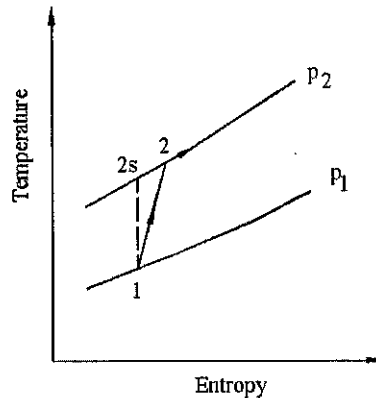
Figure A.2 An isentropic and polytropic compression processes

To find the isentropic processor relationship the derivation starts form the *T-ds* second equation, i.e.

$$Tds = dh - vdp \tag{A.7}$$

For isentropic process $Tds = 0$ and replacing $dh = c_p dT$ and using the state equation ($pv = RT$) and solving for specific volume and substituting these into Eq. (A.7) gives:

$$0 = c_{p,avg} \frac{dT}{T} - R \frac{dp}{p} \tag{A.8}$$

135

Integration gives;

$$\frac{p_2}{p_1} = \left(\frac{T_2}{T_1}\right)^{\frac{c_{p,avg}}{R}}$$ (A.9)

This equation can be simplified by introducing the specific heat ratio, γ and the fact that, $c_p - c_v = R$.

$$\frac{c_{p,avg}}{R} = \frac{c_{p,avg}}{c_{p,avg} - c_{v,avg}} = \frac{\gamma}{\gamma - 1}$$ (A.10)

Hence substituting this into Eq. (A.9) results:

$$\frac{p_2}{p_1} = \left(\frac{T_2}{T_1}\right)^{\frac{\gamma}{\gamma - 1}}$$ (A.11)

A.3   Relationships for Polytropic Process

The isentropic efficiency considers only the start and end states of the compression and expansion processes and pays no attention to the actual paths the compression and expansion processes take. Since the work is not a thermodynamic property and depends on the actual path, the polytropic analysis endeavours to account for the path taken during the compression and expansion processes in determining the actual work.

In a polytropic process, the compression or expansion process takes place in small steps. Calculating the work for the polytropic process involves the summation of the work for each step. The definition of polytropic efficiency is given as:

$$\eta_p = \frac{dh_s}{dh}$$ (A.12)

Applying the T-ds second equation, i.e.

$$Tds = dh_s - vdp$$ (A.13)

For isentropic process $Tds = 0$, i.e., $dh_s = vdp$ and replacing $dh = c_p dT$ gives,

136

$$\eta_p = \frac{vdp}{c_p dT} \tag{A.14}$$

Using the state equation ($pv = RT$) and solving for specific volume and substituting in Eq. (A.10) gives:

$$\eta_p = \frac{R\frac{1}{p}dp}{c_p\frac{1}{T}dT} \tag{A.15}$$

Integrating the expression gives the following equation.

$$\eta_p = \frac{R\int_1^2 \frac{1}{p}dp}{\int_1^2 c_p(T)\frac{1}{T}dT} = \frac{R}{c_{p,avg}}\frac{\ln\left(\frac{p_2}{p_1}\right)}{\ln\left(\frac{T_2}{T_1}\right)} \tag{A.16}$$

$$\eta_p = \frac{\gamma-1}{\gamma}\frac{\ln\left(\frac{p_2}{p_1}\right)}{\ln\left(\frac{T_2}{T_1}\right)} \tag{A.17}$$

Given the polytropic efficiency and pressure ratio, the compressor discharge temperature can be calculated from:

$$T_2 = T_1\left(\frac{P_2}{P_1}\right)^{\frac{\gamma-1}{\gamma}\frac{1}{\eta_p}} \tag{A.18}$$

Similarly, for an expansion process expanding from state 1 to 2, the polytropic efficiency is given by:

$$\eta_p = \frac{\ln\left(\frac{T_2}{T_1}\right)}{\left(\ln\left(\frac{p_2}{p_1}\right)\right)^{\frac{\gamma-1}{\gamma}}} \tag{A.19}$$

137

The expander (turbine) exit temperature is calculated from

$$T_2 = T_1 \left(\frac{p_2}{p_1} \right)^{\eta_p (\gamma - 1)/\gamma} \qquad\qquad (A.20)$$

Therefore the compressor isentropic efficiency is

$$\eta_c = \frac{\left(\dfrac{p_2}{p_1} \right)^{\frac{\gamma-1}{\gamma}} - 1}{\left(\dfrac{p_2}{p_1} \right)^{\frac{\gamma-1}{\gamma} \frac{1}{\eta_p}}} \qquad\qquad (A.21)$$

The turbine isentropic efficiency is

$$\eta_t = \frac{1 - \left(\dfrac{p_2}{p_1} \right)^{\eta_p (\gamma-1)/\gamma}}{1 - \left(\dfrac{p_2}{p_1} \right)^{(\gamma-1)/\gamma}} \qquad\qquad (A.22)$$

Appendix B: Published Literature Compressor and Turbine Raw Data

B.1 Published Literature Compressor Performance Map Raw Data [72]

Table B.1 Published compressor relative corrected speed data

0.3	0.4	0.5	0.6	0.7	0.8	0.9	1	1.1	1.2

Table B.2 Published literature compressor pressure ratio data at eleven points for each given relative speed

1.4875	1.4698	1.4522	1.4346	1.4171	1.3997	1.3819	1.3636	1.3447	1.3253	1.3053
2.2703	2.206	2.1421	2.0788	2.016	1.9539	1.89	1.8222	1.7508	1.6764	1.5993
3.1211	3.0303	2.9402	2.8509	2.7623	2.6746	2.5843	2.488	2.3864	2.2802	2.1701
4.1121	4.0014	3.8911	3.7814	3.6725	3.5642	3.4519	3.3312	3.2028	3.0677	2.9267
5.4241	5.2863	5.1479	5.0091	4.8702	4.7311	4.5828	4.4172	4.2359	4.0405	3.8329
7.3013	7.1247	6.9431	6.7568	6.5663	6.372	6.1498	5.8782	5.5626	5.2088	4.8237
10.4205	10.168	9.8971	9.6091	9.3052	8.987	8.5879	8.0516	7.3984	6.653	5.8434
13.5715	13.285	12.9837	12.6685	12.3402	12	11.5904	11.0611	10.4246	9.6964	8.8939
14.6504	14.3937	14.1379	13.8726	13.6018	13.3257	13.0157	12.6453	12.2183	11.7393	11.2136
15.2538	15.0727	14.8897	14.705	14.5187	14.3307	14.1308	13.908	13.664	13.3993	13.115

Table B.3 Published literature compressor efficiency at eleven points for each given relative speed

0.7411	0.7353	0.7291	0.7225	0.7153	0.7075	0.6986	0.6879	0.6753	0.6605	0.6434
0.7706	0.7648	0.7583	0.7508	0.7423	0.7328	0.7204	0.7032	0.6805	0.6518	0.6159
0.7845	0.7804	0.7758	0.7705	0.7646	0.758	0.7494	0.7372	0.7212	0.701	0.6761
0.8053	0.8026	0.7995	0.796	0.792	0.7875	0.7811	0.7726	0.7607	0.7457	0.7272
0.835	0.8337	0.832	0.8298	0.8272	0.8241	0.8191	0.8107	0.7989	0.7832	0.7636
0.8576	0.8582	0.8581	0.8573	0.8558	0.8535	0.848	0.8367	0.8193	0.7953	0.7645
0.8611	0.8639	0.8656	0.8661	0.8655	0.8635	0.856	0.8383	0.8099	0.7699	0.7178
0.8522	0.8533	0.8538	0.8536	0.8527	0.851	0.8461	0.8355	0.8189	0.796	0.7665
0.8088	0.8084	0.8077	0.8067	0.8054	0.8037	0.8008	0.7955	0.7878	0.7776	0.7649
0.7587	0.7578	0.7569	0.7558	0.7547	0.7534	0.7518	0.7494	0.7462	0.7423	0.7377

Table B.4 Published literature compressor flow rate at eleven points for each given relative speed (converted to SI unit [kg/s])

11.37311	11.45081	11.52693	11.60155	11.67467	11.74624	11.81628	11.88482	...
11.95186	12.01736	12.08132						
15.99893	16.17569	16.34294	16.50083	16.64939	16.78878	16.91892	17.03985	...
17.15193	17.25508	17.34943						
21.109	21.27656	21.43228	21.57626	21.70875	21.82982	21.93972	22.03843	...
22.12634	22.20345	22.27013						
27.07879	27.23859	27.3851	27.51851	27.63916	27.74717	27.84247	27.92566	...
27.99674	28.05598	28.1037						
34.61816	34.80037	34.96503	35.11227	35.24277	35.35658	35.45392	35.53521	...
35.6008	35.65101	35.68612						
44.22577	44.47652	44.70024	44.8971	45.06784	45.21303	45.33292	45.42822	...
45.49935	45.54725	45.57215						
57.01022	57.38203	57.70708	57.98636	58.22097	58.41198	58.56012	58.6669	...
58.73344	58.76075	58.76166						
69.38687	69.62334	69.83353	70.0172	70.1751	70.30795	70.41555	70.49883	...
70.55816	70.59418	70.60719						
73.81601	73.86037	73.90242	73.94147	73.97858	74.013	74.04494	74.07442	...
74.1015	74.12609	74.14836						
76.37794	76.38102	76.38356	76.38624	76.38887	76.39137	76.39363	76.39599	...
76.39812	76.40003	76.40189						

B.2 Published Literature Turbine Performance Map Raw Data [71]

Table B.5 Values of published turbine relative corrected speed data

0.3	0.4	0.5	0.6	0.7	0.8	0.9	1	1.1	1.2	1.3

Table B.6 Published literature turbine pressure ratio data at twenty points

1.1	1.2	1.4	1.6	1.7	1.8	2	2.2	2.4	2.6	2.8	...
3	3.2	3.4	3.6	3.8	4	4.2	4.4	4.6			

Table B.7 Published literature turbine efficiency data at twenty points for each given relative speed

0.83	0.731	0.626	0.569	0.549	0.533	0.507	0.488	0.474	0.462	0.451	...
0.443	0.436	0.43	0.424	0.419	0.415	0.411	0.408	0.405			
0.893	0.827	0.736	0.682	0.662	0.646	0.62	0.6	0.585	0.573	0.563	...
0.554	0.546	0.54	0.534	0.529	0.527	0.524	0.522	0.52			
0.912	0.884	0.814	0.766	0.749	0.733	0.709	0.691	0.676	0.663	0.652	...
0.646	0.641	0.637	0.633	0.63	0.626	0.623	0.619	0.615			
0.9	0.911	0.866	0.828	0.813	0.8	0.778	0.76	0.745	0.735	0.727	...
0.721	0.715	0.709	0.702	0.696	0.69	0.685	0.68	0.675			
0.867	0.919	0.9	0.872	0.859	0.849	0.828	0.811	0.799	0.789	0.78	...
0.772	0.763	0.754	0.746	0.739	0.733	0.727	0.722	0.717			
0.817	0.91	0.918	0.901	0.892	0.884	0.864	0.846	0.836	0.825	0.816	...
0.804	0.794	0.785	0.776	0.769	0.762	0.756	0.75	0.744			
0.753	0.89	0.925	0.918	0.913	0.906	0.889	0.874	0.861	0.85	0.838	...
0.826	0.815	0.805	0.796	0.788	0.781	0.775	0.769	0.763			
0.676	0.859	0.922	0.926	0.924	0.919	0.905	0.89	0.877	0.865	0.852	...
0.839	0.828	0.818	0.809	0.801	0.794	0.787	0.781	0.775			
0.589	0.82	0.912	0.927	0.928	0.925	0.913	0.899	0.886	0.874	0.86	...
0.847	0.836	0.826	0.817	0.809	0.801	0.794	0.788	0.782			
0.486	0.774	0.896	0.921	0.926	0.925	0.916	0.902	0.889	0.878	0.864	...
0.851	0.84	0.83	0.821	0.813	0.805	0.798	0.791	0.785			
0.379	0.721	0.873	0.91	0.919	0.921	0.915	0.902	0.889	0.878	0.864	...
0.852	0.84	0.831	0.822	0.813	0.806	0.799	0.792	0.786			
0.265	0.661	0.845	0.895	0.907	0.912	0.909	0.897	0.886	0.875	0.861	...
0.849	0.838	0.829	0.82	0.812	0.804	0.797	0.791	0.785			

Table B.8 Published literature turbine flow rate data at twenty points for each given relative speed (converted to SI unit [kg/s])

11.02631	15.29166	18.8182	19.44372	19.44372	19.44372	19.44372	19.44372	19.44372	19.44372	...
19.44372	19.44372	19.44372	19.44372	19.44372	19.44372	19.44372	19.44372	19.44372	19.44372	
10.39992	14.47471	18.31123	19.40011	19.44372	19.44372	19.44372	19.44372	19.44372	19.44372	...
19.44372	19.44372	19.44372	19.44372	19.44372	19.44372	19.44372	19.44372	19.44372	19.44372	
10.09872	13.88314	17.81187	19.22916	19.42821	19.44372	19.44372	19.44372	19.44372	19.44372	...
19.44372	19.44372	19.44372	19.44372	19.44372	19.44372	19.44372	19.44372	19.44372	19.44372	
10.03169	13.49677	17.36842	18.99002	19.32078	19.44021	19.44372	19.44372	19.44372	19.44372	...
19.44372	19.44372	19.44372	19.44372	19.44372	19.44372	19.44372	19.44372	19.44372	19.44372	
10.12653	13.27636	16.99814	18.72483	19.14545	19.36557	19.43201	19.43201	19.43201	19.43201	...
19.43201	19.43201	19.43201	19.43201	19.43201	19.43201	19.43201	19.43201	19.43201	19.43201	
10.27376	13.11127	16.61031	18.35748	18.83137	19.11969	19.29502	19.29502	19.29502	19.29502	...
19.29502	19.29502	19.29502	19.29502	19.29502	19.29502	19.29502	19.29502	19.29502	19.29502	
10.49476	13.04717	16.30003	18.01589	18.5094	18.84016	19.12262	19.14311	19.14311	19.14311	...
19.14311	19.14311	19.14311	19.14311	19.14311	19.14311	19.14311	19.14311	19.14311	19.14311	
10.77663	13.07468	16.07992	17.73167	18.23659	18.57818	18.92826	19.00202	19.00202	19.00202	...
19.00202	19.00202	19.00202	19.00202	19.00202	19.00202	19.00202	19.00202	19.00202	19.00202	
11.11295	13.1865	15.95347	17.52297	18.01999	18.36568	18.75381	18.88377	18.88992	18.88992	...
18.88992	18.88992	18.88992	18.88992	18.88992	18.88992	18.88992	18.88992	18.88992	18.88992	
11.47503	13.35803	15.89961	17.37662	17.85666	18.19825	18.60248	18.76669	18.79683	18.79683	...
18.79683	18.79683	18.79683	18.79683	18.79683	18.79683	18.79683	18.79683	18.79683	18.79683	
11.88366	13.58575	15.91717	17.29788	17.75538	18.08731	18.49183	18.67448	18.73215	18.73332	...
18.73332	18.73332	18.73332	18.73332	18.73332	18.73332	18.73332	18.73332	18.73332	18.73332	
12.31891	13.85651	15.99211	17.27563	17.70708	18.02584	18.41983	18.60921	18.69322	18.69322	...
18.69322	18.69322	18.69322	18.69322	18.69322	18.69322	18.69322	18.69322	18.69322	18.69322	

Appendix C: Statistical Evaluation

Error is the difference between the predicted output from the model and the measured output from the validation data set. Thus, error represent the portion of the validation data not explained by the model. In order to do that each model prediction result is compared with actual data from which the error is obtained. Mathematically, this is conceptualized as:

$$\text{measured value} = \text{model value} \pm \text{error} \tag{C.1}$$

The error is a combined effect of the assumptions, interpolation and terminating criteria that are used in the simulation model. For the investigation the quality of the prediction statistical evaluation is carried out. Minitab was used to examine the error. Minitab is a statistical program with a spreadsheet-like data worksheet [91]. It is capable of manipulating and transforming this data and can produce graphical and numerical summaries. Minitab also allows one to perform a wide variety of statistical computations. The following are the common statistical test and evaluation parameters that are used for the error analysis.

C.1 Measures of Position

A commonly used measure of the centre of a batch of data is mean. If the data are $x_1, x_2, x_3, ..., x_n$, then the mean is:

$$\bar{x} = \frac{\sum_{i=1}^{n} x_i}{n} \tag{C.2}$$

C.3 Measures of Dispersion

The sample standard deviation provides a measure of the spread of the data. If the column contains $x_1, x_2, x_3, ..., x_n$ with mean $\bar{x}$, then the standard deviation is:

$$s = \sqrt{\frac{\sum_{i=1}^{n} (x_i - \bar{x})^2}{n-1}} \tag{C.3}$$

Variance is a measure of how far the data are spread about the mean. Sample variance equals the standard deviation squared.

C.4 Anderson-Darling Normality Test

Anderson_Darling (A^2) measures the area between the fitted line (based on chosen distribution) and the nonparametric step function (based on the plot points). The statistic is a squared distance that is weighted more heavily in the tails of the distribution. Smaller Anderson–Darling values indicate that the distribution fits the data better.

Another quantitative measure for reporting the result of the normality test is the p-value. A small p-value is an indication that the null hypothesis is false. P-values are often used in hypothesis tests, where you either reject or fail to reject a null hypothesis. The p-value represents the probability of making a Type I error, which is rejecting the null hypothesis when it is true. The smaller the p-value, the smaller is the probability that you would be making a mistake by rejecting the null hypothesis.

If one knows A^2 one calculate the P-value.

$$A'^2 = A^2 \times \left(1 + \frac{0.75}{n} + \frac{2.25}{n^2}\right)$$ (C.4)

Depending on A'^2, one will calculate P with the following equations:

If $0.600 > A'^2 > 0.340$, $P = \exp\left(0.9177 - 4.279 A'^2 - 1.38\left(A'^2\right)^2\right)$ (C.5)

If $0.600 > A'^2 > 0.340$, $P = \exp\left(0.9177 - 4.279 A'^2 - 1.38\left(A'^2\right)^2\right)$ (C.6)

If $0.340 > A'^2 > 0.200$, $P = 1 - \exp\left(-8.318 + 42.796 A'^2 - 59.938\left(A'^2\right)^2\right)$ (C.7)

If $A'^2 < 0.600$, $P = 1 - \exp\left(-13.436 + 101.14 A'^2 - 223.73\left(A'^2\right)^2\right)$ (C.8)

144

C.5 Distribution Shape

Minitab also analyse the skewness of the distribution and skewness is the measure of asymmetry. A negative value indicates to the left, and a positive value indicates skewness to the right. A zero value does not necessarily indicate symmetry. The formula for skewness is:

$$b_1 = \frac{n}{(n-1)(n-2)} \sum \left[(x_i - \bar{x})/s \right]^3 \qquad (C.9)$$

Kurtosis is one measure of how different a distribution is from the normal distribution. A positive value typically indicates that the distribution has a sharper peak, thinner shoulders, and flatter tails than the normal distribution. A negative value means that a distribution has a flatter peak, fatter shoulders, and thinner tails than the normal distribution and is given by:

$$b_2 = \frac{n(n+1)}{(n-1)(n-2)} \sum \left[(x_i - \bar{x})/s \right]^4 - \frac{3(n-1)^2}{(n-2)(n-3)} \qquad (C.10)$$

C.6 Confidence Intervals

C.6.1 Confidence Interval for the Mean

A $(1-\alpha)$ 100% confidence interval for the true mean based on the sample standard deviation is given by:

$$\bar{x} - \frac{t_{n-1,\alpha/2}s}{\sqrt{n}} \quad \text{to} \quad \bar{x} + \frac{t_{n-1,\alpha/2}s}{\sqrt{n}} \qquad (C.11)$$

where $t_{\alpha/2}$ is in general the $(1-\alpha)$ 100th percentile of the t-distribution with (n - 1) degrees of freedom and obtained from tables of the t distribution.

C.6.2 Confidence Interval for Standard Deviation

Minitab calculates a $(1-\alpha)$100 % confidence interval for the true standard deviation, α . The confidence interval goes from:

145

$$\sqrt{\frac{(n-1)s^2}{\chi^2_{n-1,\alpha/2}}} \quad \text{to} \quad \sqrt{\frac{(n-1)s^2}{\chi^2_{n-1,1-\alpha/2}}} \qquad\qquad (C.12)$$

where $\chi^2_{n,\alpha}$ is in general is the $(1-\alpha)$ 100th percentile of the chi-square distribution with n degrees of freedom.

The aforementioned concepts and formula were used for statical evaluation of the errors between the simulated and actual data. The results are included in Chapter 4.